THE UNIVERSITY OF ALBERTA

THE EFFECTS OF STRAIN-HARDENING ON THE ULTIMATE LOAD CAPACITY OF STEEL FRAMES

A THESIS

SUBMITTED TO THE FACULTY OF GRADUATE STUDIES IN PARTIAL FULFILMENT OF THE REQUIREMENTS FOR THE DEGREE

of

MASTER OF SCIENCE

DEPARTMENT OF CIVIL ENGINEERING

by

IVAN FREDERICK KRAEMER

EDMONTON, ALBERTA

APRIL, 1962

SYNOPSIS

Results are reported for load tests of two hinge-supported rectangular portal frames. One frame was subjected to a vertical load applied at midspan; the other to a vertical load at midspan and a horizontal force applied at the top of one column.

A secondary portion of the test consisted of a load test on a simple span beam subjected to two equal loads symmetrically placed on each side of midspan.

Strain-hardening effects became evident at approximately ultimate load in each frame and caused substantial increases in the load carrying capacity in excess of that predicted by the simple plastic theory. For the frame subjected to a vertical load applied at midspan, the final load obtained was approximately thirty-three percent in excess of that predicted by simple plastic design calculations. For the frame subjected to a vertical load at midspan and a horizontal force applied at the top of one column, the final load was approximately eighteen percent in excess of the theoretical ultimate load.

ACKNOWLEDGMENTS

The successful completion of the studies herein reported was made possible by the fine cooperation of many individuals. To all those who in any manner aided in the work, the author expresses his sincere thanks.

The test specimens were provided by the Canadian Institute of Steel Construction, Western Regional Committee, Alberta Division.

The author is especially grateful to Professor J. Longworth for his supervision and assistance in this investigation, and for his constructive criticisms during the preparation of the report.

Special thanks go to R. Brown and his entire Civil Engineering shop staff for their splendid cooperation.

The author also wishes to thank fellow graduate students T. James, J. Gregg, W. Landers, C. Howard, and W. Truch.

Acknowledgment is made to L. Sprinkhuysen, L. Nichols, and D. Nichols for their help during the instrumentation and testing.

For the typing and proof reading of the manuscript, the author wishes to thank Miss L. Mason.

TABLE OF CONTENTS

LIST OF FIGURES

CHAPTER 1: INTRODUCTION

1-1 Strain-Hardening Related to Ultimate Load

The application of plastic analysis to structural design is made possible by the important property of steel known as ductility. Beyond the elastic limit, steel is able to absorb large deformations without fracture. Plastic design makes conscious use of this ductility up to the point where strain-hardening begins. In Figure 1(a) an actual stress-strain diagram for a typical A7 steel illustrates the property of ductility. An idealized stress-strain curve shown in Figure 1(b) represents a very close approximation to the actual behaviour of structural steel.[1,2] After the elastic limit is reached, elongations from 8 to 15 times the elastic strain occur at constant stress. An increase in strength is then exhibited as the material strain-hardens. Strain-hardening is the remarkable phenomonen of most metals that occurs during plastic straining. As plastic straining proceeds, the crystal lattice suffers severe distortions and rotations causing an increased resistance to further deformations.[3] Therefore the property of strain-hardening acts essentially as an added margin of safety when the ultimate load is used as the design criterion for structural analysis; the ultimate load being defined as that load causing failure due to excessive deformations.

Average values obtained from standard coupon tests for the determination of material properties indicate that the strain at the onset of strain-hardening, e_{st}, is approximately equal to 15 times the yield strain. Presumably, strains of this magnitude would have to be attained before an actual structure would experience strain-hardening. This fact seems to indicate that an actual structure would have to

---

(1) Numbers in parenthese refer to references listed in Bibliography.

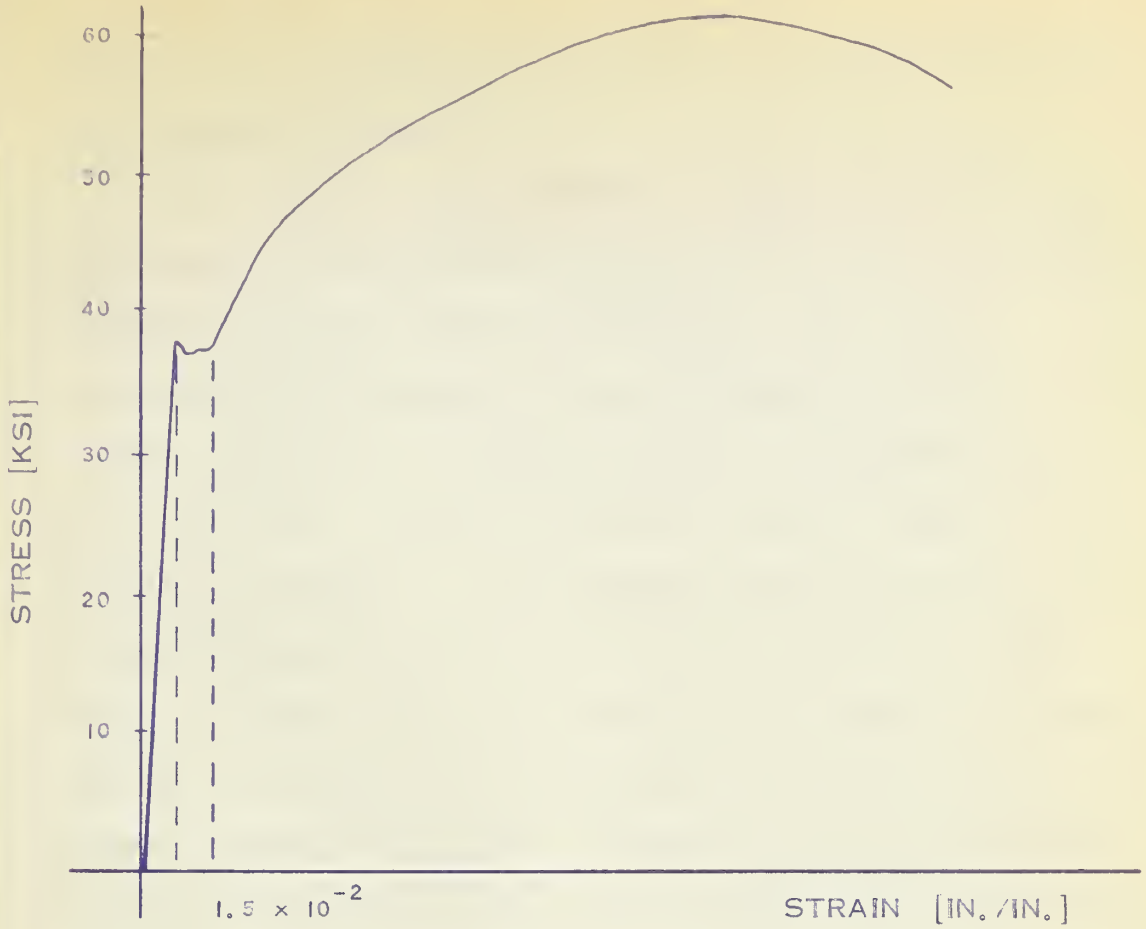

FIG. 1(a) STRESS – STRAIN DIAGRAM
FOR A7 STRUCTURAL STEEL

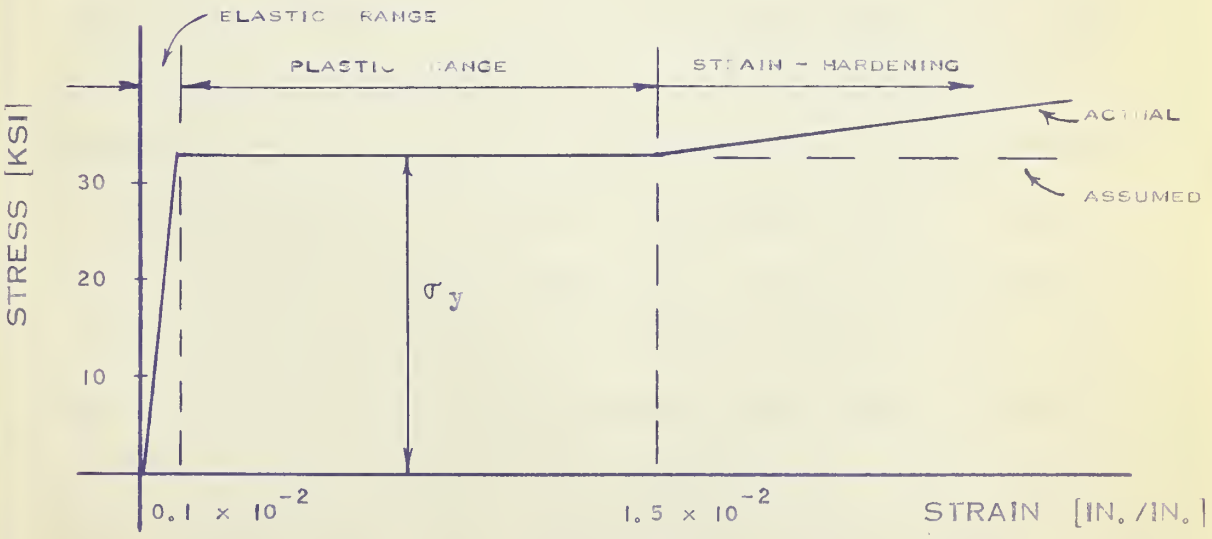

FIG. 1(b) IDEALIZED STRESS—STRAIN
DIAGRAM FOR A7 STRUCTURAL STEEL

experience large deflections and rotations at constant load before strain-hardening began.

For a simply supported beam, the approximate position at which strain-hardening theoretically begins is shown in moment vs. curvature and load vs. deflection diagrams. In an idealized moment-curvature relationship, shown in Figure 2, curvature is directly proportional to bending moment up to the plastic moment. Beyond this point, curvature increases at constant moment. Strain-hardening will begin at a point where the curvature is equal to the strain-hardening strain divided by one-half of the depth of the section. A typical theoretical load-deflection diagram for a simple beam with equal loads positioned symmetrically on both sides of the midspan is shown in Figure 2(b). Loads are directly proportional to deflection up to the ultimate load, at which further deflection occurs at constant load. With the onset of strain-hardening, increased deflection is accompanied by an increase in load. In Figure 2(c), a theoretical load-deflection curve is shown for a simple beam subjected to a central concentrated load. For a given moment-curvature diagram (including strain-hardening), increased deflections are accompanied by an increase in load due to the effect of strain-hardening in the region of the plastic hinge.[4] There is thus a considerable range of deflection in the former case over which the load remains constant at the theoretical collapse value. This is due to the fact that the central portion of the beam is subjected to a constant bending moment, so that large curvatures are developed over a finite length of the beam when this moment approaches the fully plastic value. A similar analysis applied to a continuous beam or two-pinned frame becomes indeterminate due to the redistribution of

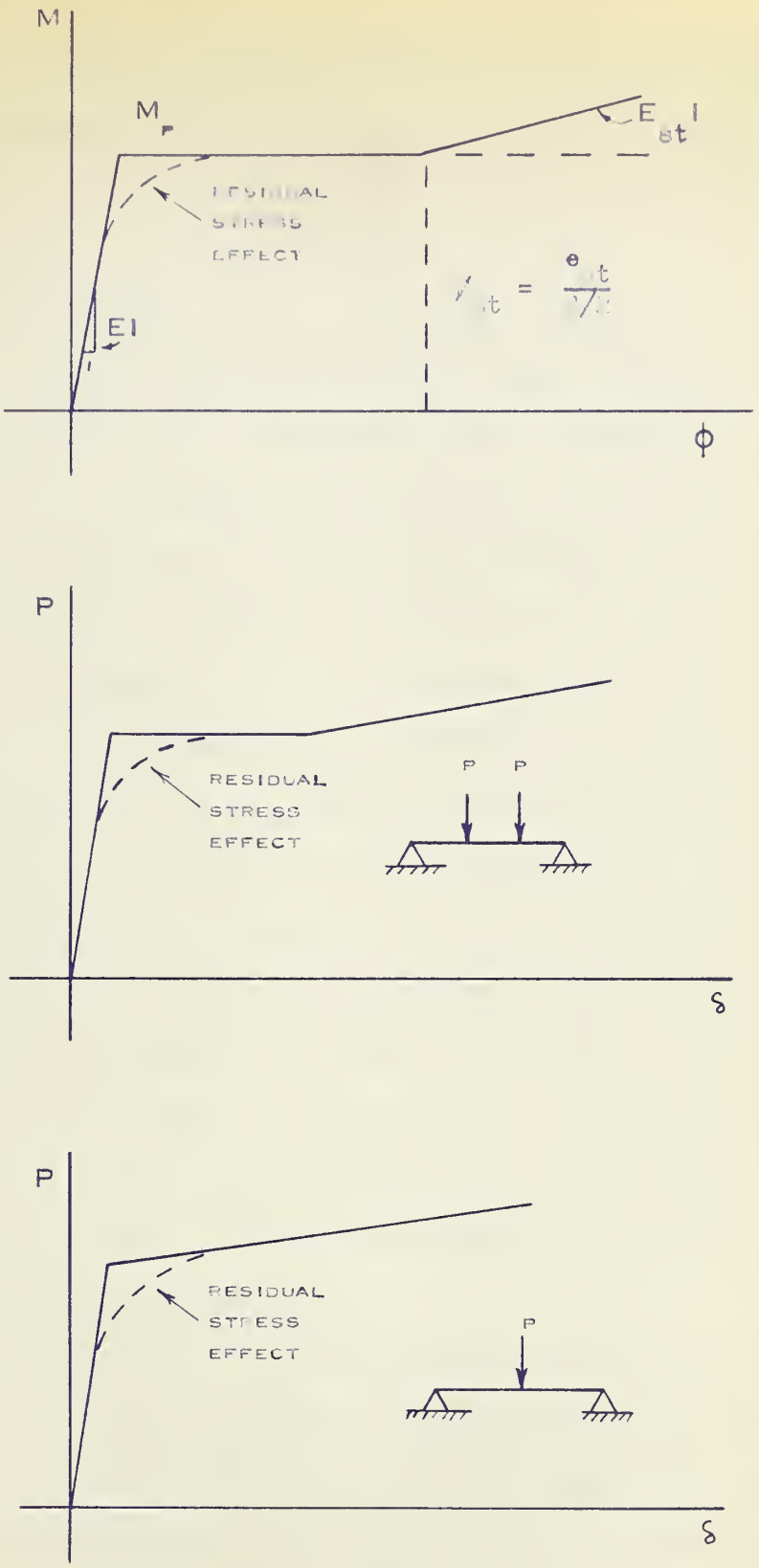

FIG. 2 INFLUENCE OF STRAIN – HARDENING UPON MOMENT – CURVATURE AND LOAD – DEFLECTION RELATIONSHIPS

moments. In general, however, applying the above discussion of beams to a rectangular portal frame loaded with a single concentrated force at the midspan would indicate that strain-hardening begins near the ultimate load.

1-2 Residual Stresses

The effect of residual stress, shown by dotted lines in Figures 2(a), (b) and (c) causes the section to yield at a lower load than predicted. In general, residual stresses are caused by differential cooling, cold-bending, and welding. The presence of residual stresses has no effect on the ultimate moment capacity.[1] These stresses do, however, cause the $M - \Theta$ and $P - \delta$ curves to be nonlinear as shown in Figure 2. Such departures from the straight line relationship is of little consequence when compared with the large rotations and deflections that occur when the plastic hinge forms. Tests at Lehigh University [5,6] show the magnitude of these residual stresses in large wide flange sections to be approximately 0.3 times the yield stress, with the maximum stresses occurring at the edges of the flanges. Since residual stresses cause initial yielding at a lower load than predicted, it would seem logical to assume that these stresses would also cause a section to enter the strain-hardening range sooner than expected.

1-3 Experimental Investigations

Previous tests on rectangular portal frames at Lehigh University[7] show an immediate increase in load carrying capacity at or near the point where the calculated ultimate load is just reached.

A more recent series of tests conducted at the University of California were reported in 1960.[8] The tests attempted to show deflection stability of frames under repeated loads. However, one of the frames tested was subjected to a proportional loading with the

applied loads increasing in magnitude at the same rate. These tests are of particular interest in connection with the present studies at the University of Alberta for two reasons; one being that a similar loading frame was used for the tests conducted here, and the second being that a similar size test specimen was used. Results showed a conservative value for the ultimate load capacity in comparison to that obtained by the simple plastic theory. The authors attributed the increased load carrying capacity to strain-hardening effects.

1-4 Previous Investigation at the U. of A.

A series of tests conducted in 1961 by Channon[9] introduced studies in plastic analysis at the University of Alberta. In this investigation results were reported on four rectangular portal frames, one loaded with a concentrated vertical force at the midspan of the frame beam, one loaded with a concentrated horizontal force at the corner, and two loaded with both concentrated vertical and horizontal forces. The first frame tested failed at a load slightly lower than its predicted capacity due to insufficient lateral support. However when additional support was provided, the remaining three test frames exhibited ultimate load carrying capacities greater than those predicted by the simple plastic theory. The excess in ultimate load capacity was attributed to the effect of strain-hardening at the plastic hinges.

Derived moment-curvature curves in general showed poor agreement with the idealized moment-curvature curves. This poor correlation between test results and theoretical calculations for the moment-curvature relationship can possibly be attributed to two main factors. The magnitudes of frame reactions were not measured and therefore it was necessary to make certain assumptions in order to compute bending moments. For the two frames in which equal vertical

and horizontal loads were applied at the midspan of the beam and at the top of the column, the calculated horizontal reactions were assumed to be equal to those determined by an elastic analysis of the frame up to the load calculated to form the first plastic hinge. For loads greater than this value, the increase in horizontal load was assumed to be taken entirely by the horizontal reaction at the windward column while the horizontal reaction at the leeward column remained constant. For the frame loaded with a concentrated horizontal load applied at the top of the column, each horizontal reaction was assumed to carry one-half of the applied load. For the frame in which a concentrated vertical load was applied at the beam midspan, the horizontal reactions were assumed as equal to values determined by an elastic analysis of the frame up to the load at which the first plastic hinge formed. For loads greater than this value, the horizontal reactions were calculated assuming a moment equal to the theoretical plastic moment acting at the midspan of the beam. A second factor that contributed to the poor agreement between test results and theoretical calculations for the moment-curvature relationships was the method by which curvature was measured. Strain gauges were the only instrumentation used for this measurement. They proved to be unsatisfactory, since readings had to be discontinued before the end of the test, thus providing an incomplete picture of the curvatures. These readings were discontinued because some strain values went beyond the range of the strain indicators, while in other cases, the gauge itself ceased to function properly.

1-5 Present Investigation

In light of Channon's results, it was decided to implement three main improvements in the instrumentation. Firstly, the

horizontal reaction was measured at the left support, which eliminated the assumptions concerning the distribution of the horizontal reactions. Secondly, a different method was used to measure curvature. A mechanical device, similar to that used at Lehigh University[7] was used instead of electrical resistance strain gauges. The third change in instrumentation involved the measurement of the applied loads. Channon used bourdon pressure gauges for all load readings. In the present tests, all loads were measured using newly acquired load cell equipment.

The present investigation deals with load tests on steel frames identical to those used in Channon's tests with a view to examining the effects of strain-hardening on the ultimate load capacity.

CHAPTER 2: SCOPE OF INVESTIGATION

2-1 Object of Investigation

The investigation described in this thesis was designed to examine the effects of strain-hardening on the ultimate load capacity of steel frames.

The major portion of the program consisted of load tests on two hinge-supported rectangular frames loaded as shown in Figure 3. Frame No. 1 was loaded with a vertical force at the beam midspan. Frame No. 2 was loaded with a vertical force at the beam midspan and a horizontal force applied at the top of one column. Loads were proportioned such that the ratio of vertical to horizontal load was 2:1.

A beam was loaded as shown in Figure 3 with two equal forces symmetrically placed on each side of the midspan. The primary reason for testing the beam was to obtain an experimental moment-curvature relationship for the 4 I 9.5 material used for the test specimens.

In the test program, attention was focussed on the following characteristics:

1. Actual load-carrying capacity as compared to the calculated capacity.
2. Actual deflections as compared to computed deflections.
3. Actual moment-curvature relationships as compared to computed values.
4. Strain distribution at sections where plastic hinges were predicted.
5. Failure mechanism in each frame at ultimate load.

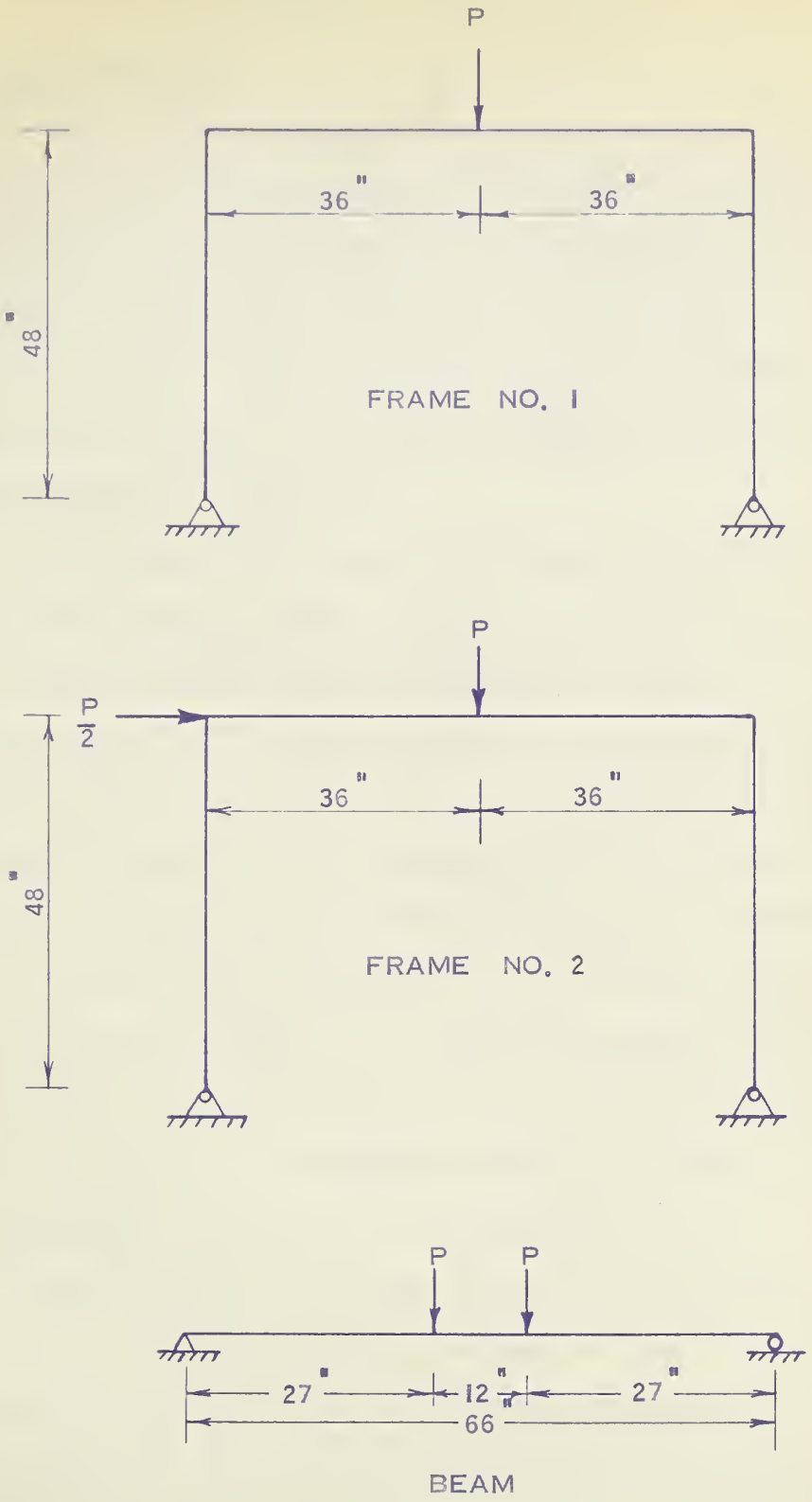

FIG. 3 – LOADING CONDITIONS FOR FRAMES AND BEAM

CHAPTER 3: TEST SPECIMENS

3-1 Frame Specimens

The two frame specimens tested in this program were of the same design as those tested by Channon.[9] They were of uniform section throughout with column and beam sections cut from 4 I 9.5 material. They had a column height of four feet and a beam span of six feet, as shown in Figure 4. The holes at the column bases allowed the insertion of one and one-eighth inch diameter finished pins for supporting the specimens in the loading frame.

The corner details, shown in Figure 5, were welded in order to obtain the greatest possible rigidity. The welds in the connections were proportioned such that the maximum weld stress at ultimate load did not exceed 1.65 times the allowable weld stresses given in the present elastic design codes. This is in accordance with the new C.S.A. S16 1961 Specification for Steel Structures for Buildings and with the A.I.S.C. Supplementary Rules for Plastic Design and Fabrication.

Flange plates were welded to the beam at the frame corners so that the plastic hinges at the corners would form in the column section. The corner connections were well stiffened to assure that local buckling would not occur in the connections before the ultimate load was reached. The horizontal stiffener in the column web was designed to distribute the thrust from the lower flange of the beam and reduce the web crippling tendency. Diagonal stiffeners were used to resist the high shear stresses encountered in the web. Vertical bearning stiffeners were provided at the center of the beam to prevent web crippling under the vertical concentrated load.

The column flanges were coped at the base, as shown in Figure 5, so the frames could be fitted into the hinge support provided in the loading frame. Doubler plates were used to increase the bearing capacity of the column web at the hinge. The one and one-eighth inch diameter holes provided for the hinge pins were reamed to reduce the rotation resistance at the support as much as possible. Rotation indicator brackets, shown in detail in Figure 6, were welded to the fillets of the test specimens. They were positioned near points where plastic hinges were predicted. Figure 4 shows their positions on the frame.

3-2 Beam Specimen

The beam specimen used was cut from the same material as the two frames. The beam was six feet in length. Vertical bearing stiffeners were placed on each side of the web at the two loading positions (see Figure 6). Two rotation indicator brackets were welded to the fillets of the beams, straddling the midspan of the beam.

3-3 Specimen for Material Properties

The fabricator supplied a five foot length of the 4 I 9.5 section from the same stock as was used for the two frames and the beam. This was used to determine residual stresses, modulus of elasticity, and yield strength of the steel.

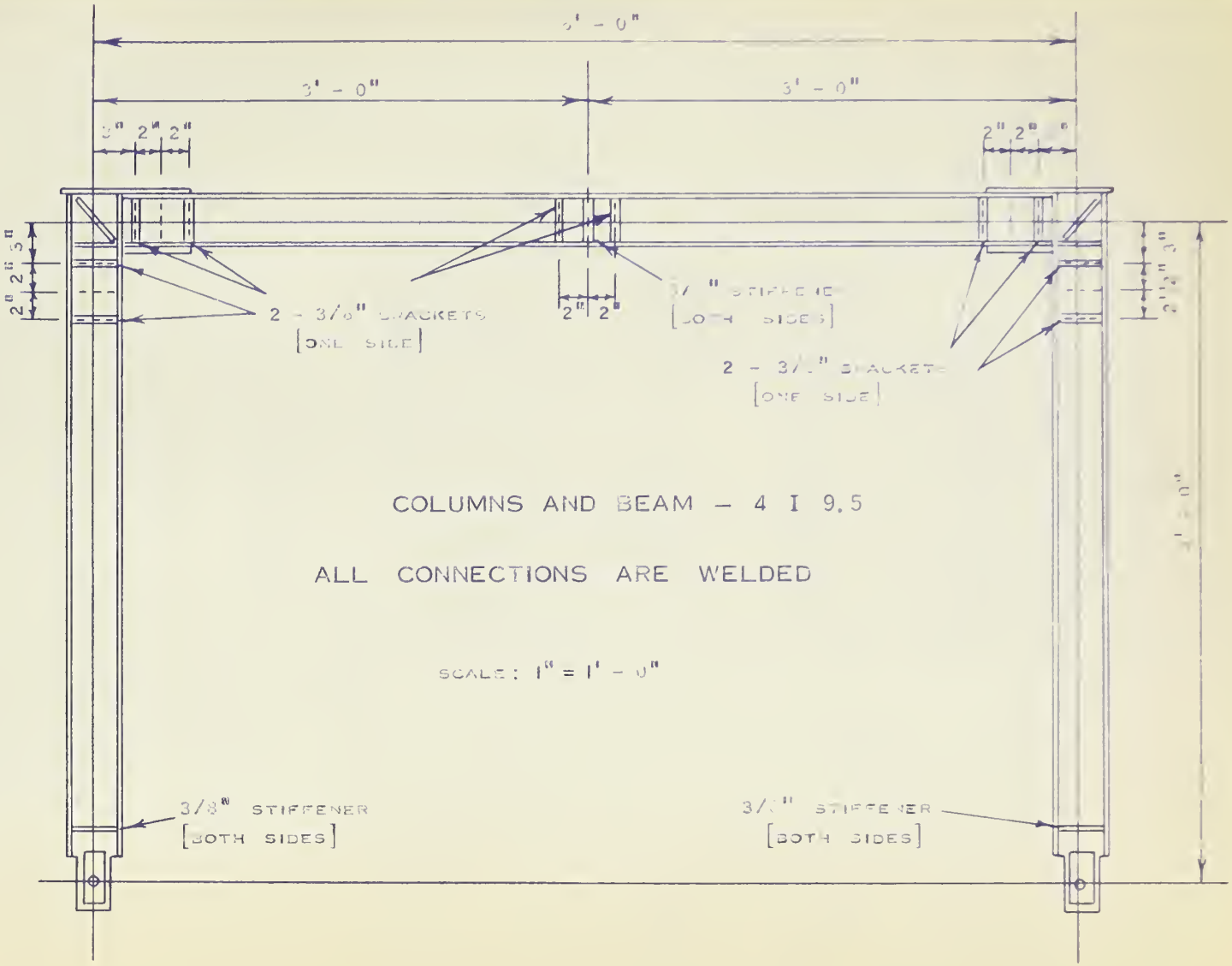

FIG. 4 – DETAILS OF TEST FRAME

CORNER CONNECTION

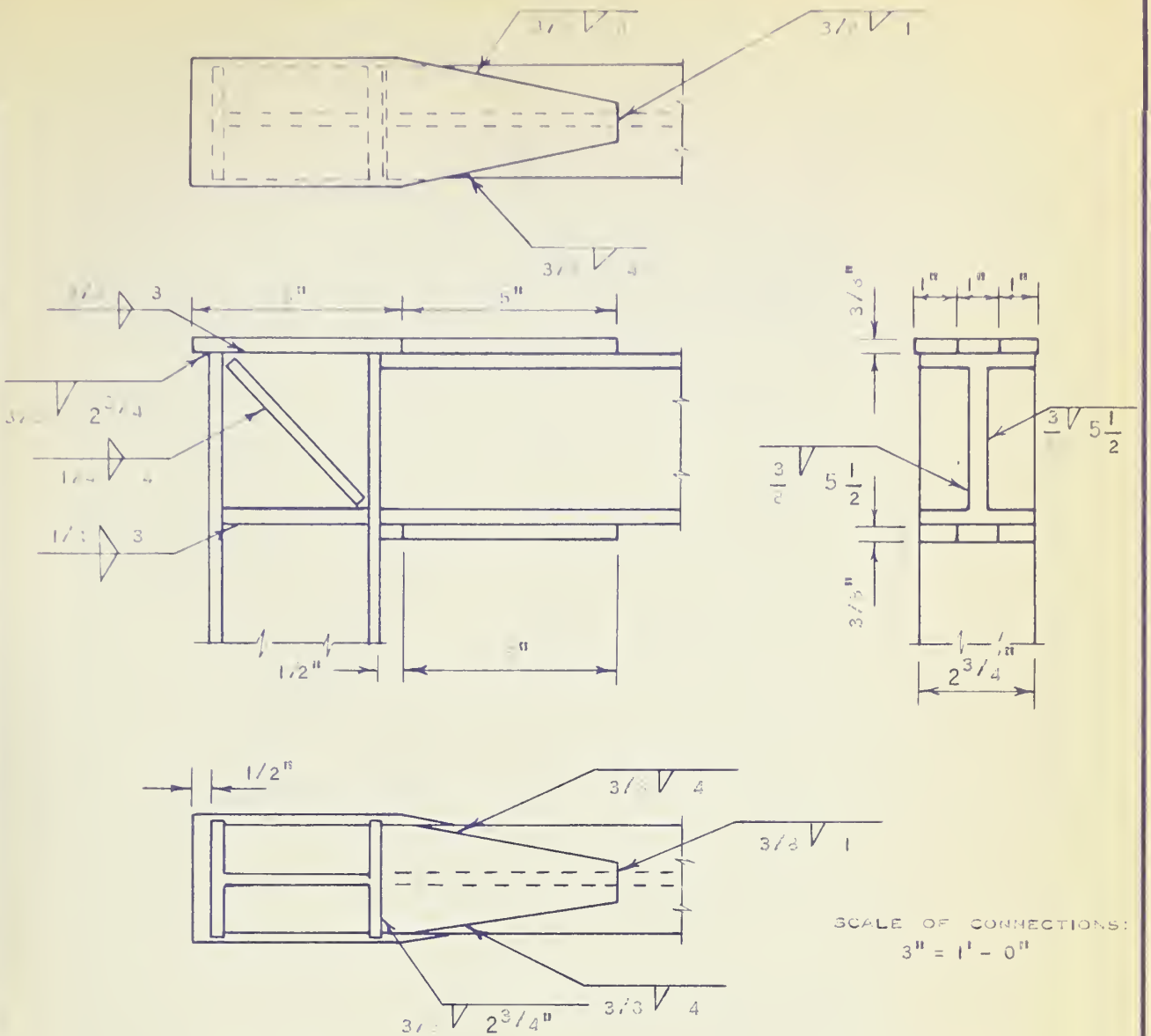

SCALE OF CONNECTIONS:
3" = 1' - 0"

HINGE CONNECTION

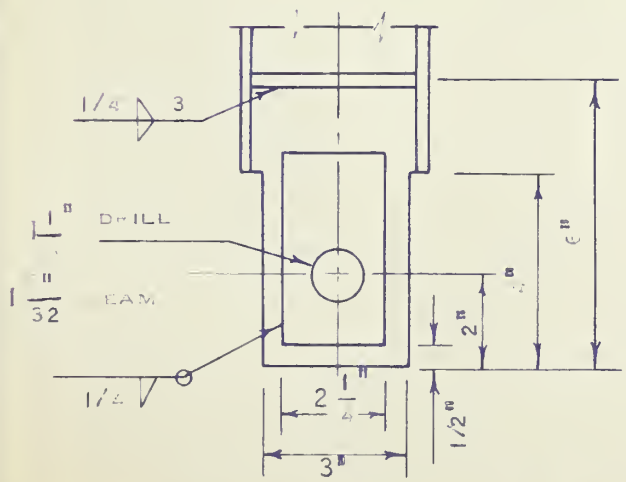

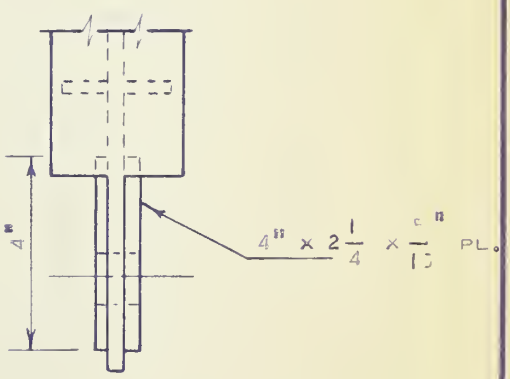

NOTE ALL STIFFENERS AND BRACKETS CUT FROM 3/16" PLATE.

FIG. 5 – DETAILS OF TEST FRAME CONNECTIONS

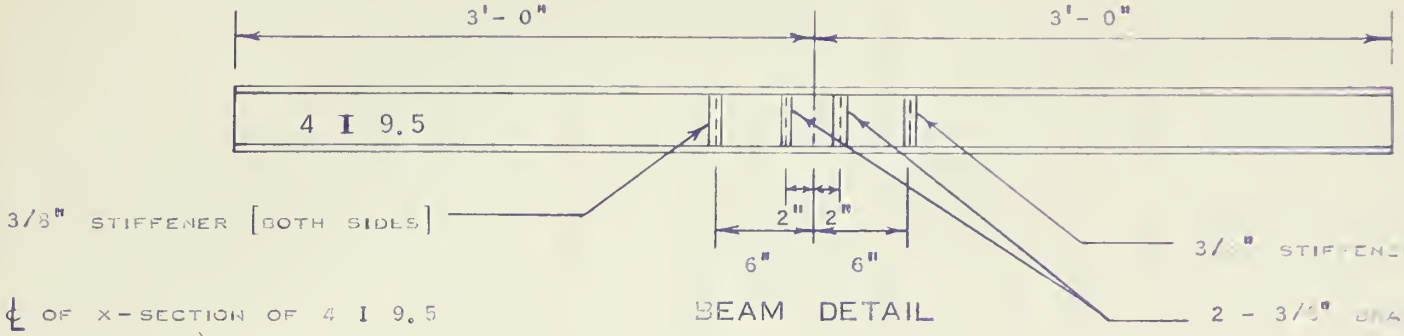

BEAM DETAIL

℄ OF X-SECTION OF 4 I 9.5

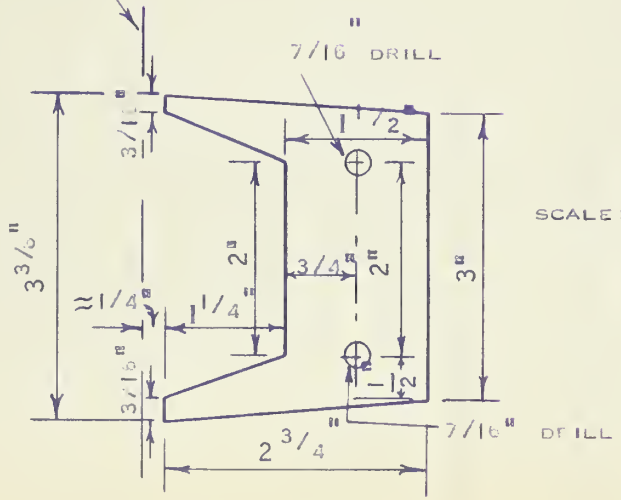

SCALE: HALF SIZE

BRACKET DETAIL

NOTE: ALL STIFFENERS AND BRACKETS CUT FROM 3/8" PLATE

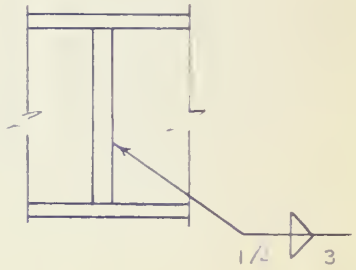

WELDING DETAIL OF STIFFENER

FIG. 6 – DETAILS OF TEST BEAM

4-1 Frame Specimens

Loads were applied to the test frames by means of hydraulic rams. The jacks were firmly attached to a loading frame, designed specifically for this type of investigation.[9] Due to the fact that a heavy roller mechanism was used to allow horizontal movement of the vertical jack, it was found to be more convenient to test the frame specimens in an upside down position with the hinge supports attached to the upper beam of the loading frame.

The loading system used for Frame No. 1 is shown in Figure 7. One "Blackhawk RC-251" hydraulic jack with a capacity of twenty tons and a plunger travel of six inches was used to apply the vertical load. The base of the jack was bolted to the roller mechanism. In this particular test, no movement of the roller mechanism took place. A ten ton capacity " Blackhawk RC-159" hydraulic ram was used as the horizontal reaction jack. It had a plunger travel of six inches, and was bolted in a horizontal position directly to the left column of the loading frame.

The loading system used for Frame No. 2 is shown in Figure 8. Vertical load was applied by equipment described above for Frame No. 1. A horizontal load was applied to the left frame leg at a point in line with the mid-depth of the beam. The ratio of vertical to horizontal load was 2:1. Movement of the roller mechanism under the vertical load occurred as a result of the horizontal load. Due to the difference in loading, the horizontal reaction jack had to be placed in the opposite direction to that for Frame No. 1. The jack was bolted to a 6" wide flange section, which was in turn secured to the top beam of the loading frame, as seen in Figure 8. The horizontal load jack and the horizontal

reaction jack were "Blackhawk RC-159" rams.

Lateral support was provided for the frames by two 8" channel sections bolted at the ends to the columns of the loading frame. Structural angles projecting from the backs of the two channels provided restraint to movement in the lateral direction.

4-2 Beam Specimen

The test beam was placed on two hinged supports spaced 66 inches apart. A simple span condition was obtained by introducing a one-inch diameter roller under the beam at the right support. Figure 9 shows the loading system used for the beam. Two "Blackhawk RC-161" hydraulic jacks with a capacity of ten tons each and a plunger travel of ten inches were placed twelve inches apart and symmetrical with respect to the midspan of the beam. Both rams were operated with a single "Blackhawk P-59" pump allowing equal loads to be maintained on the rams throughout the test. The base plates attached to the jacks were bolted together by a steel bar to hold the jacks parallel throughout the test. The jacks were bolted to the beam section of the loading frame which had been lowered after the completion of the frame tests. Lateral support was provided for the beam in the same manner as in the testing of the frame specimens.

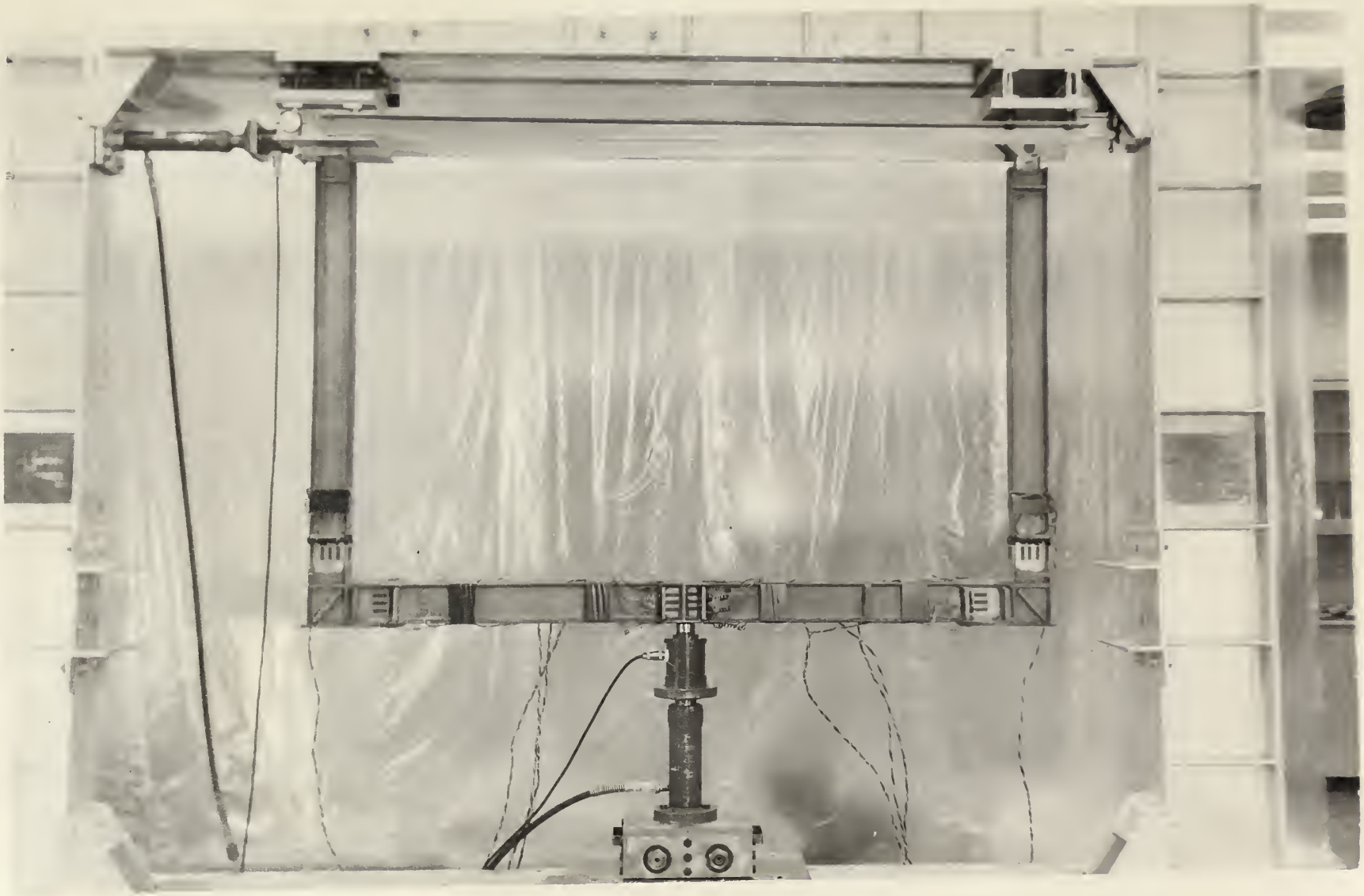

FIG. 7 – LOADING SYSTEM FOR FRAME NO. 1

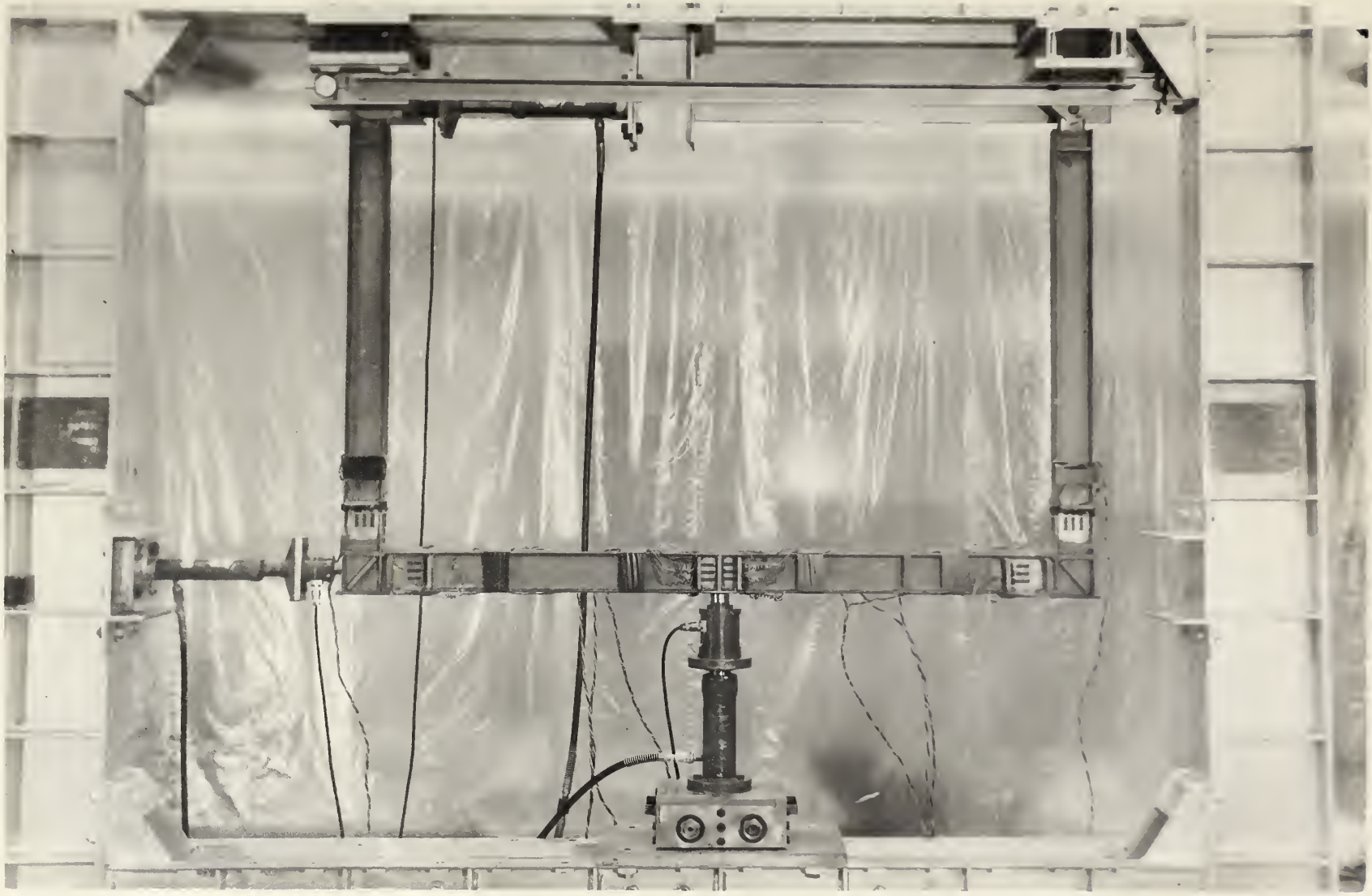

FIG. 8 — LOADING SYSTEM FOR FRAME NO. 2

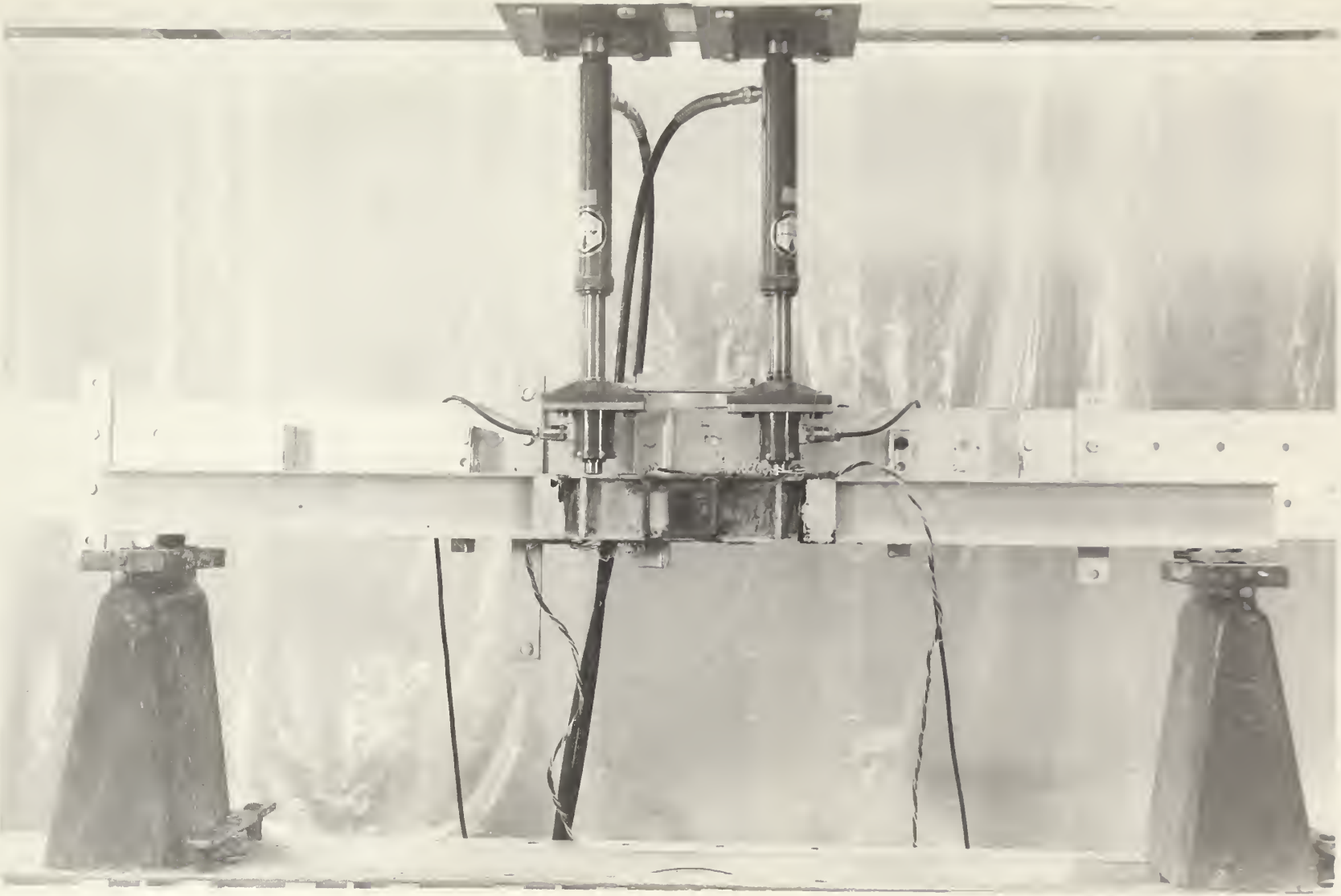

FIG. 9 – LOADING SYSTEM FOR BEAM

CHAPTER 5: INSTRUMENTATION

5-1 Load Measurement

Loads applied through the hydraulic rams were measured by means of "Kyowa" load cells which were bolted to bearing plates screwed to the ends of the hydraulic rams, as show in Figures 11 and 12. These load cells were connected through a 3-point switching box to a "Type SLW-210PA Kyowa Self-Balancing Indicator."

For testing Frame No. 1, the vertical load was measured by a "Kyowa LC-20/1" load cell, having a capacity of twenty tons. The horizontal reaction load was measured by a "Kyowa LC-5/3" load cell, with a capacity of five tons.

For testing Frame No. 2, the vertical load and horizontal reaction load were measured by the identical load cells described above for Frame No. 1. One additional "Kyowa" five-ton load cell, LC-5/1, was used to measure the horizontal load.

Figure 10 gives an overall view of the complete test set-up, showing all the instrumentation used.

5-2 Frame Reaction Measurement

In order to measure the horizontal reaction at one of the supports, a horizontal reaction assembly, shown in Figure 13, was used. On each side of the hinge support, provision was made for angle iron tie-bars to extend from one frame leg to the other. The tie-bars were securely fastened to the right hinge support as shown in Figure 14, and allowed to roll freely at the left support. As the frame was loaded, distance between the columns was kept constant by applying the necessary force to maintain the initial dial gauge reading. A set of rollers placed over this hinge support allowed free movement of the entire horizontal reaction assembly.

5-3 Curvature Measurement

Rotation indicators were used to measure relative rotation of two neighbouring cross sections (see Figure 15). These indicators consisted of two parallel steel angles, 25 inches long, connected to brackets which were welded to the frame at the fillets and symmetrically placed on each side of the section at which the curvature was to be measured. The relative rotation of these arms was measured by means of two dial gauges mounted at known distances above and below the frame axis. In some cases, the steel angles were bolted at the ends, and a single dial at the opposite end was used to measure rotation. The curvature at a section equals the measured angle divided by the distance (4 inches) between the two arms. Denoting two consecutive dial readings as R_1 and R_2 respectively, the change in curvature $\Delta \phi$ is given by:

$$\Delta \phi = \frac{R_1 - R_2}{4 \times 25} = 0.01 (R_1 - R_2) \quad \text{radians/ inch.}$$

The curvature as measured by this rotation is accurate to about 10^{-5} radians or 2 seconds.

In the frame tests, five rotation indicators were used as shown in Figure 10. One indicator was placed at the midspan of the beam, and four at the corners; two attached to the columns and the other two attached to the beam. Exact positions of the brackets on the frame are detailed in Figure 4.

5-4 Frame Deflection Measurements

Two dial gauges, reading to 0.001 inch, and having a two-inch travel were used to measure deflections at the midspan of the beam and at the right corner of the frame. In testing Frame No. 1, deflections

at the left corner were measured by a one-inch travel dial indicator, reading to 0.001 inch.

As a check on the dial gauges, readings were taken on two steel scales, graduated in 1/100 of an inch by means of surveyor's levels. Figure 16 shows typical equipment for deflection measurements. In testing Frame No. 1, one scale was attached at the midspan of the beam and the horizontal cross-hair of the first level was used to take the vertical deflection readings at each load. The second scale was attached to the right column at a point directly between the two arms of the rotation indicator. The second level was focused on this scale from approximately ten feet, and at each load increment, horizontal movement was recorded by using the vertical cross-hair.

In testing Frame No. 2, one scale was attached at the midspan of the beam as before; however the second scale was attached to the left column at a point directly between the two roation indicator lever arms. A dial gauge was not used here, but was used instead to measure the horizontal movement of the roller mechanism.

5-5 Strain Measurements

Electrical resistance strain gauges were mounted on each frame to measure strain at locations where plastic hinges were expected to form. Eighty Type A-3, SR-4 gauges were mounted on each frame, and placed on each side of the section. Sixteen were placed on each column near the corner, and eight more positioned on each end of the beam near the corner. Sixteen gauges were placed on each side of the stiffener at the midspan of the beam. Exact positions are shown in Figure 17.

The surface of the frame specimens had been sandblasted by the

fabricator to remove the mill scale. The surfaces were further prepared to give a smooth finish before mounting the strain gauges. A rotary-disc sander was used for grinding the flanges. For the insides of the flanges and for the webs, a small air-driven grinder worked very satisfactorily. After grinding, emery cloth was used to produce a smoother finish. After the surface had been cleaned thoroughly with acetone, the "SR-4" gauges were cemented in position with C.I.L. Household Cement. Care was taken to squeeze out any air bubbles in the cement so that the gauges were in intimate contact with the metal. The cement was allowed to dry for approximately two weeks. All gauges were checked with an ohmeter before wiring, and any defective gauges were replaced. One coat of neoprene was used to waterproof and protect the gauges.

After the frame was set in place in the loading frame, the lead wires from the gauges were connected to four "Baldwin-Lima-Hamilton" 20-point Switching Units. Strain readings were taken with four "Baldwin-Lima-Hamilton Type 4, SR-4 Strain Indicators."

5-6 Beam Instrumentation

Figure 18 gives an overall view of the instrumentation used for the beam set-up. A "Kyowa" load cell was attached to each of the two loading jacks, and connected through a 3-point switching-box to the "Kyowa Self-Balancing Indicator." The two load cells, LC-5/1 and LC-5/3, each had a capacity of five tons. Curvature was measured at the midspan by a rotation indicator. Vertical deflection at the midspan of the beam was measured in a similar manner to that used in the frame tests. A two-inch travel dial gauge, measuring to 0.001 inch was positioned directly under the midspan of the beam. A check on these deflection readings was provided by readings taken with a surveyor's level on a steel scale

mounted at midspan.

The procedure for preparing the surfaces and mounting the strain gauges was identical to that employed for the frame specimens. Twenty gauges were mounted at the midspan of the beam as shown in Figure 19. A "Baldwin-Lima-Hamilton Switching Unit" and Indicator were used to measure strain.

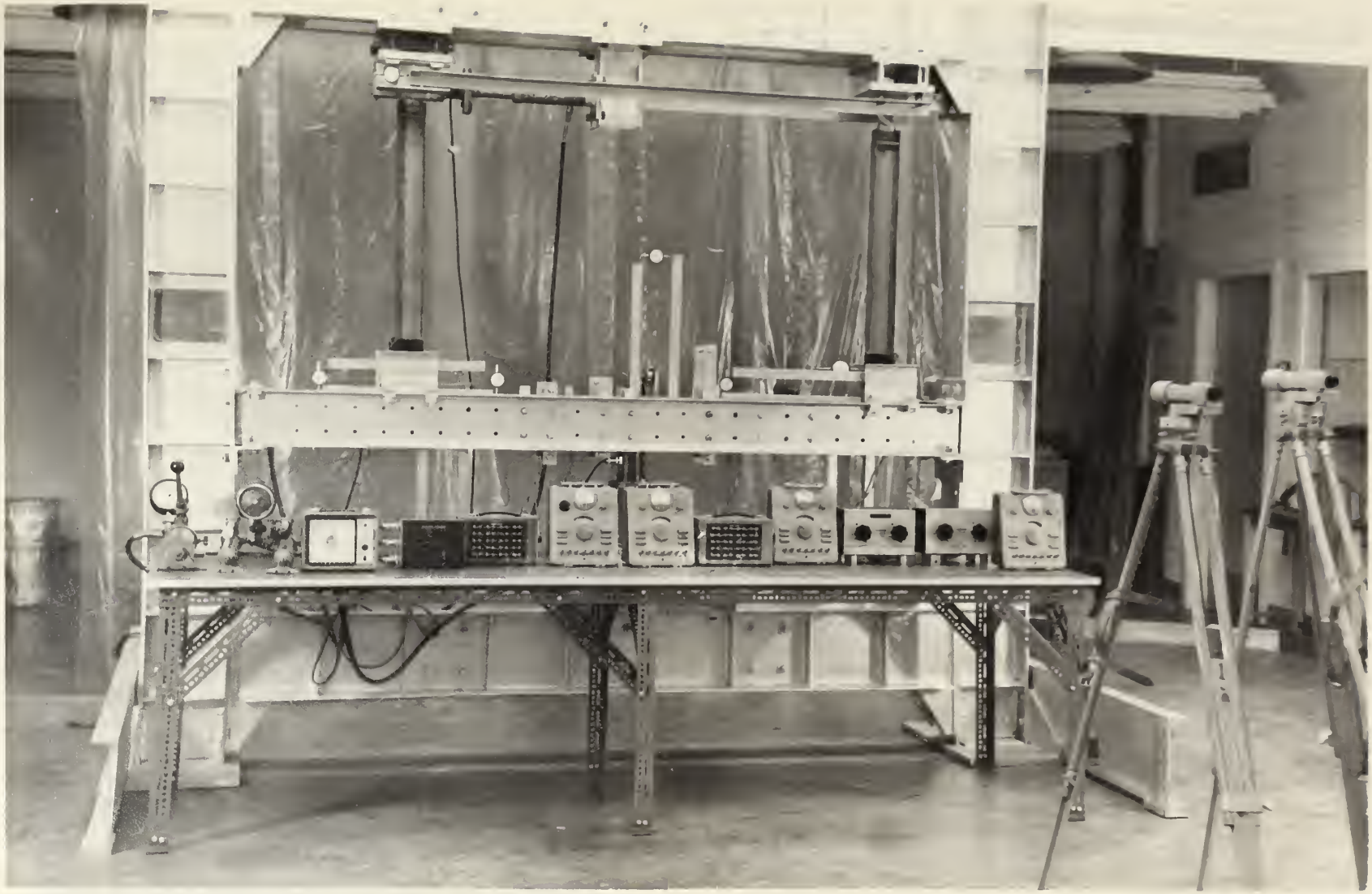

FIG. 10 – GENERAL VIEW OF FRAME TEST EQUIPMENT

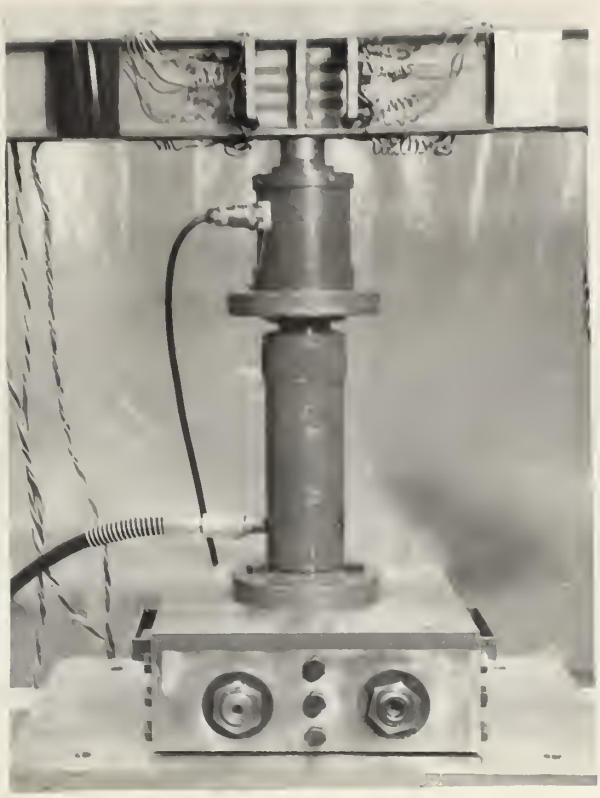

FIG. 11 – VERTICAL JACK WITH 20 TON LOAD CELL

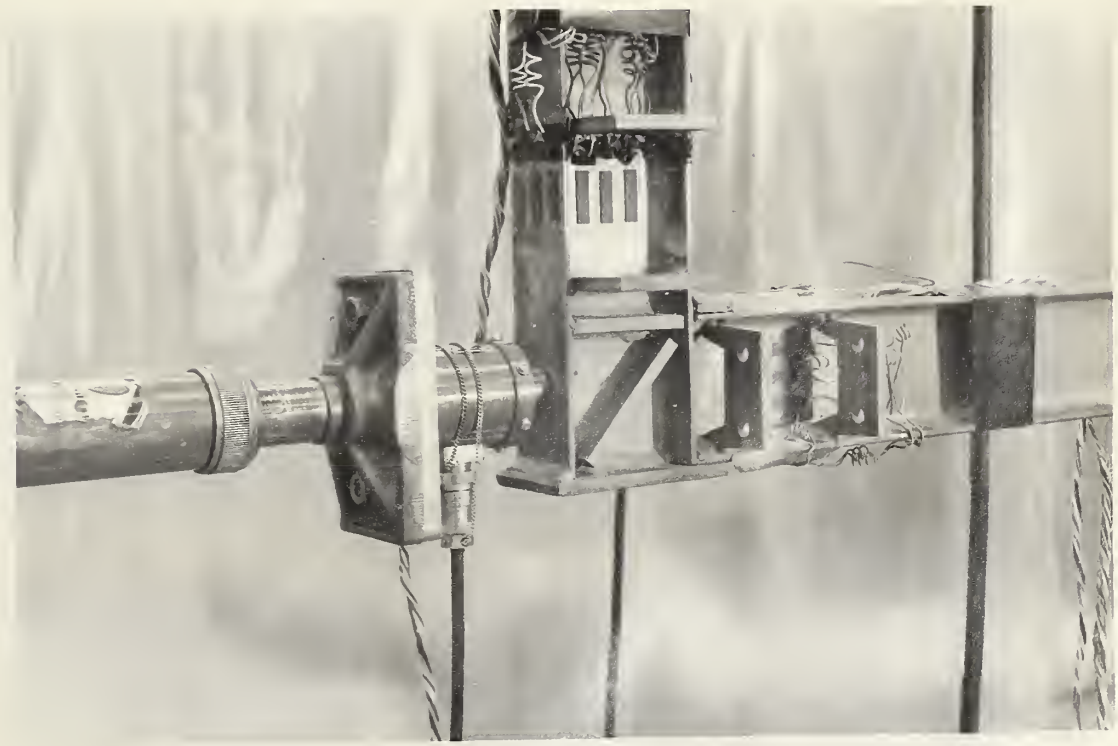

FIG. 12 – HORIZONTAL JACK WITH 5 TON LOAD CELL

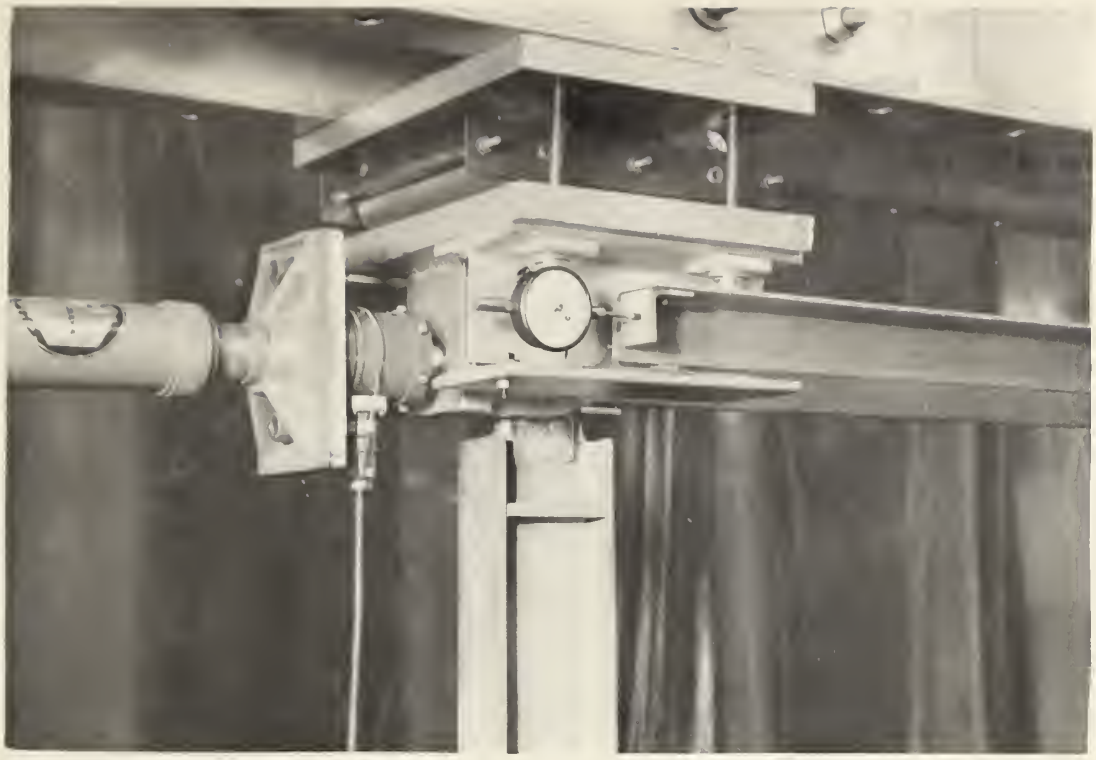

FIG. 13 – HORIZONTAL REACTION ASSEMBLY – LEFT SUPPORT

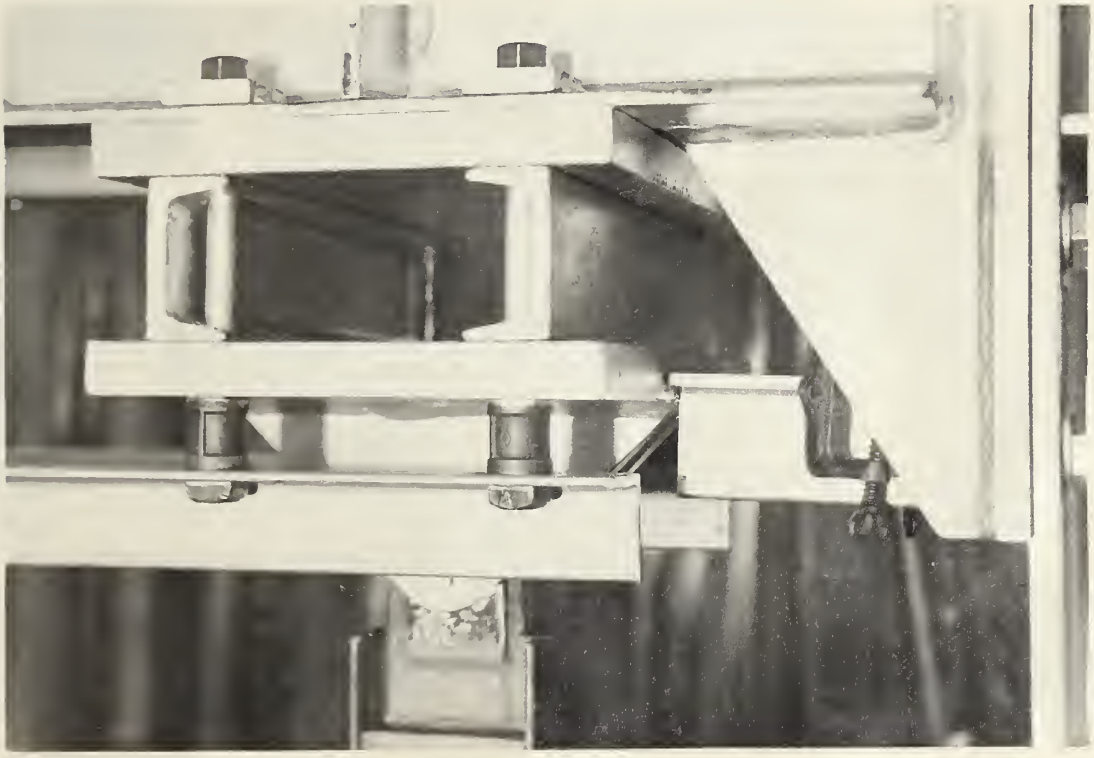

FIG. 14 – HORIZONTAL REACTION ASSEMBLY – RIGHT SUPPORT

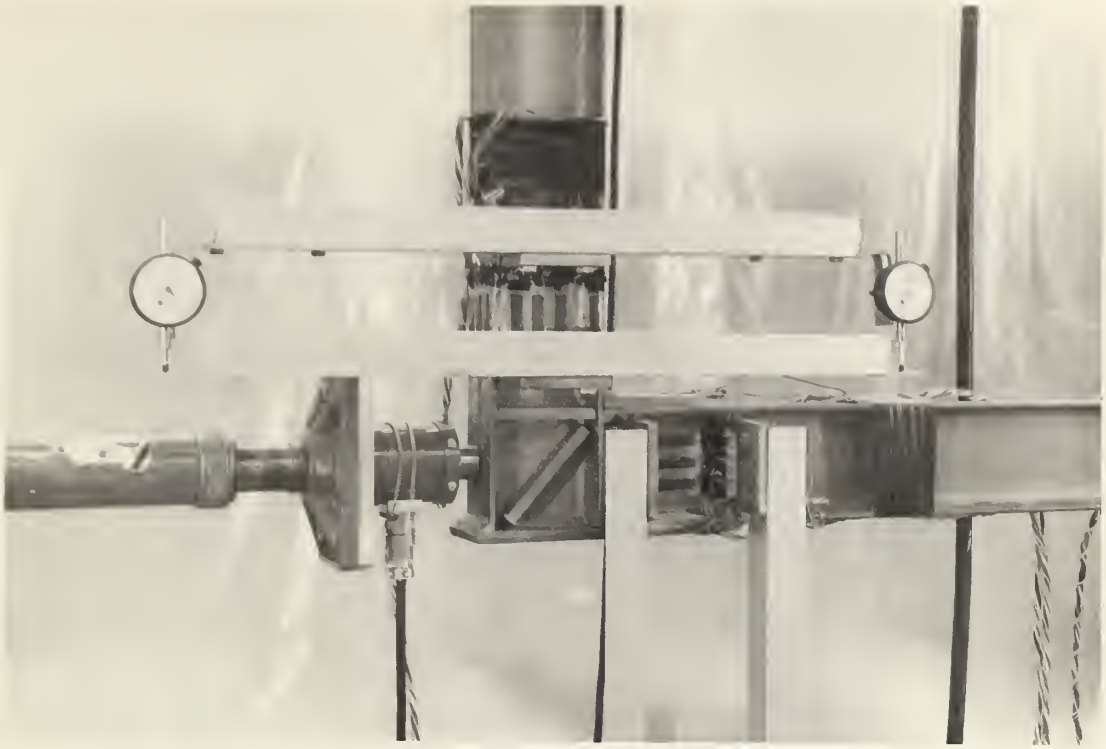

FIG. 15 – ROTATION INDICATOR APPARATUS

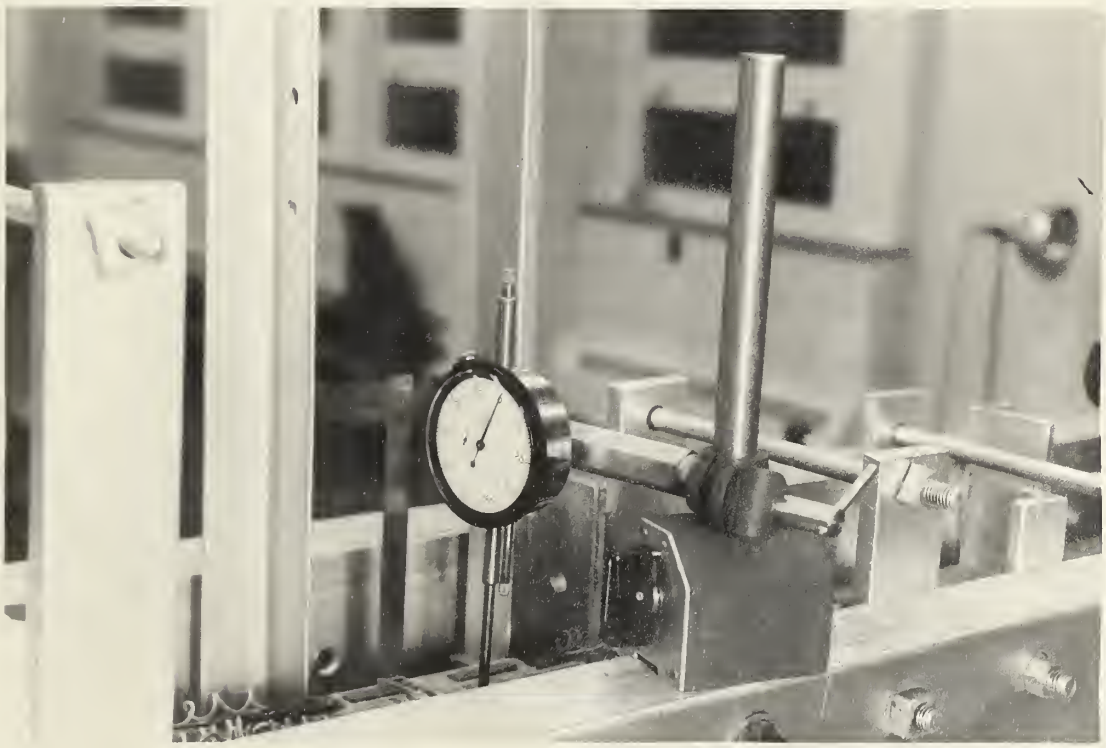

FIG. 16 – DIAL AND SCALE INSTALLATION AT BEAM MIDSPAN

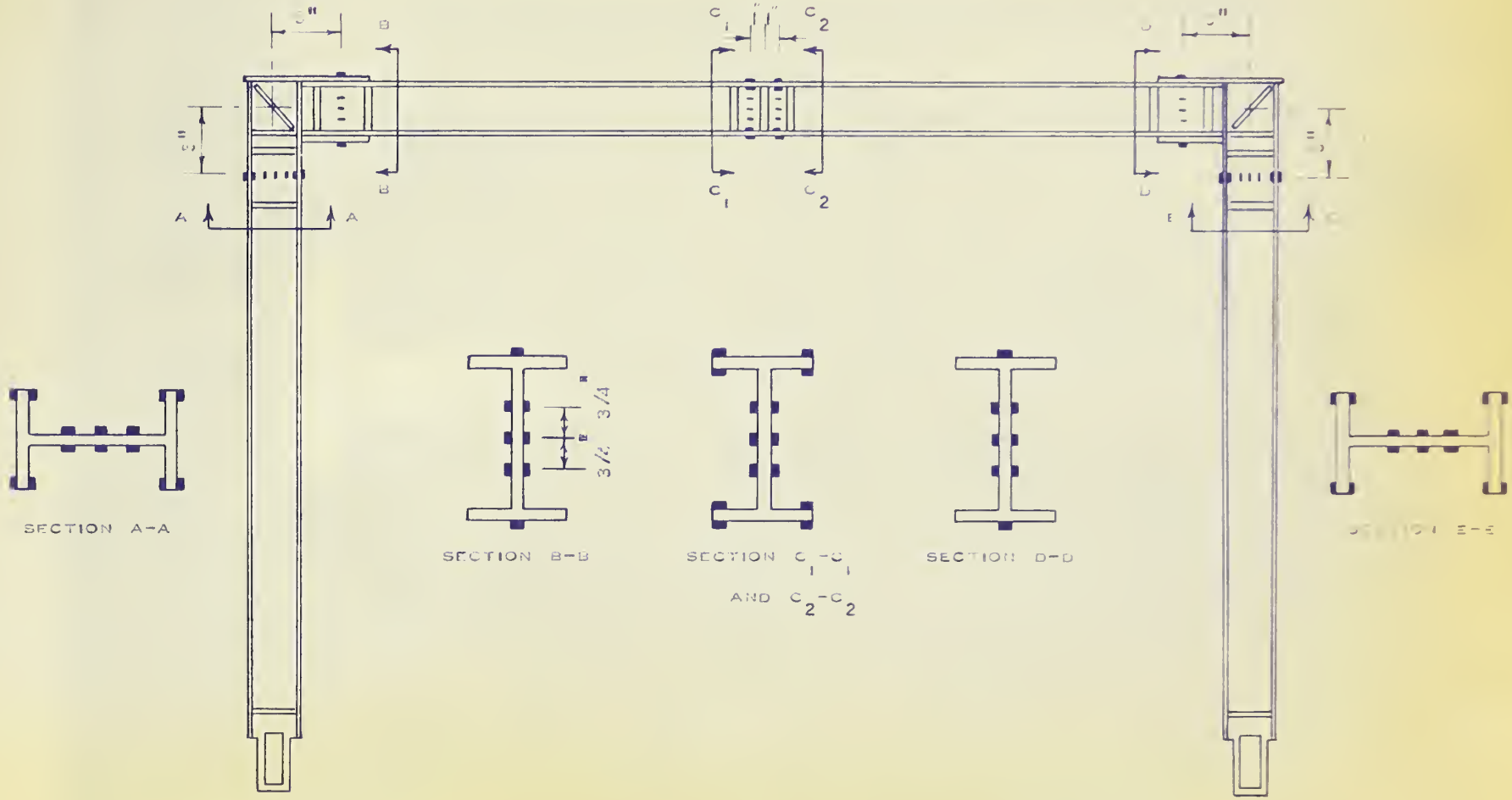

FIG. 17 – STRAIN GAUGE LOCATIONS ON FRAMES

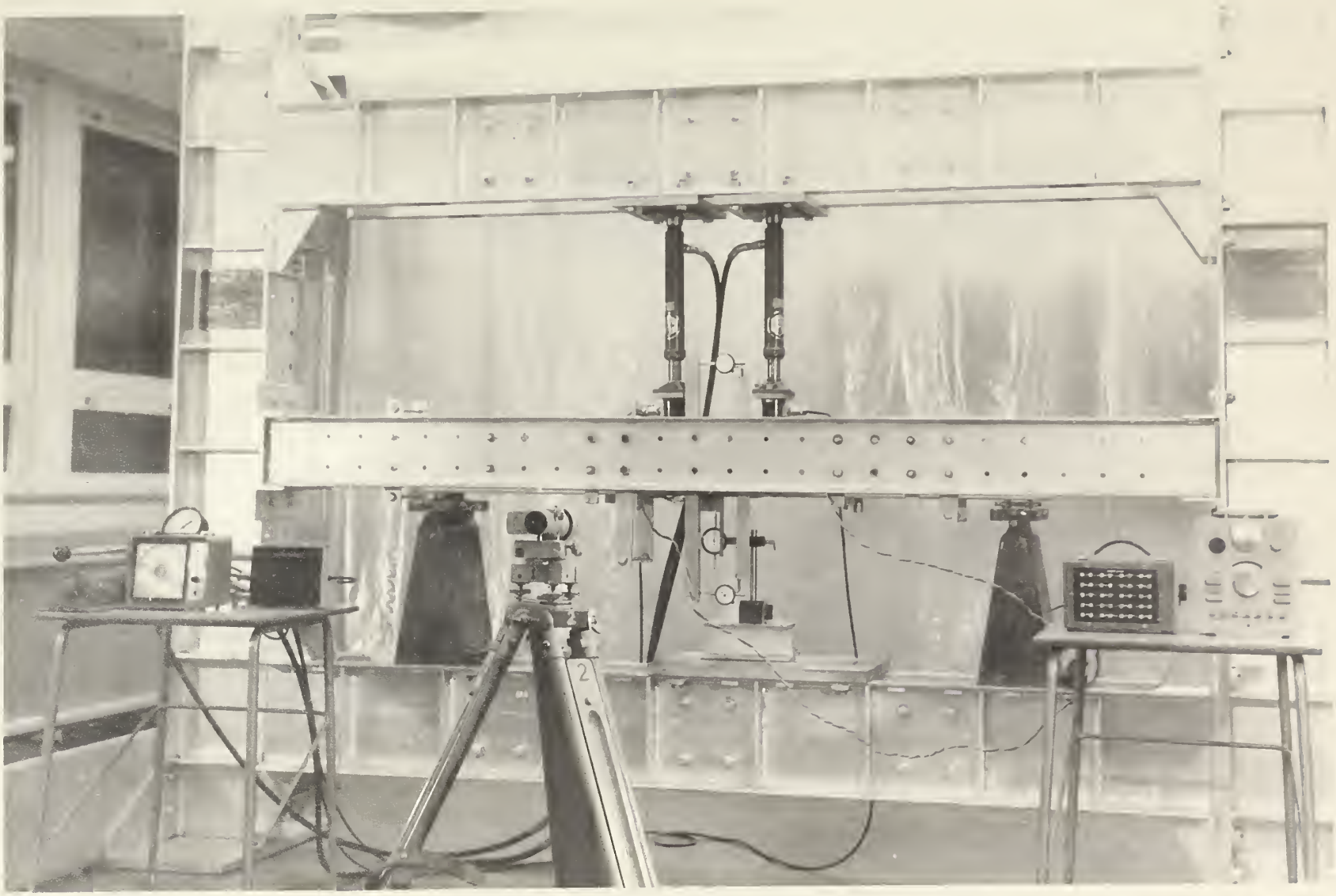

FIG. 18 – GENERAL VIEW OF BEAM TEST EQUIPMENT

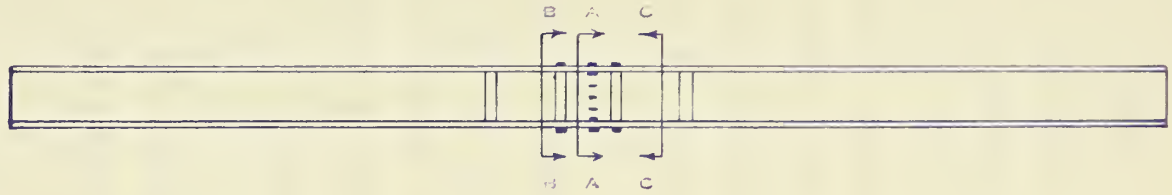

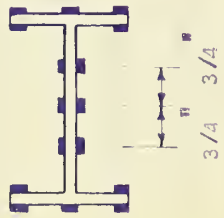

SECTION A-A

SECTION B-B & C-C

FIG. 19 — STRAIN GAUGE LOCATIONS ON BEAM

CHAPTER 6: EXPERIMENTAL PROCEDURE

6-1 Frame Test Procedure

After frame alignment was completed and before the actual test was run, a trial test was performed, the purpose of which was to give a check on the complete test set-up. Readings on all gauges were taken during a loading up to approximately one-third of the load calculated to give initial yield.

The main test was then carried out. Nine men were employed in testing Frame No. 1. Four men were employed in reading the four strain indicators at each load increment. A fifth was in charge of applying load, while the sixth man maintained the load on the horizontal reaction jack. The seventh man took the load readings from the self-balancing indicator and plotted a load vs. horizontal reaction curve. The eighth man was in charge of recording all the dial gauges on the rotation indicators. The duties of the ninth man included reading and recording the vertical and horizontal deflections by means of dial gauges and surveyor's levels. He then reduced the dial readings and plotted a load-deflection curve as the tests progressed. In testing Frame No. 2, ten men were employed, the extra man in this case being required to maintain the load on the horizontal jack.

At the beginning of each test, zero readings were taken on all dials and instruments. The loads were then applied in equal increments. These loads were read on the "Kyowa Self-Balancing Indicator", which was calibrated prior to the actual testing.

In the testing of Frame No.1, load was applied in increments of 1000 pounds up to a load of 17000 pounds, after which the load increment was reduced to 500 pounds. The test was discontinued at a load of 20,000 pounds. All dial readings, strain readings, and

deflection measurements were taken up to the 20,000 pound load. The test was discontinued at this load due to the fact that both frame legs had begun to buckle laterally. Additional lateral support was then provided for the two columns so that a larger load could be applied. Two pair of 6" channel sections, 8" long, were bolted on each side of the lateral support channel at both columns of the frame as shown in Figure 20. Plates were bolted to the flange of this small channel to prevent additional lateral buckling. After a lapse of approximately three weeks the test was continued. Strain gauge readings were not recorded for this second portion of the test. The test frame was loaded to 20,000 pounds, and then load increments of 500 pounds were applied to 23,000 pounds, at which point the test was terminated.

In testing Frame No. 2, load was applied in increments of 500 pounds on the vertical jack and 250 pounds on the horizontal jack up to a load of 11,000 pounds on the vertical jack. At this point, load was applied to the vertical and horizontal jacks in increments of 250 and 125 pounds respectively. The test was stopped at a vertical load value of 11,500 pounds, since the plunger on the horizontal jack had travelled its maximum distance. All dial readings, strain readings, and deflection measurements were taken up to this point. Load was removed and the horizontal load jack was replaced by a jack with a longer plunger travel. The next day the frame was reloaded in increments of 2000 pounds and 1000 pounds on the vertical and horizontal jacks respectively, up to a vertical load value of 10,000 pounds. Data was taken at a vertical load of 11,000 pounds and a horizontal load of 5500 pounds. Loads were then increased in increments of 250 pounds and 125 pounds on the vertical and horizontal

jacks respectively. A maximum value of 12,250 pounds for the vertical load was reached. Strain gauge readings were not taken during the second day of testing.

6-2 Beam Test Procedure

Three men were employed in testing the beam. The first man maintained the load on the jacks, while the second man read the strain indicator. The third man recorded load, deflection and rotation measurements and plotted a load-deflection curve as the test progressed.

Loads were applied in increments of 500 pounds to each jack up to value of 5500 pounds. Further information was obtained at loads of 5750, 6000, and 6100 pounds. All dial readings, strain readings, and deflection measurements were made up to and including 6100 pounds.

CHAPTER 7: MATERIAL PROPERTIES

7-1 Coupon Results

Two web coupons and two flange coupons were tested in tension to determine values of modulus of elasticity, yield point stress, and strain-hardening modulus. Figure 21 shows the dimensions of these coupons.

To determine the modulus of elasticity, stress-strain curves were plotted from data obtained from the "Baldwin Testing Machine" and from optical strain gauge equipment. These curves are shown in Figures 22 and 23. The two web specimens gave a modulus of elasticity value of 30.2×10^6 psi, while the two flange specimens gave values of 29.4×10^6 psi. An average value of 29.8×10^6 psi was used in making theoretical deflection calculations for the frames. Values of the load corresponding to the lower yield point were read from the load dial on the testing machine. The two web specimens gave lower yield point stresses of 39.3 ksi and 39.5 ksi, while the two flange specimens gave values of 38.5 ksi and 38.6 ksi. An average value of 39.0 ksi was used in computing theoretical load carrying capacities. The strain at the onset of strain-hardening was read from the graph plotted by the electric stress-strain recorder. The average value obtained for this strain was 0.0075 inches per inch. The strain-hardening modulus was also obtained from a graph plotted by the electric stress-strain recorder. The slope of the initial portion of the strain-hardening region was taken and gave values of 90 ksi and 108.5 ksi. An average value of 99.3 ksi was used.

In conducting the above tests, load was applied in 500 pound increments. Mill reports gave a yield point stress of 46.5 ksi, approximately 19 percent in excess of that calculated above.

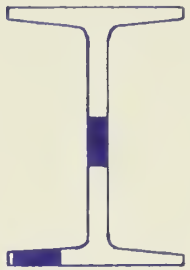

COUPON LOCATION ON CROSS SECTION

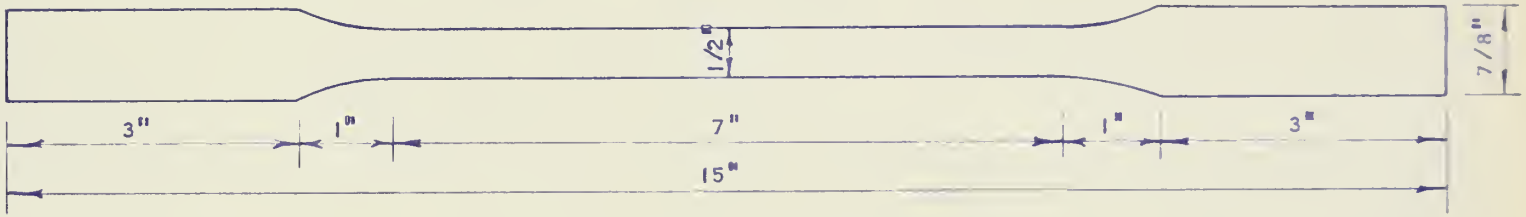

SCALE - HALF SIZE

FIG. 21 – TEST COUPON DIMENSIONS

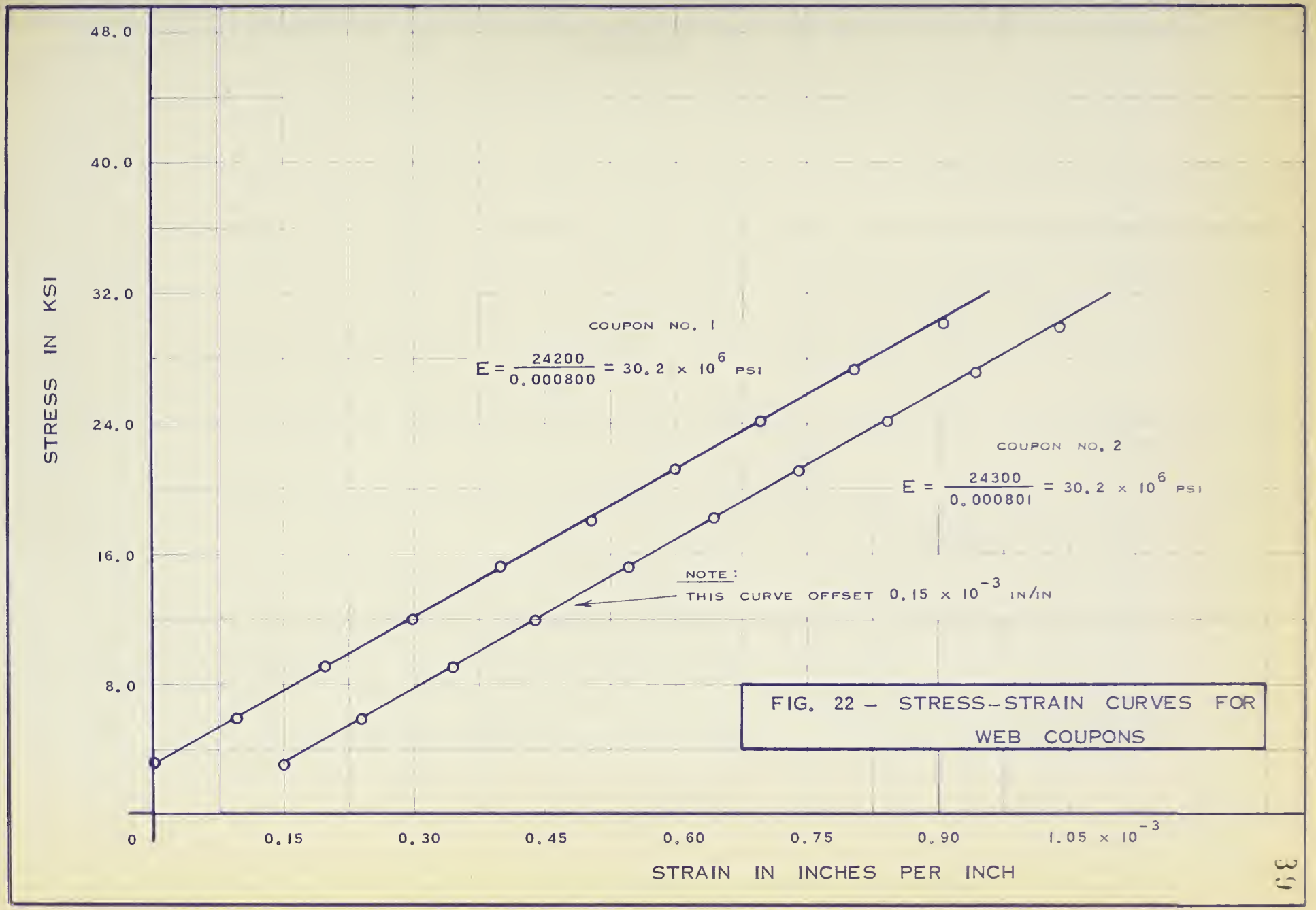

FIG. 22 – STRESS–STRAIN CURVES FOR WEB COUPONS

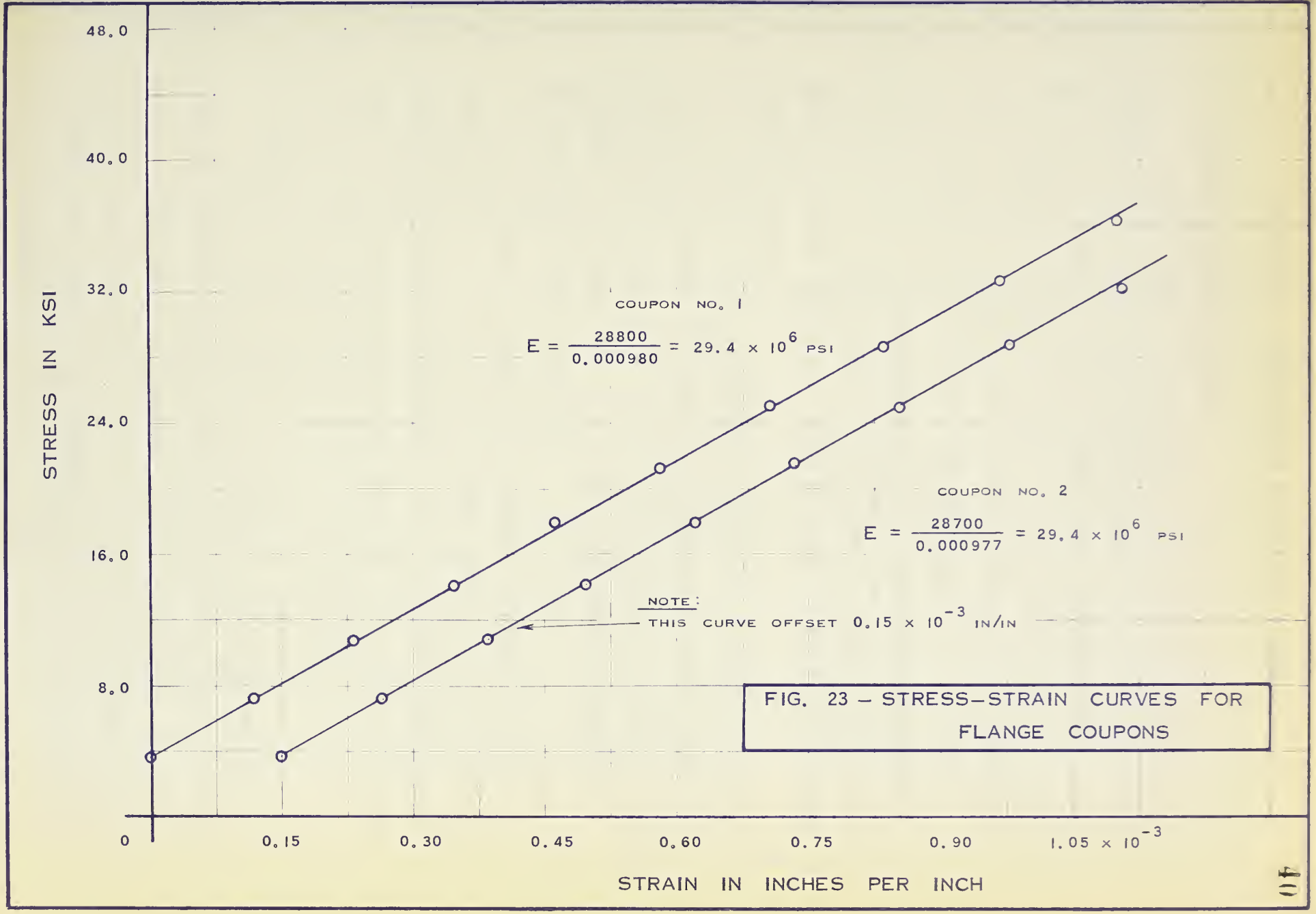

FIG. 23 – STRESS–STRAIN CURVES FOR FLANGE COUPONS

8-1 Residual Strain Measurement

A method similar to that used at Lehigh University[5,6] was adopted for the measurement of residual strains. A five foot section of 4 I 9.5, taken from the same stock as the test specimens, was used for analyzing the residual strains. A 9-inch section was cut from the center of this piece and small holes were drilled in the flanges and web of this section to properly seat gauge points. Strains were measured over an 8-inch gauge length by a "Demec Gauge" measuring to 0.0001 inch. Longitudinal saw cuts one-half inch apart straddling the gauge holes were then made. Figure 24 shows a typical layout of the sectioning process.

Where possible, readings were taken on both sides of the web and on both sides of each flange. A standard 8-inch Invar steel bar was employed throughout the test to check changes in temperature during readings. The average error in these measurements corresponds to a stress of approximately $\pm$600 psi.

Following an initial set of readings taken before the 9-inch section was cut, a second set of readings was taken when this section was cut from the five foot section. The final strains were obtained after the 9-inch section had been sawed into strips of one-half inch widths, each strip containing a pair of gauge points.

8-2 Results

Figures 25 and 26 show the distribution and magnitude of the measured residual strains. Stresses were calculated using the elastic modulus of 29.8×10^6 psi obtained from the test coupons. An average maximum value of 13,000 psi was calculated for the residual stress in the flange tips. This value is approximately one-third of the yield stress of the steel.

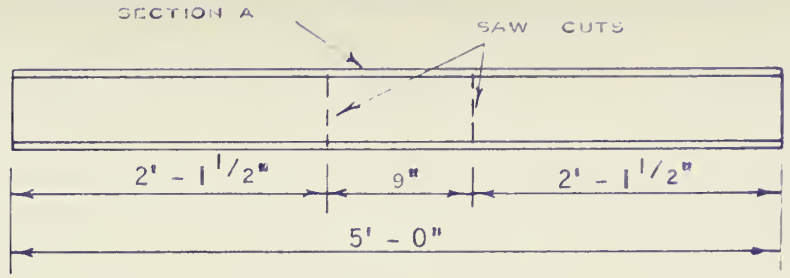

CUTTING LAYOUT

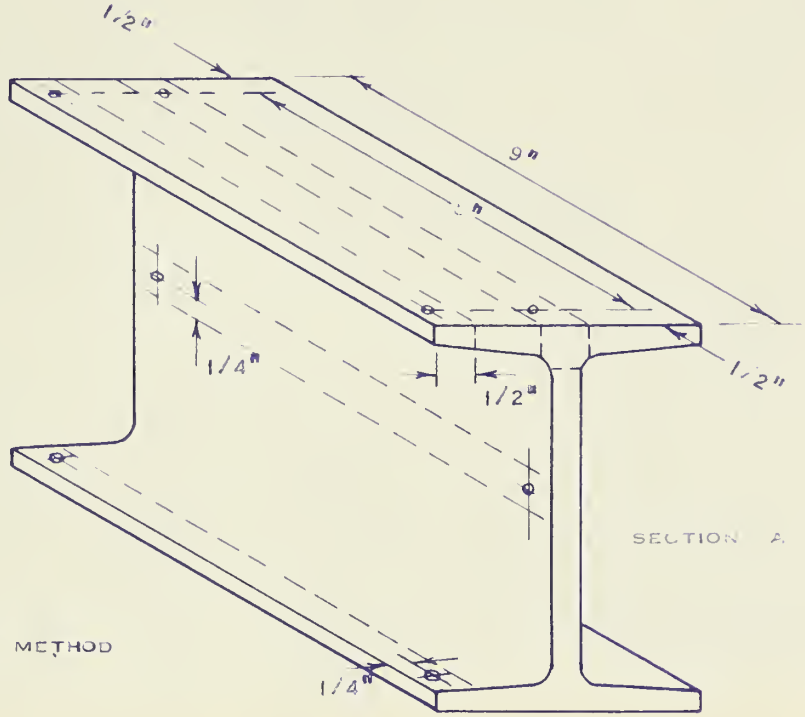

SECTIONING METHOD

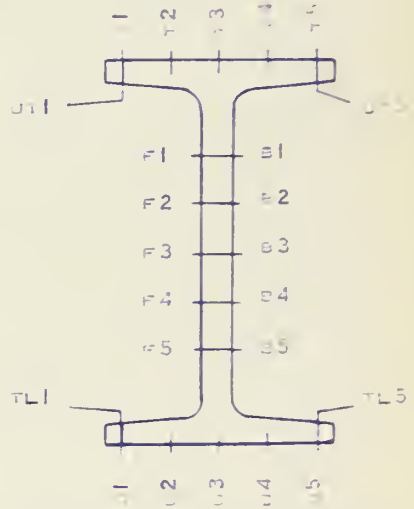

LOCATION OF GAUGE HOLES

FIG. 24 — SECTIONING METHOD FOR MEASURING RESIDUAL STRAINS

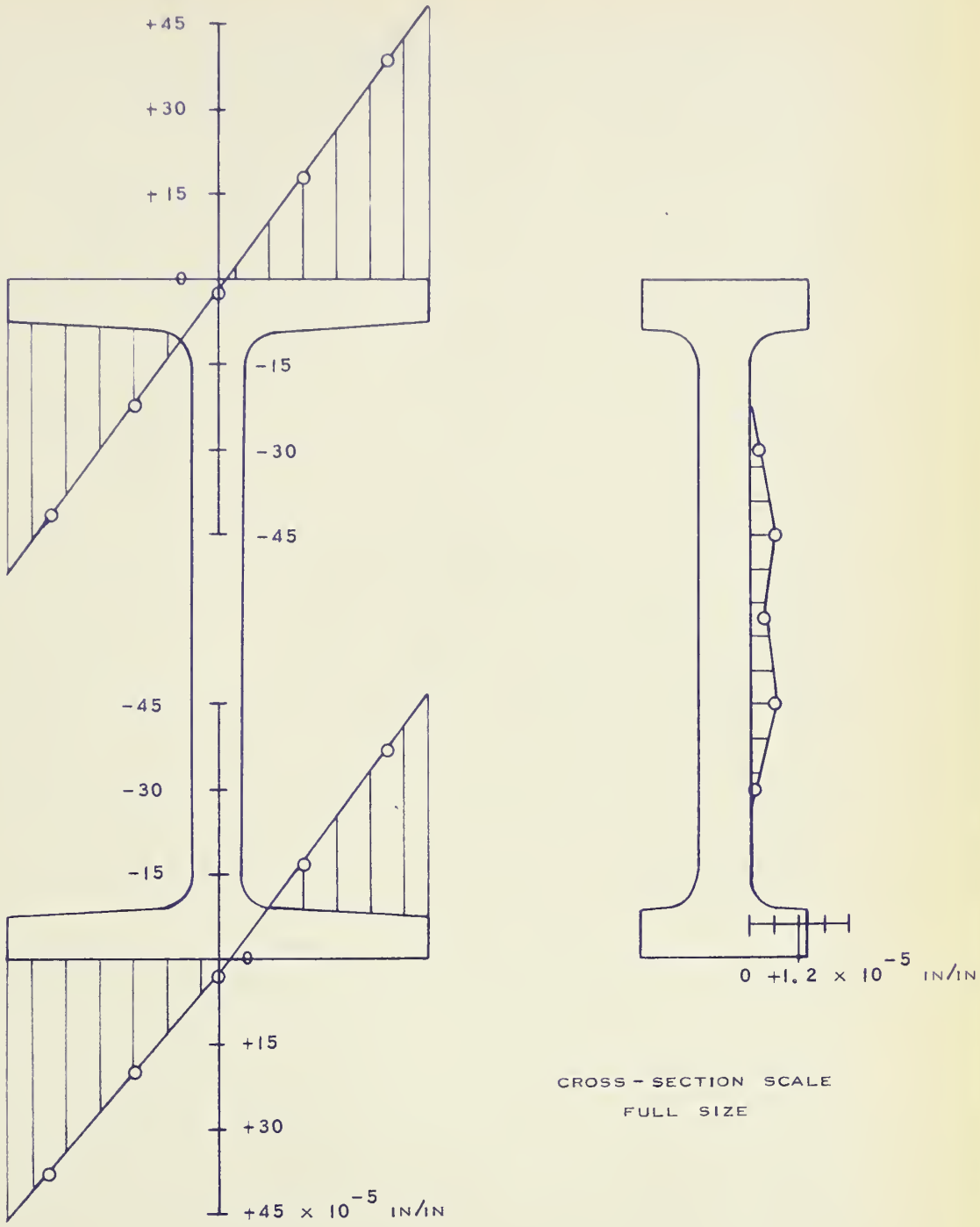

FIG. 25 – DISTRIBUTION OF RESIDUAL STRAINS AFTER INITIAL CUT

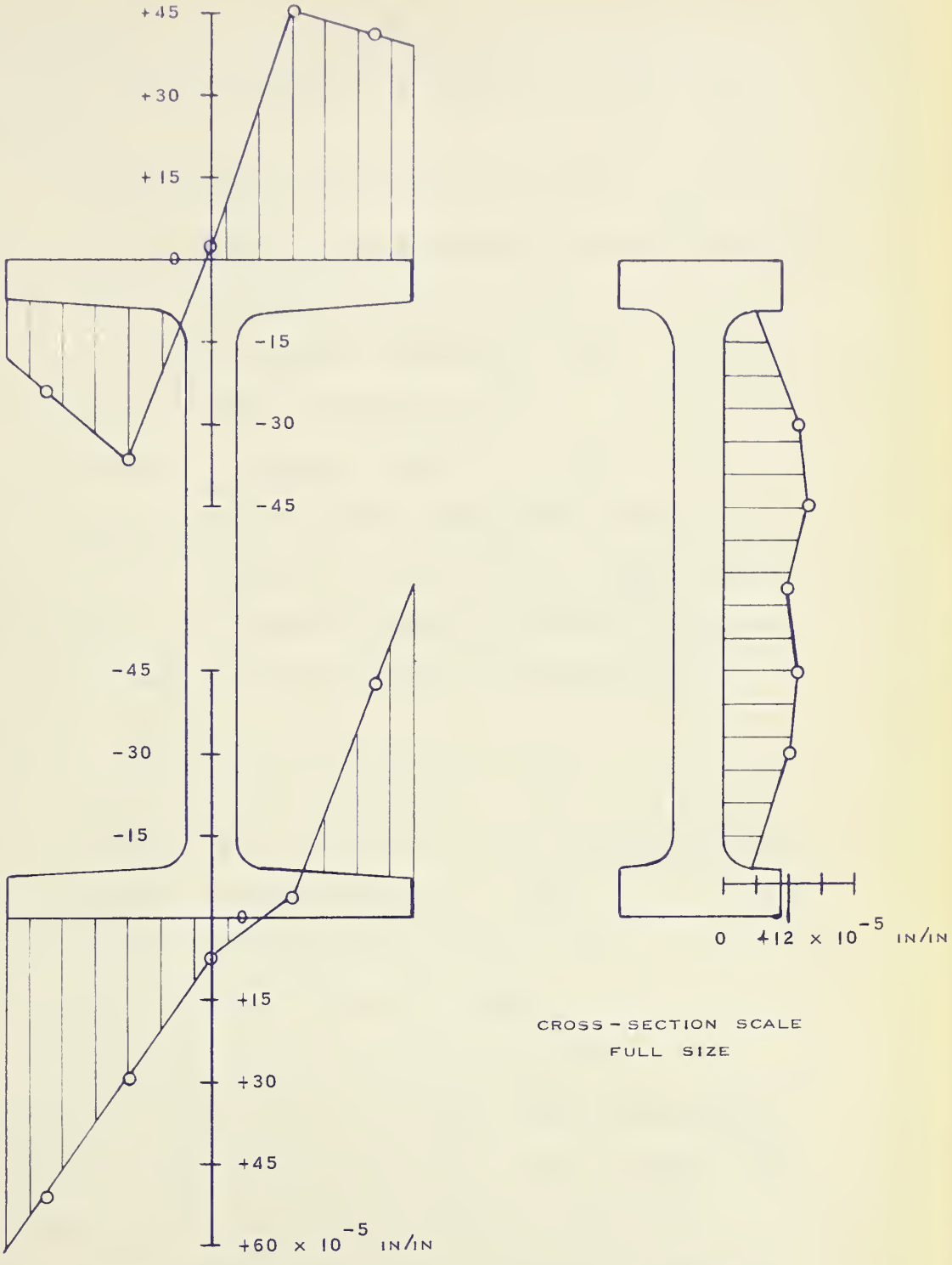

FIG. 26 – DISTRIBUTION OF RESIDUAL STRAINS AFTER FINAL SECTIONING

CHAPTER 9: TEST RESULTS

9-1 Frame Loading

Test results are presented in graphical form for Frame No.1 as follows:

1. Load vs. deflection (Figures 27 and 28).
2. Vertical load vs. left horizontal reaction (Figure 29).
3. Load vs. curvature (Figures 30 - 33).
4. Strain distributions (Figures 34 - 37).
5. Load vs. strain (Figures 38 - 41).
6. Moment vs. curvature (Figures 42 - 44).

Figure 45 shows a general view of the frame after testing, while Figures 46 - 48 show closeup views of the plastic hinges. The buckled portions of the columns are shown in Figures 49 and 50.

Test results are also presented in graphical form for Frame No. 2 as follows:

1. Load vs. deflection (Figures 51 - 53).
2. Vertical load vs. left horizontal reaction (Figure 54).
3. Load vs. curvature (Figures 55 - 57).
4. Strain distributions (Figures 58 - 60).
5. Load vs. strain (Figures 61 - 63).
6. Moment vs. curvature (Figures 64 and 65).

Figure 66 shows a general view of the frame after testing, while Figures 67 and 68 show closeup views of the plastic hinges. The buckled portion of the right column is shown in Figure 69.

The load-deflection curves were plotted using dial indicator readings wherever possible. For Frame No. 2, both vertical and horizontal deflections were plotted against load.

In addition to the observed deflections, a plot of theoretical deflections was made in each case to provide a means of comparing actual test results with those predicted by the simple plastic theory. In calculating theoretical deflections, plastic hinges were assumed to form at the corners of the line diagram, representing the center lines of the frame members. Theoretical deflections prior to the formation of the first plastic hinge were calculated using the Maxwell-Mohr equations, while deflections at ultimate load were calculated using the slope-deflection equations. These calculations appear in Appendix A.

Vertical load vs. left horizontal reaction curves are presented for both frames. Theoretical curves also are shown for comparison. These theoretical curves were plotted from the theoretical deflection and ultimate load calculations. On the basis of an elastic analysis, applied load vs. horizontal reaction was assumed to vary linearly up to the formation of the first plastic hinge. At this point the load-reaction relationship varies linearly at a different slope up to the calculated ultimate load. In Figure 54, a second curve is shown for values taken when the frame was reloaded as explained in Chapter 6.

Load-curvature curves were plotted using actual test data. These curves represent data obtained from rotation indicators located on the frame as shown in Figure 4.

The strain-distribution curves have been plotted for the SR-4 strain gauge data at certain specific loads. Each strain value plotted represents the average of two strain readings obtained from gauges placed on each side of the 4 inch I section.

Load-strain curves were plotted to indicate lateral buckling tendencies. The two strains used in each plot were those measured at both edges of the tension or compression flange.

Moment-curvature relationships were plotted for Frame No. 1 at the beam midspan and at the two columns. In Frame No. 2, moment-curvature was plotted for the beam midspan and for the leeward column only. Moments were calculated from the measured horizontal reaction at the left support. For both frames, the vertical reactions were calculated on the basis of statics. In Frame No. 2, the right horizontal reaction was calculated by taking the difference between the measured reaction and the applied horizontal force. Curvature values were calculated from the rotation indicator data by applying the equation given in Chapter 5. Theoretical moment-curvature relationships for the 4 I 9.5 section were plotted for comparison with the above curves. These calculations appear in Appendix A.

9-2 Beam Loading

Curves similar to those mentioned above were produced from the beam test data. Test results are presented in graphical form as follows:

1. Load vs. deflection (Figure 70).
2. Load vs. curvature (Figure 71).
3. Strain distributions (Figure 72).
4. Load vs. strain (Figure 73).
5. Moment vs. curvature (Figure 74).

Figure 75 shows a general view of the beam after testing, while Figure 76 shows a closeup of the plastic hinge.

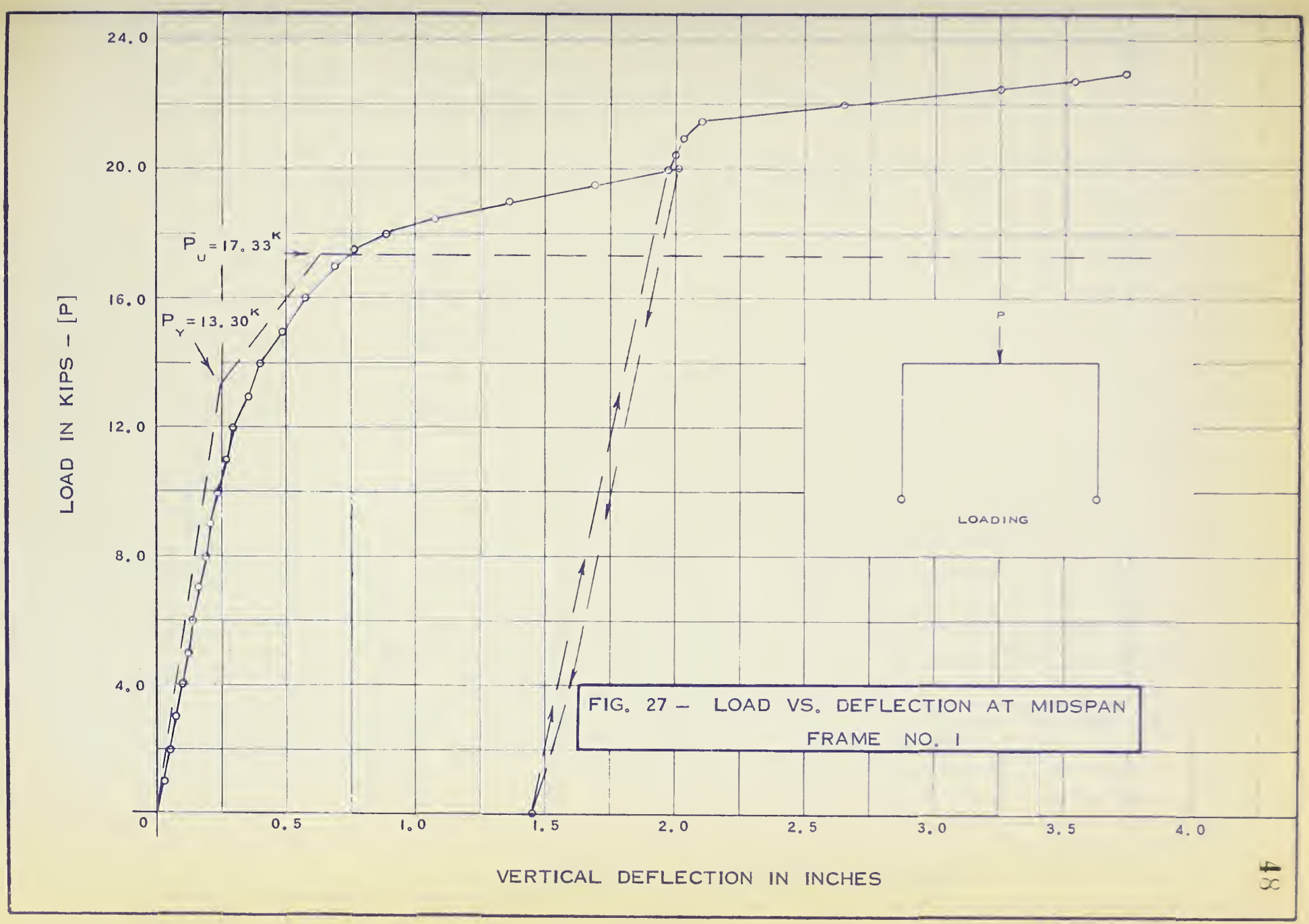

FIG. 27 – LOAD VS. DEFLECTION AT MIDSPAN
FRAME NO. 1

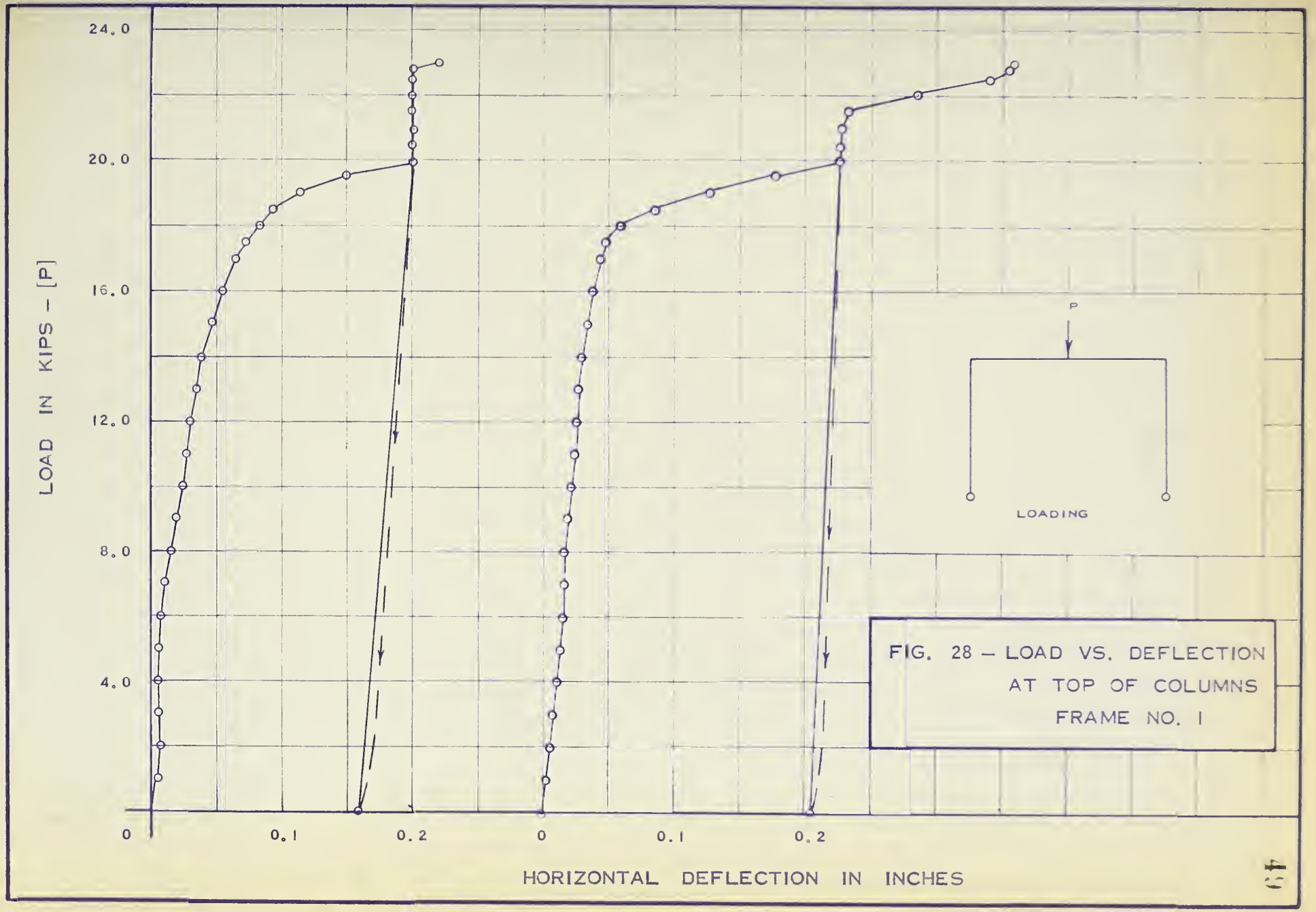

FIG. 28 – LOAD VS. DEFLECTION AT TOP OF COLUMNS FRAME NO. 1

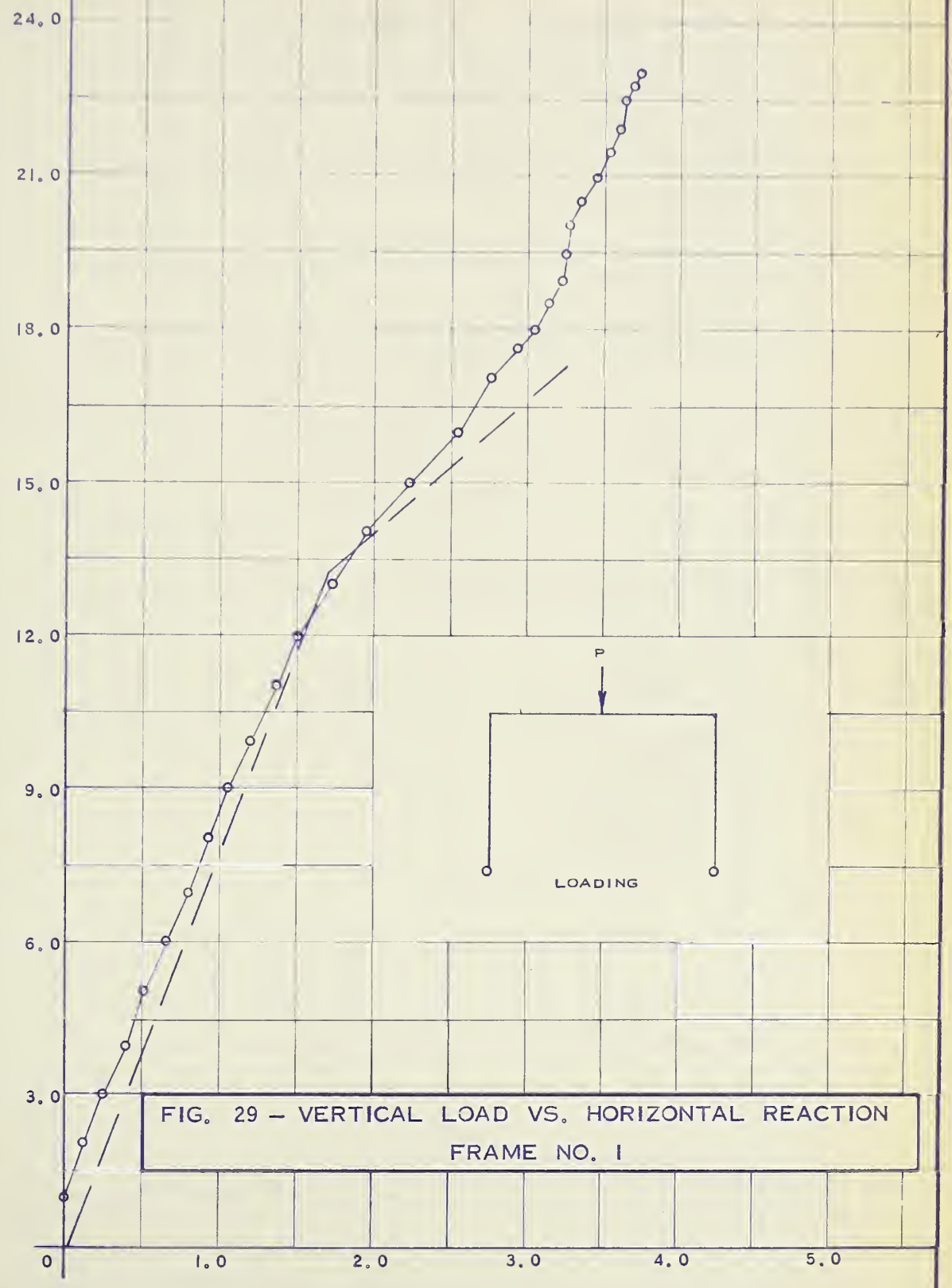

FIG. 29 – VERTICAL LOAD VS. HORIZONTAL REACTION
FRAME NO. 1

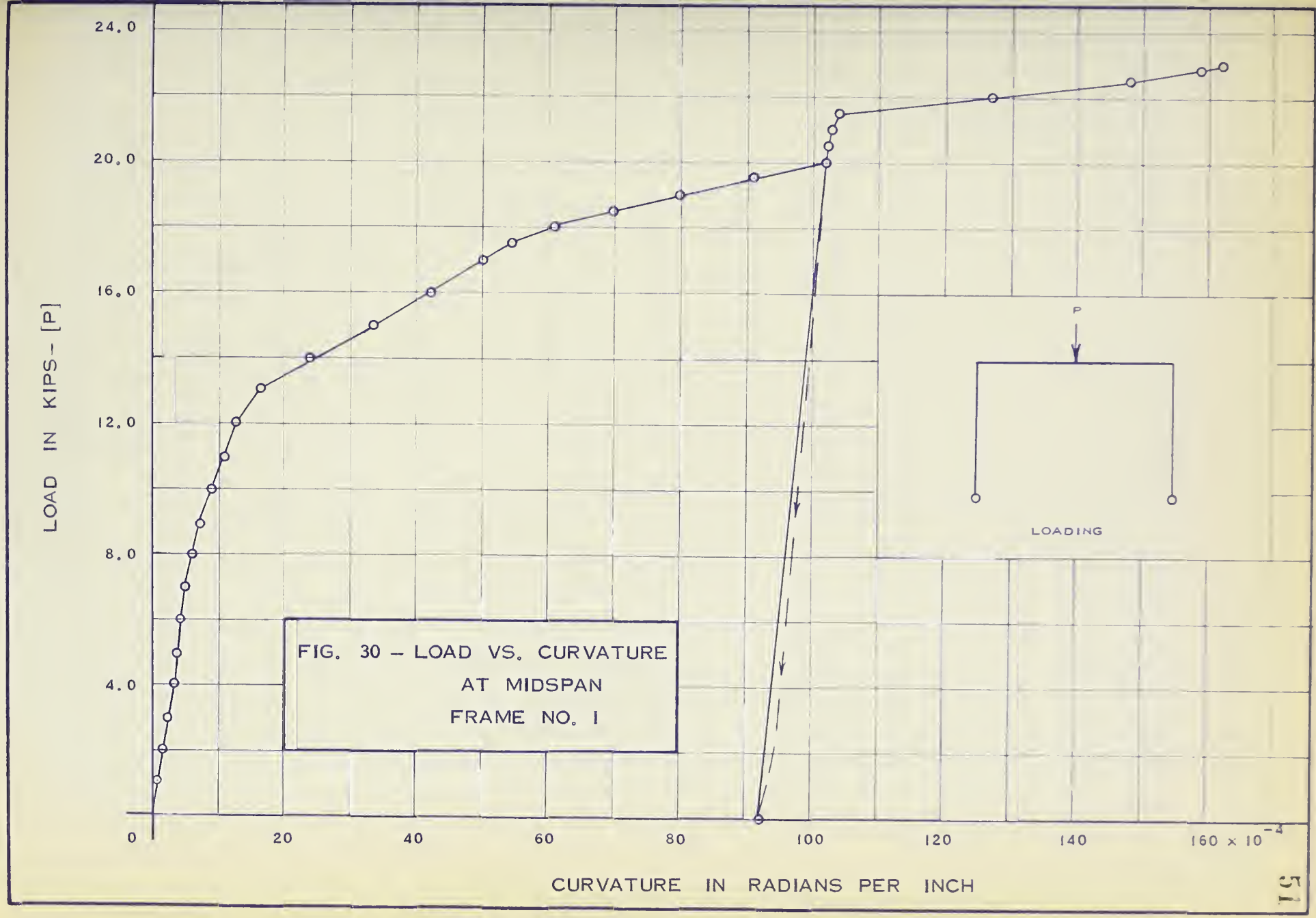
24.0
20.0
16.0
12.0
8.0
4.0
0
20
40
60
80
100
120
140
160 x 10⁻⁴
LOAD IN KIPS - [P]
CURVATURE IN RADIANS PER INCH
P
LOADING
FIG. 30 – LOAD VS. CURVATURE
AT MIDSPAN
FRAME NO. 1

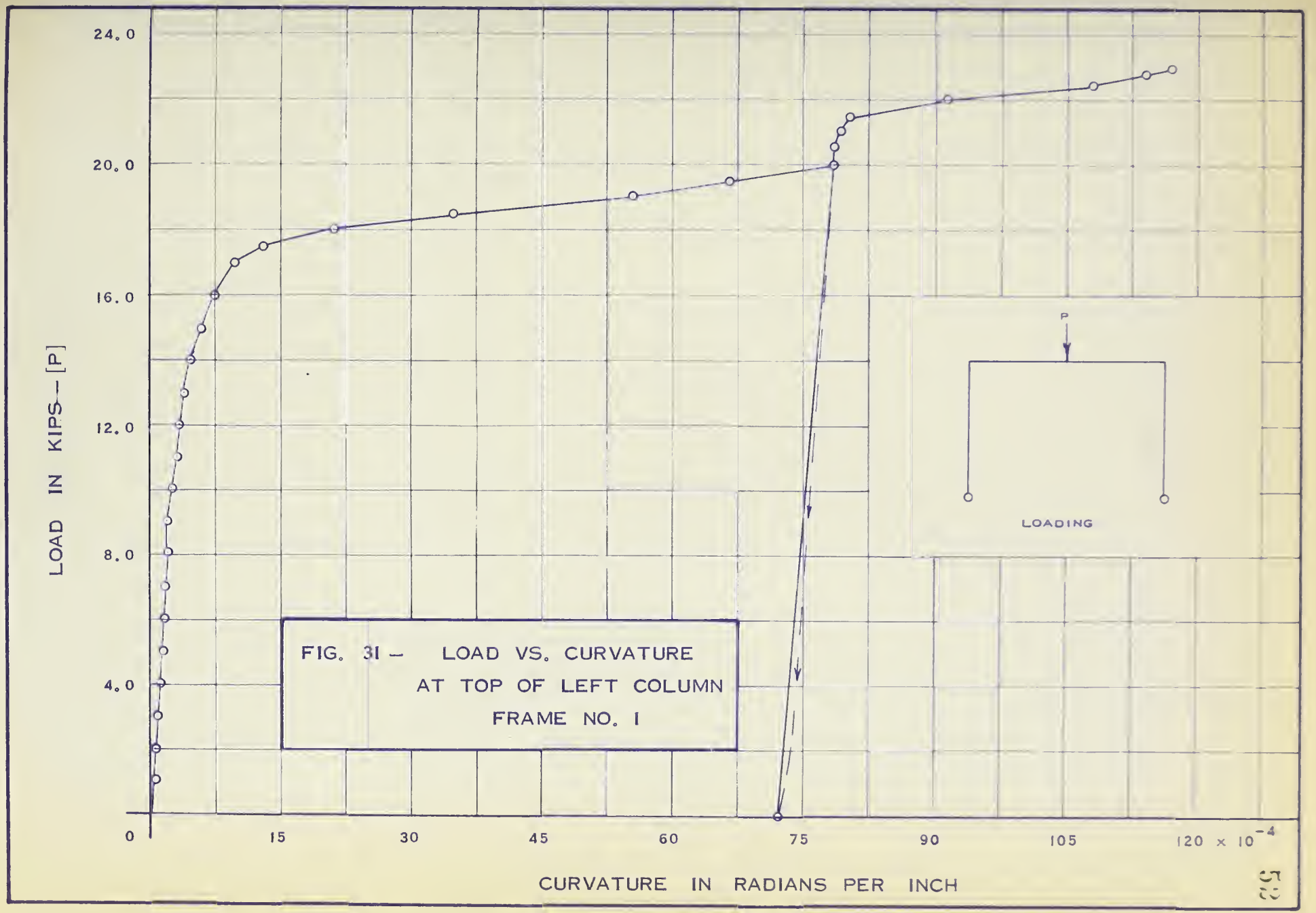

FIG. 31 — LOAD VS. CURVATURE AT TOP OF LEFT COLUMN FRAME NO. 1

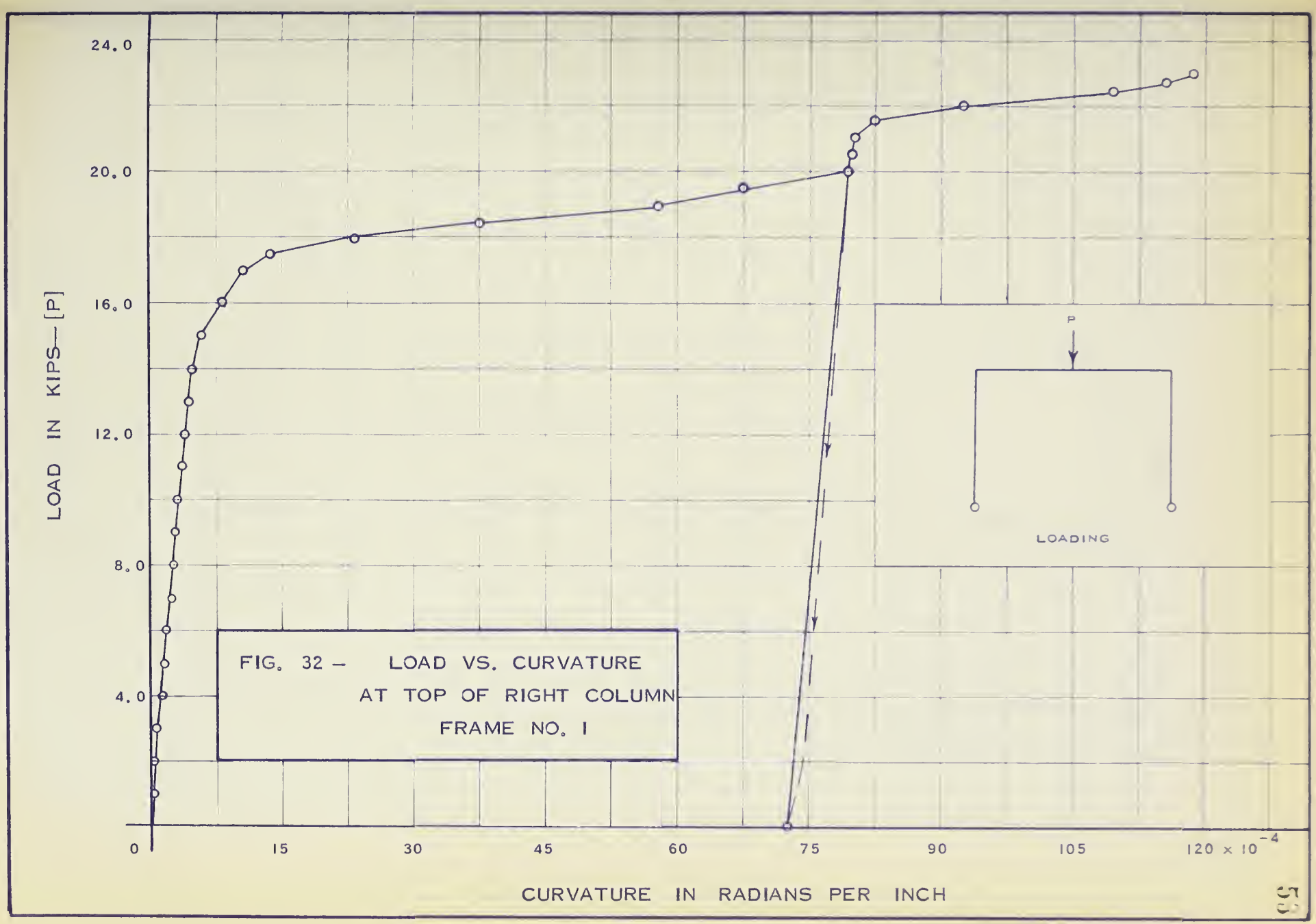

FIG. 32 — LOAD VS. CURVATURE AT TOP OF RIGHT COLUMN FRAME NO. 1

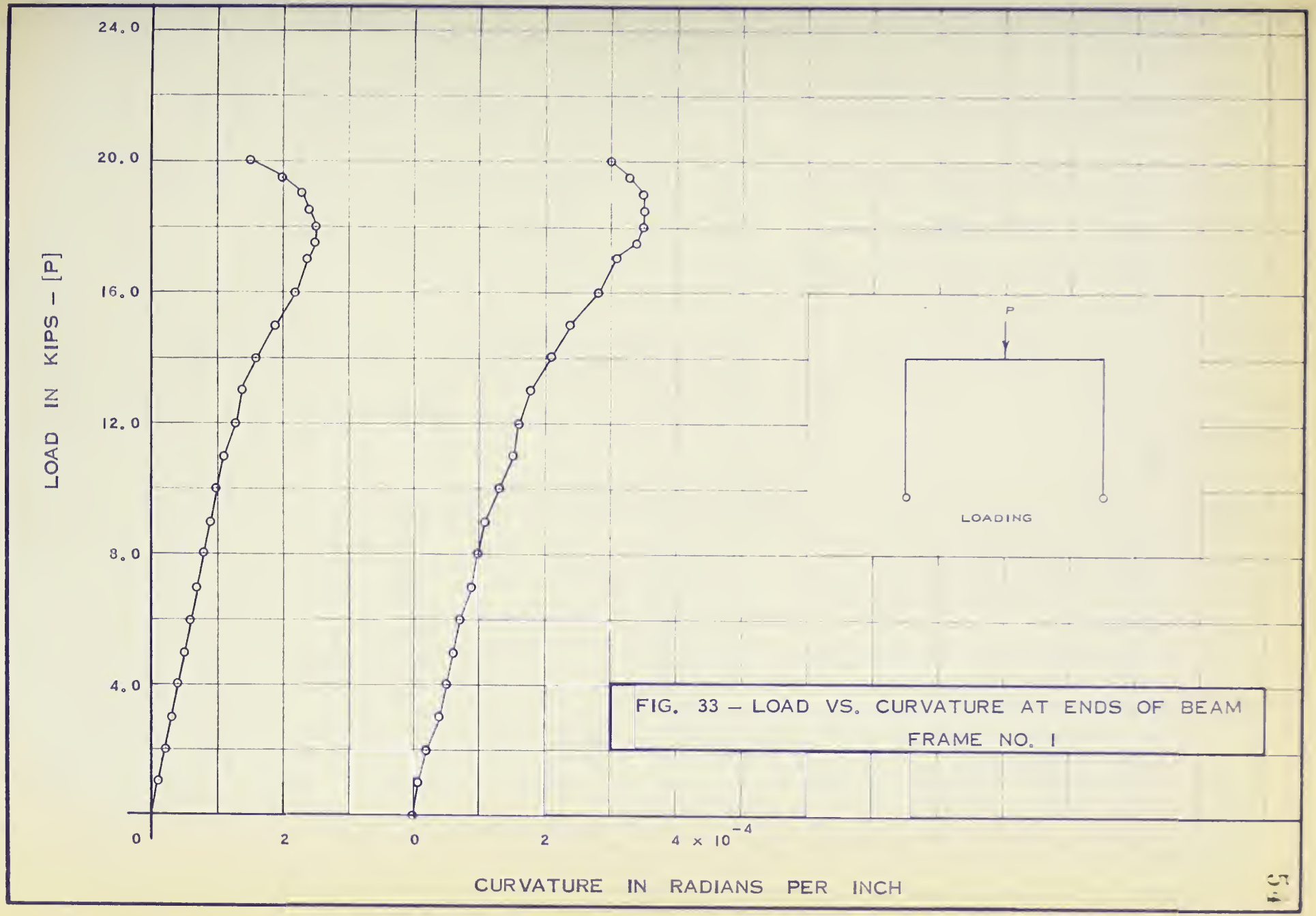

FIG. 33 – LOAD VS. CURVATURE AT ENDS OF BEAM
FRAME NO. 1

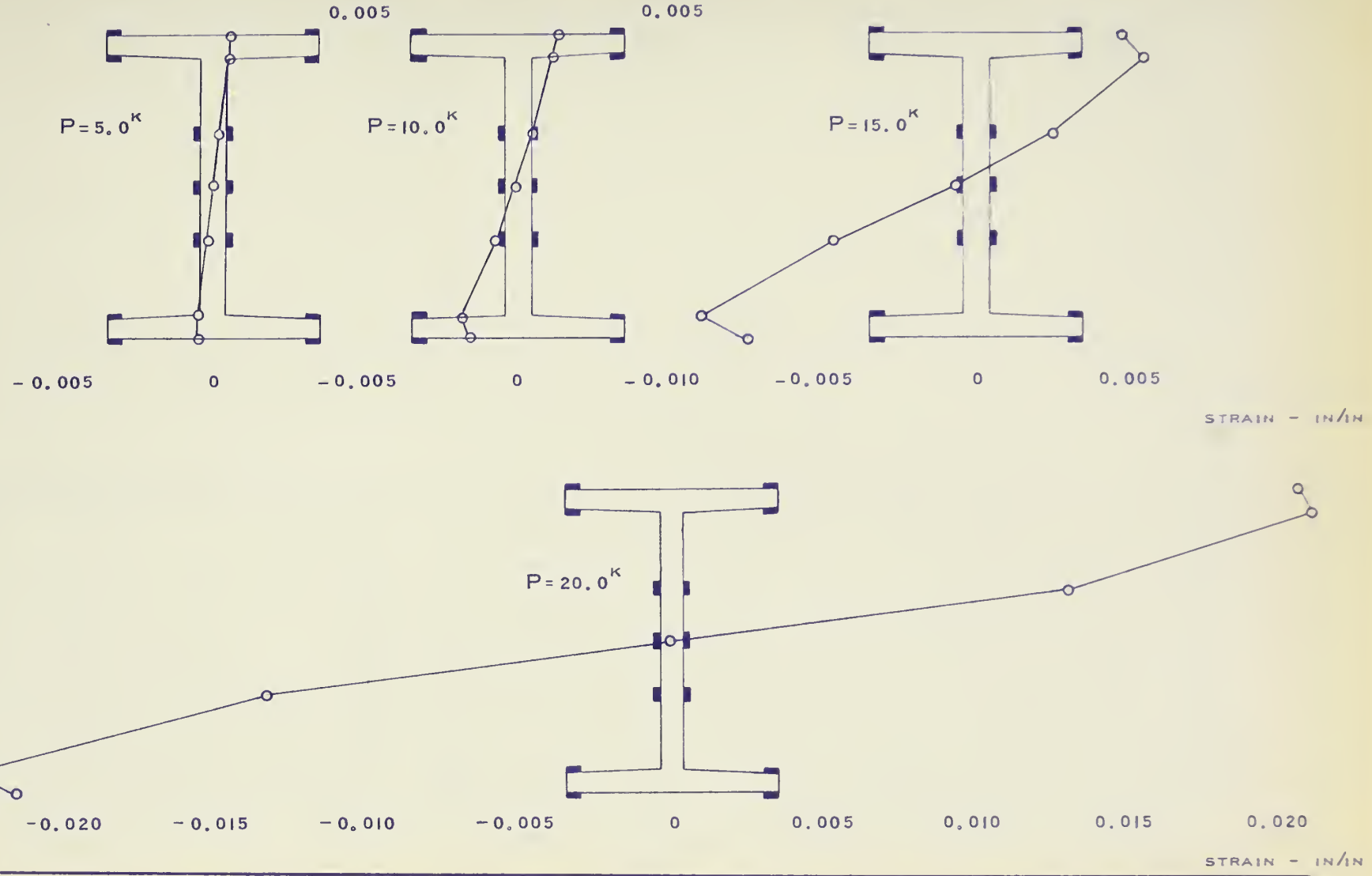

FIG. 34 – STRAIN DISTRIBUTION AT MIDSPAN – STRAINS MEASURED TO LEFT OF STIFFENER FRAME NO. 1

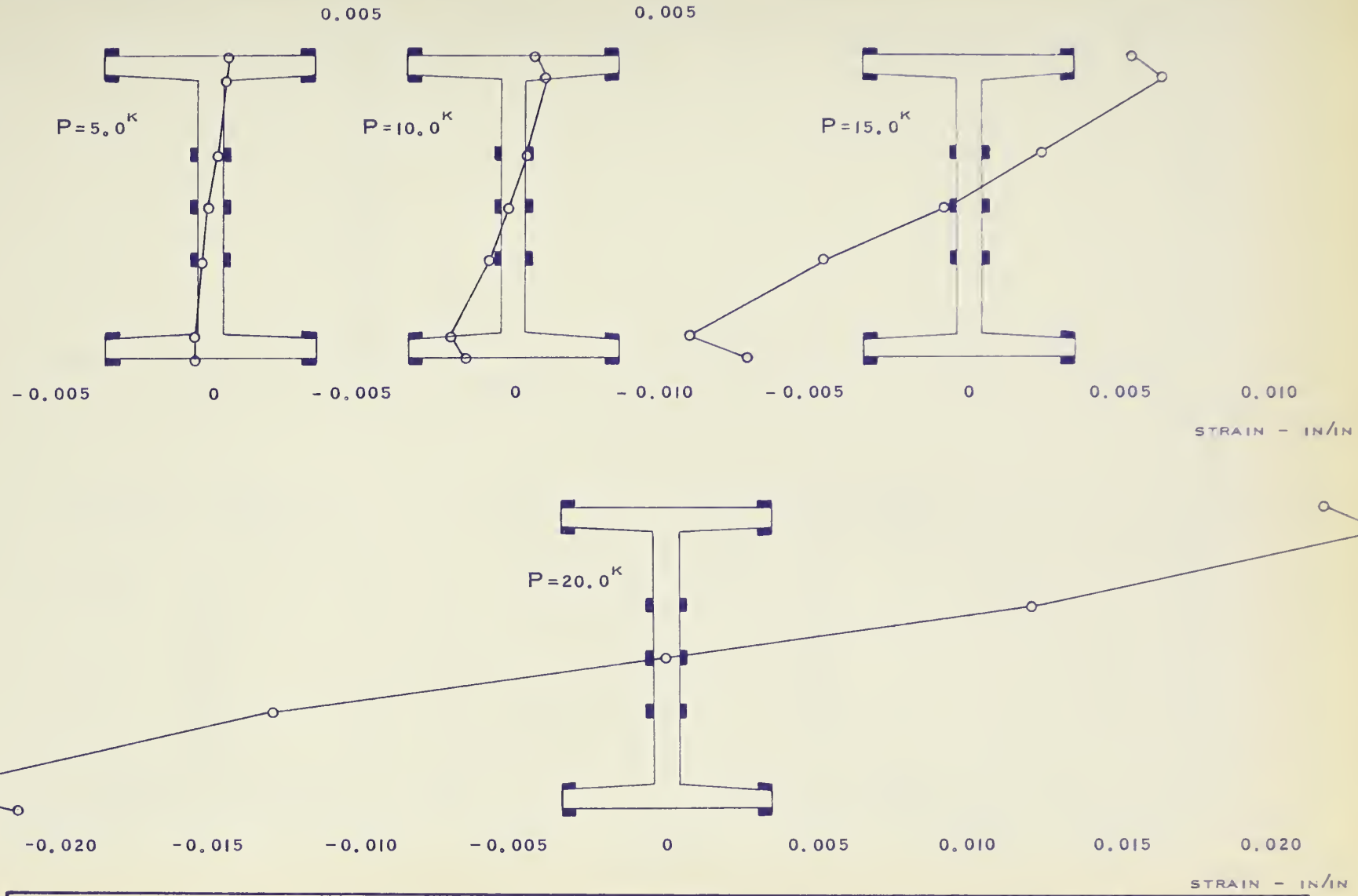

FIG. 35 – STRAIN DISTRIBUTION AT MIDSPAN – STRAINS MEASURED TO RIGHT OF STIFFENER FRAME NO. 1

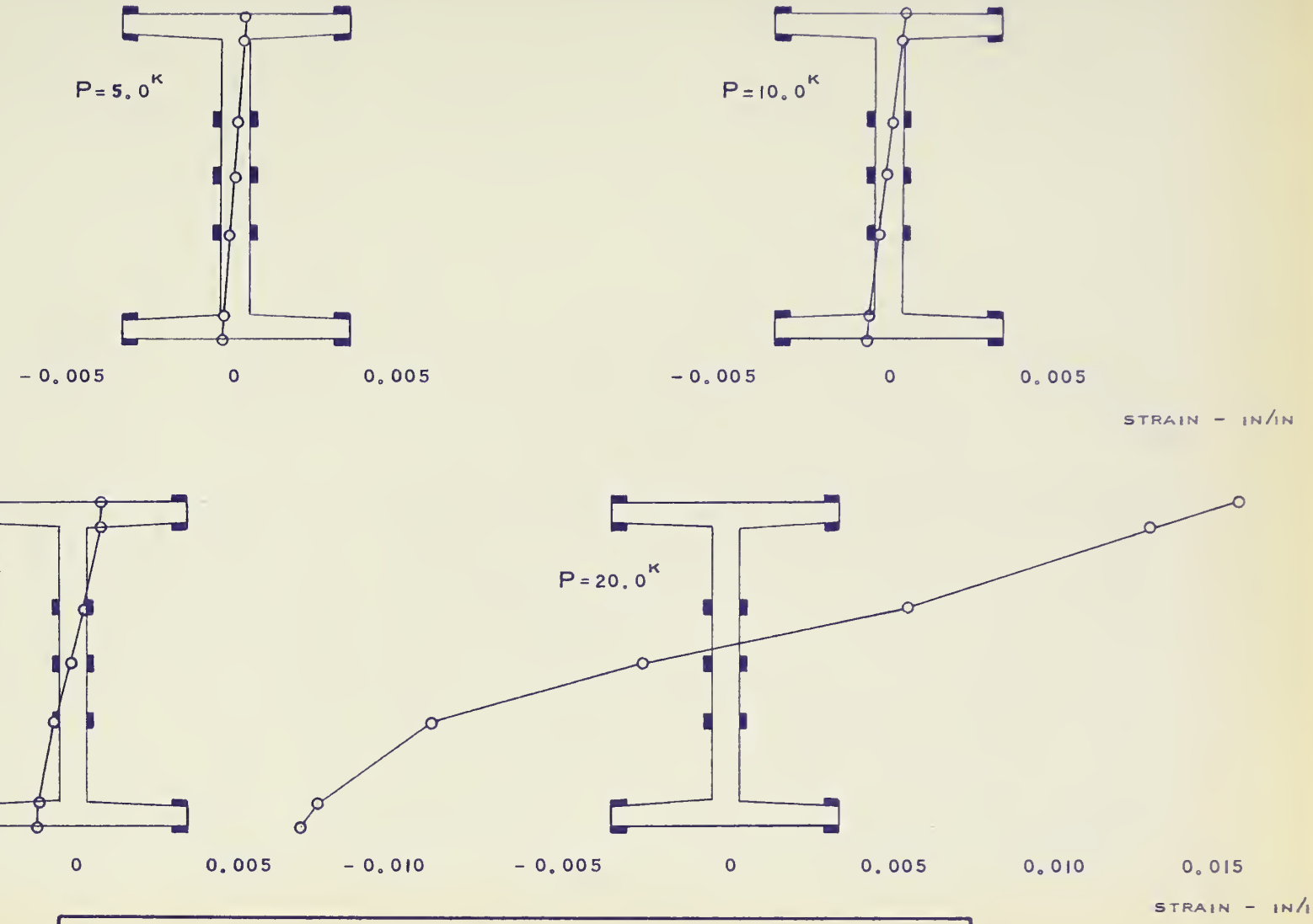

FIG. 36 — STRAIN DISTRIBUTION AT TOP OF LEFT COLUMN
FRAME NO. 1

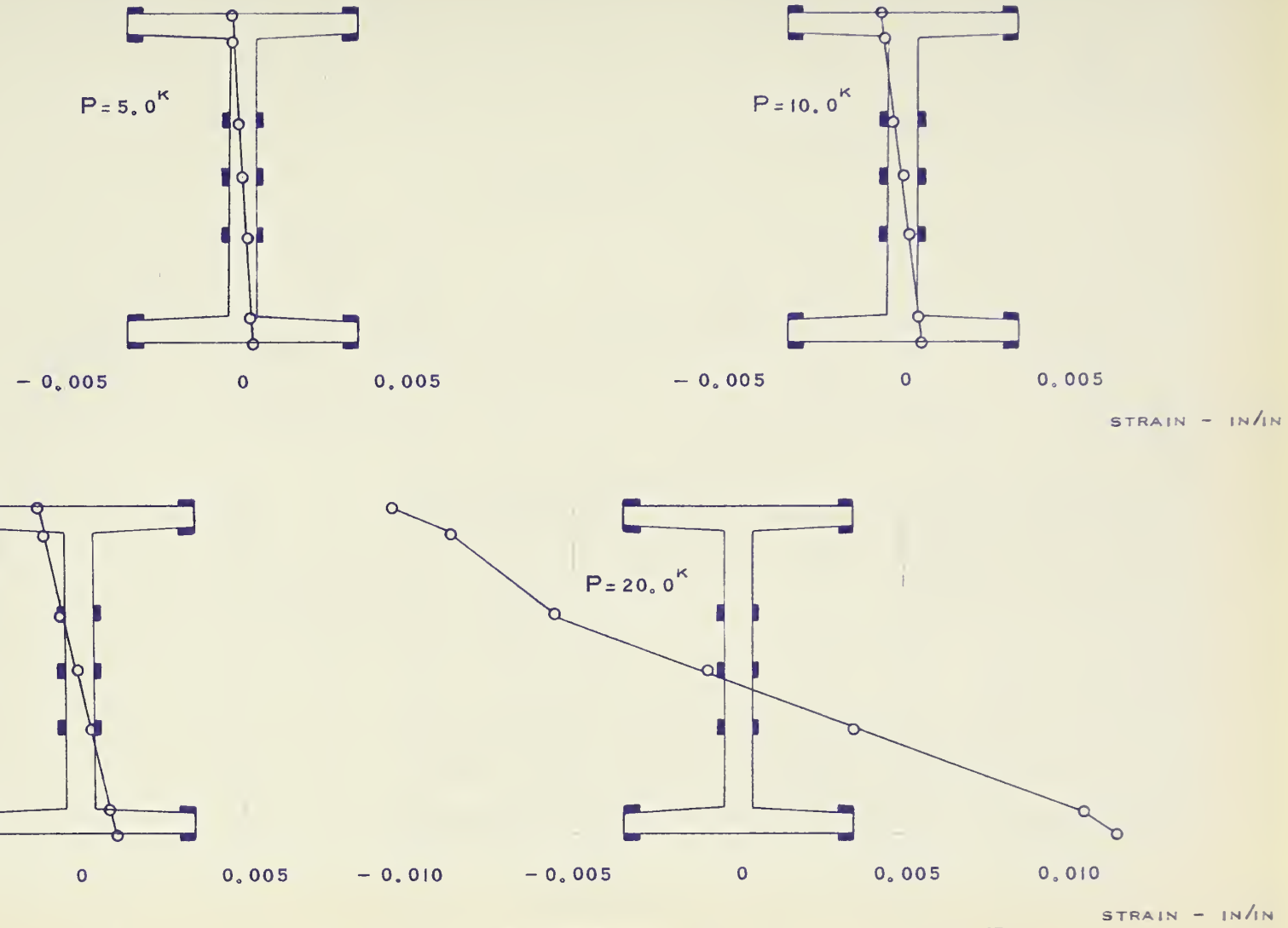

FIG. 37 – STRAIN DISTRIBUTION AT TOP OF RIGHT COLUMN
FRAME NO. 1

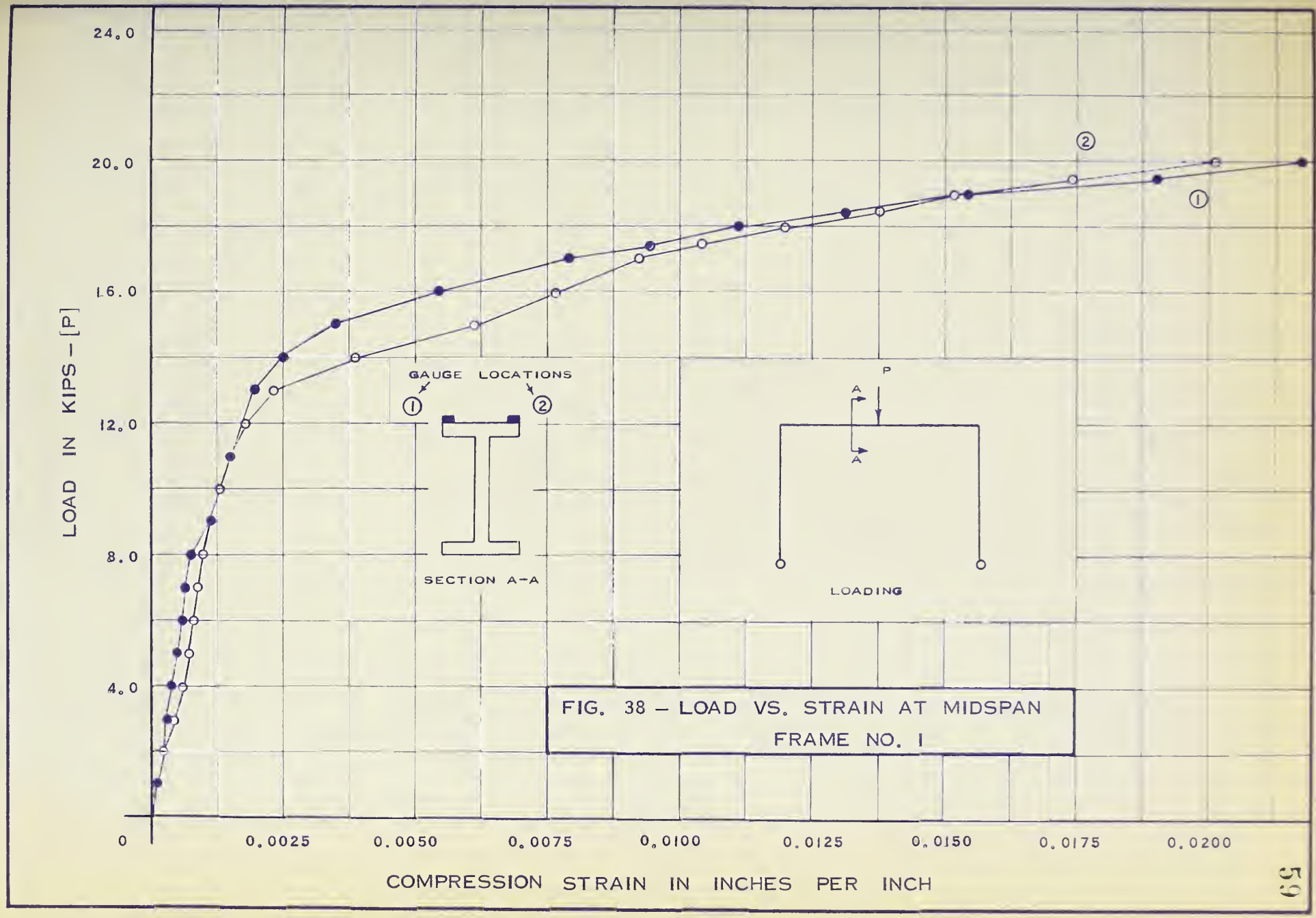

FIG. 38 – LOAD VS. STRAIN AT MIDSPAN
FRAME NO. 1

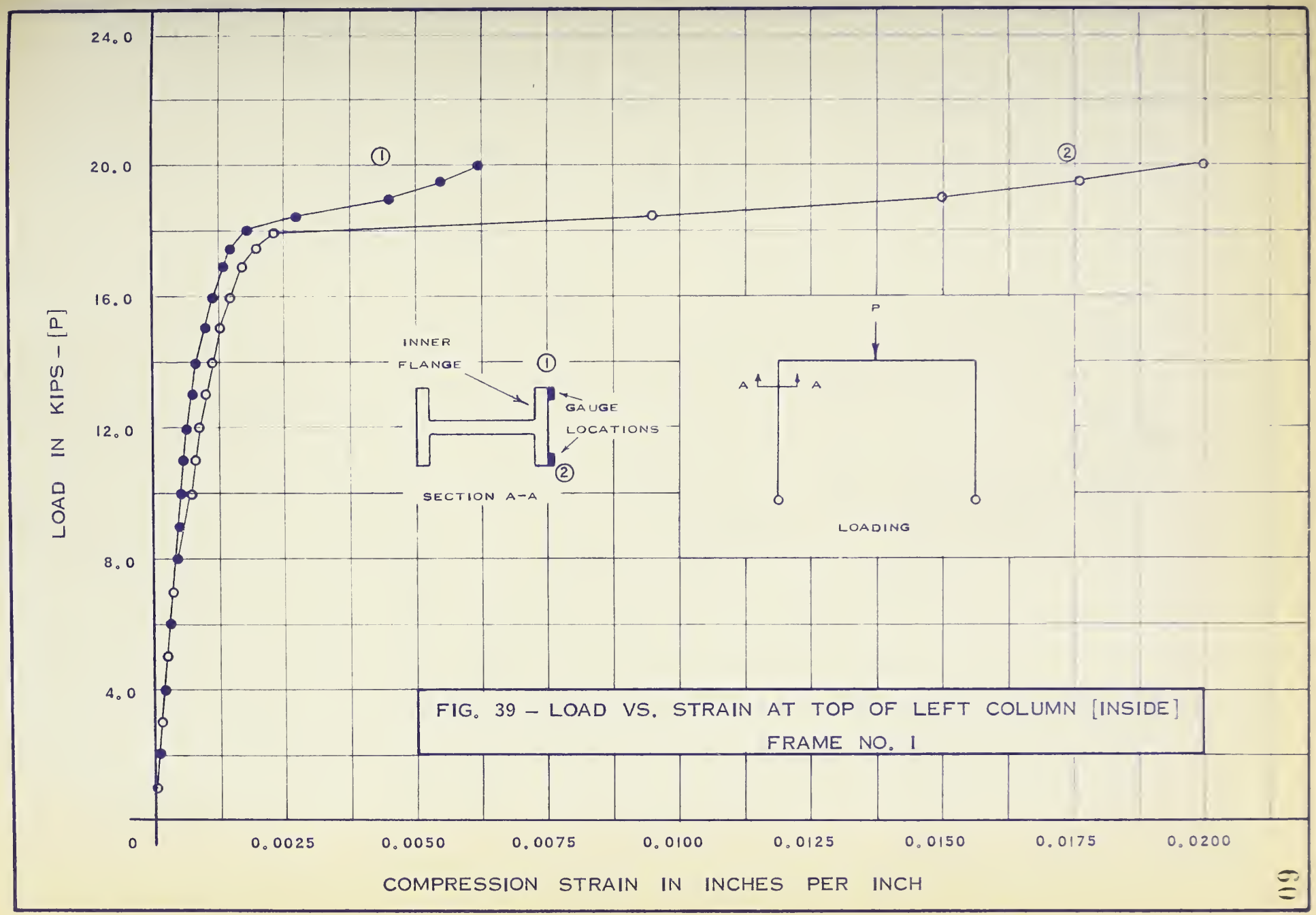

FIG. 39 – LOAD VS. STRAIN AT TOP OF LEFT COLUMN [INSIDE]
FRAME NO. 1

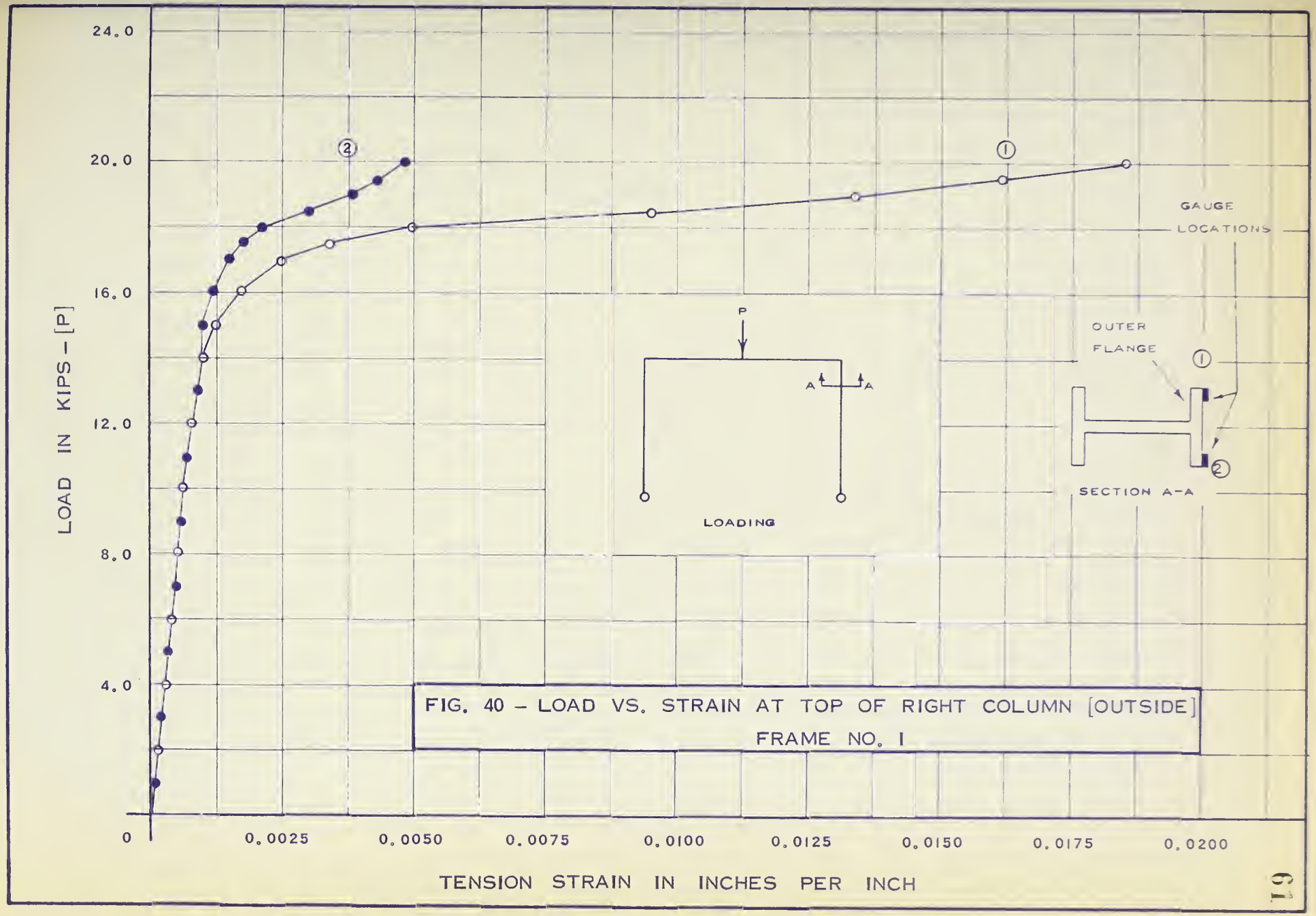

FIG. 40 – LOAD VS. STRAIN AT TOP OF RIGHT COLUMN [OUTSIDE]
FRAME NO. 1

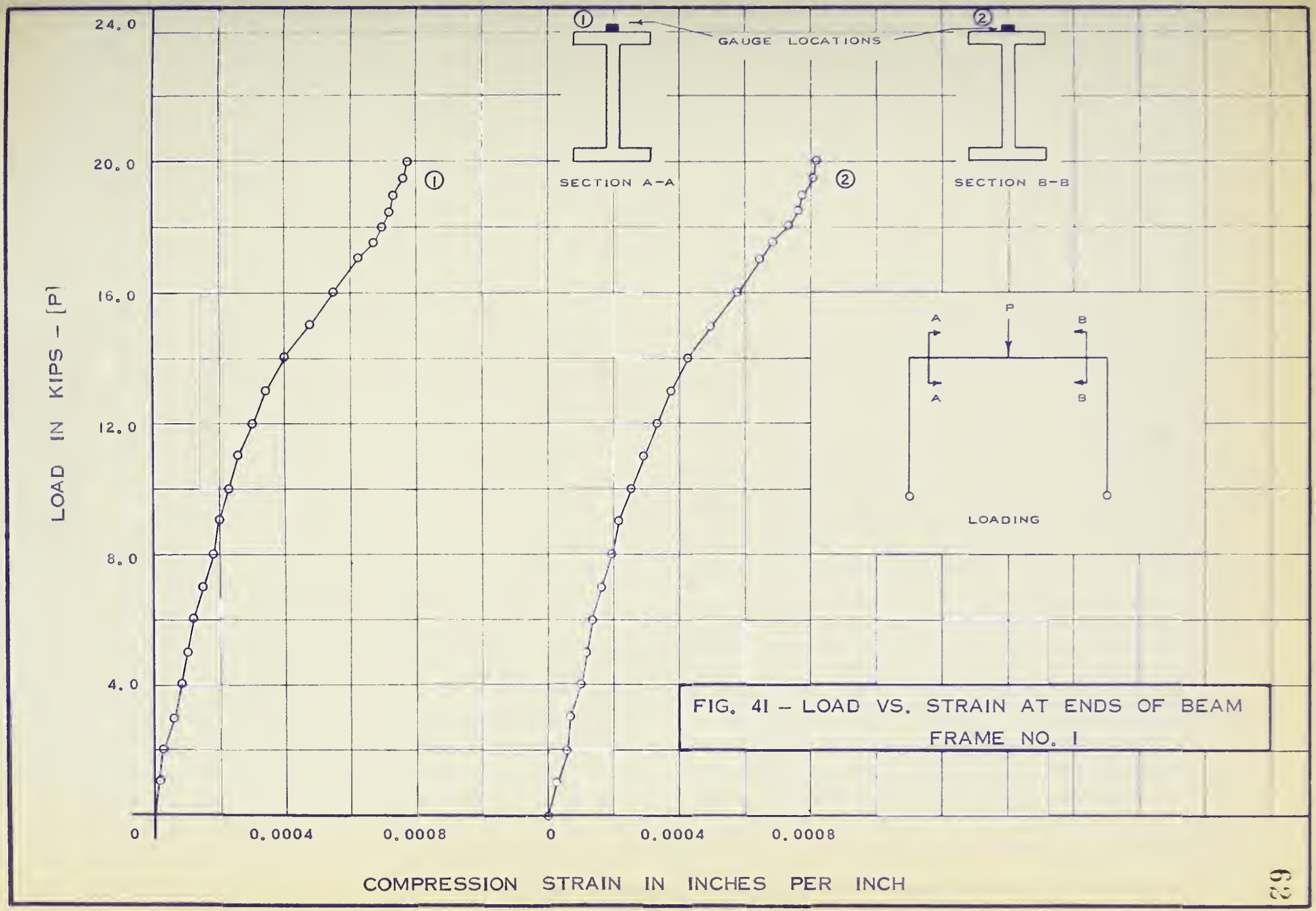

FIG. 41 – LOAD VS. STRAIN AT ENDS OF BEAM
FRAME NO. 1

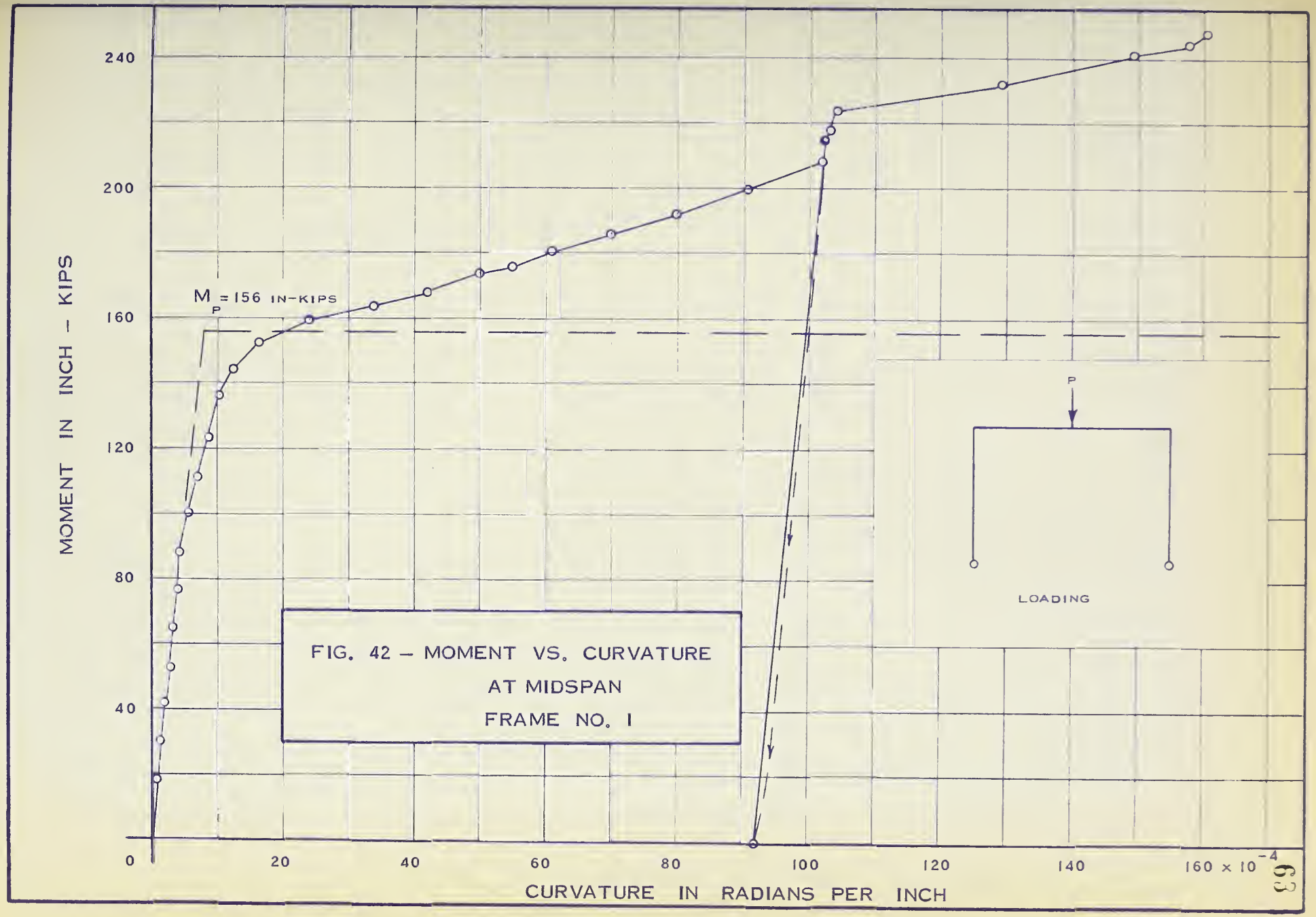

FIG. 42 – MOMENT VS. CURVATURE AT MIDSPAN FRAME NO. 1

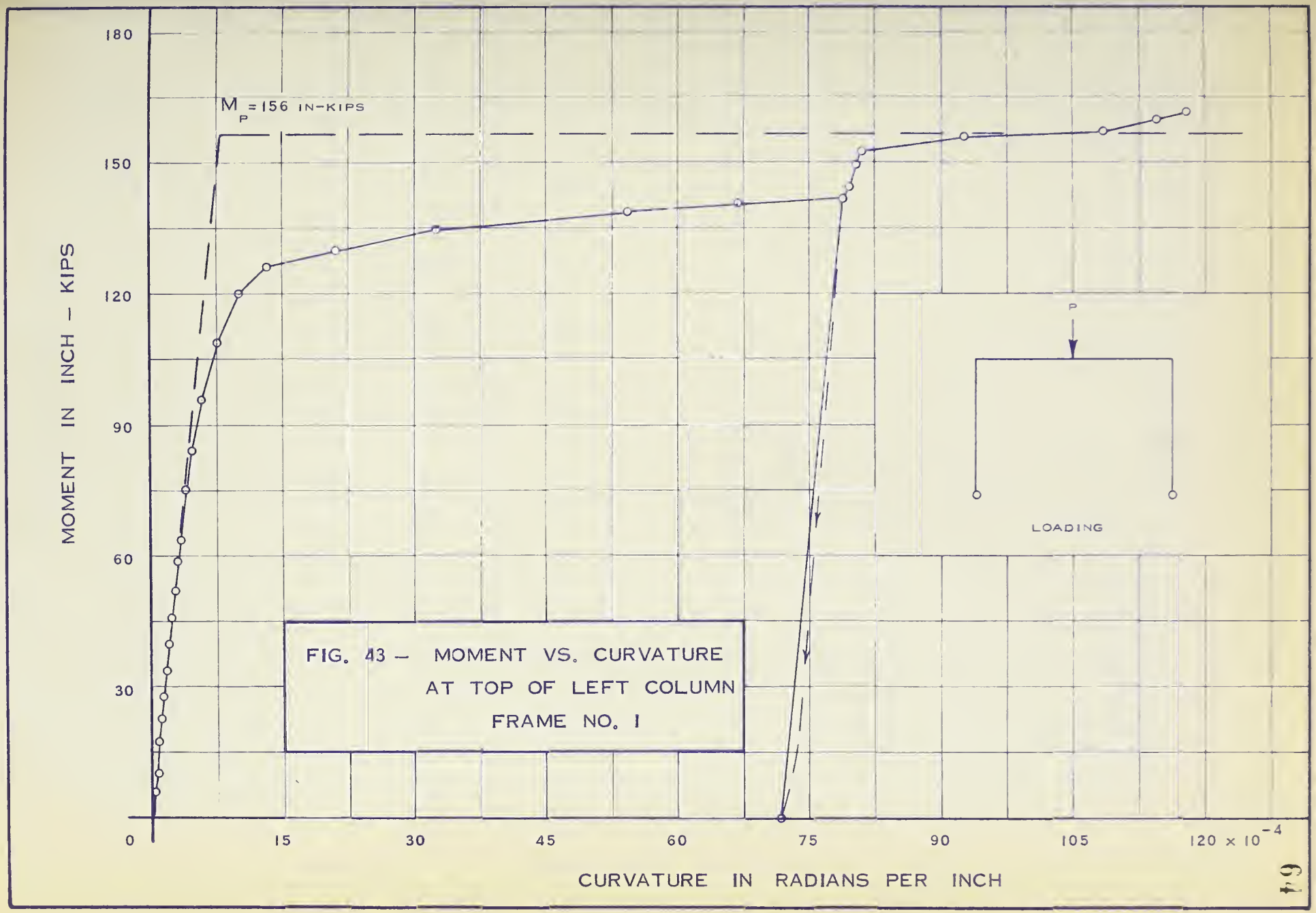

FIG. 43 — MOMENT VS. CURVATURE AT TOP OF LEFT COLUMN FRAME NO. 1

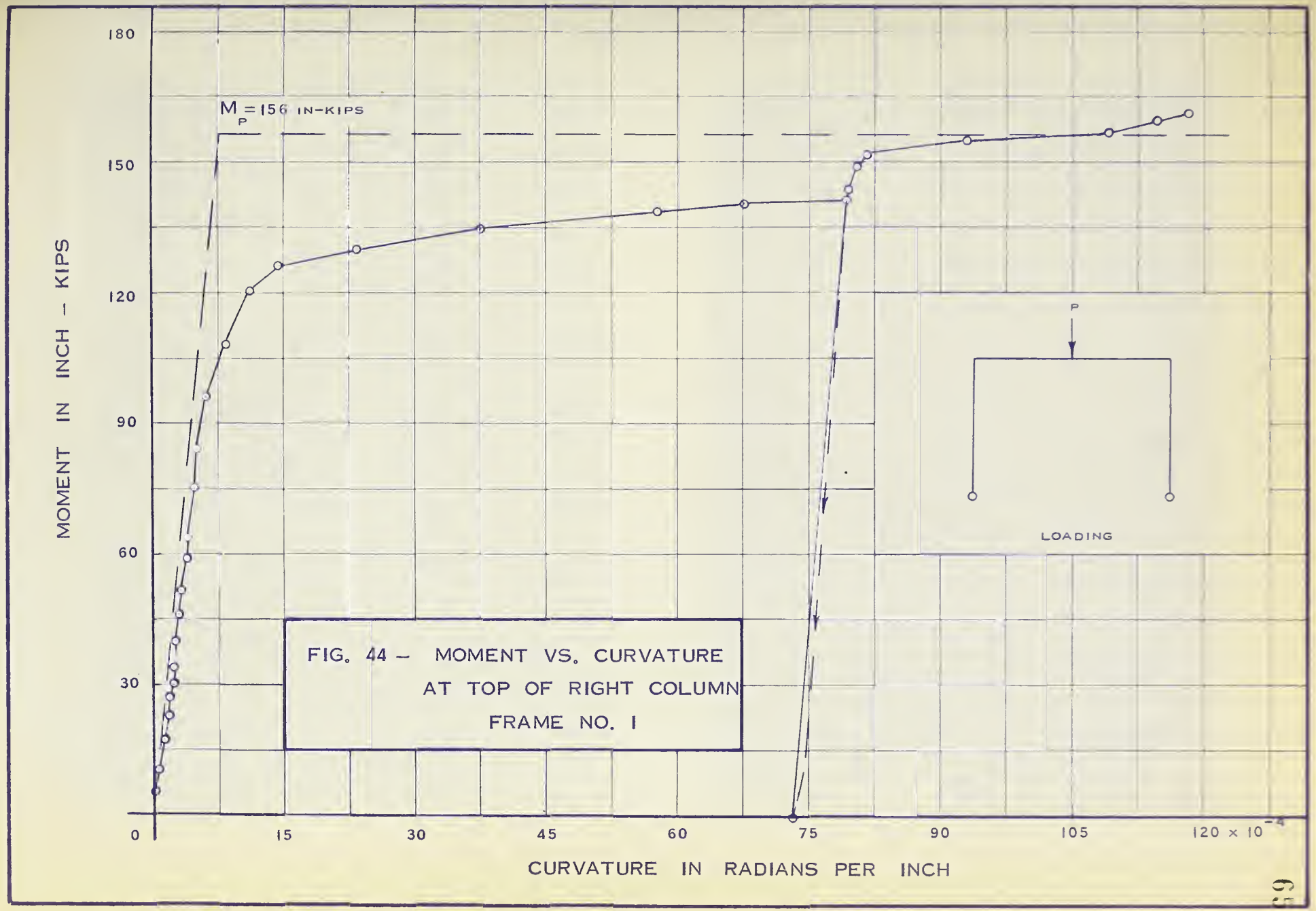

FIG. 44 – MOMENT VS. CURVATURE AT TOP OF RIGHT COLUMN FRAME NO. 1

FIG. 45 – FRAME NO. I AFTER TEST

FIG. 46 – PLASTIC HINGE AT MIDSPAN OF BEAM – FRAME NO. I

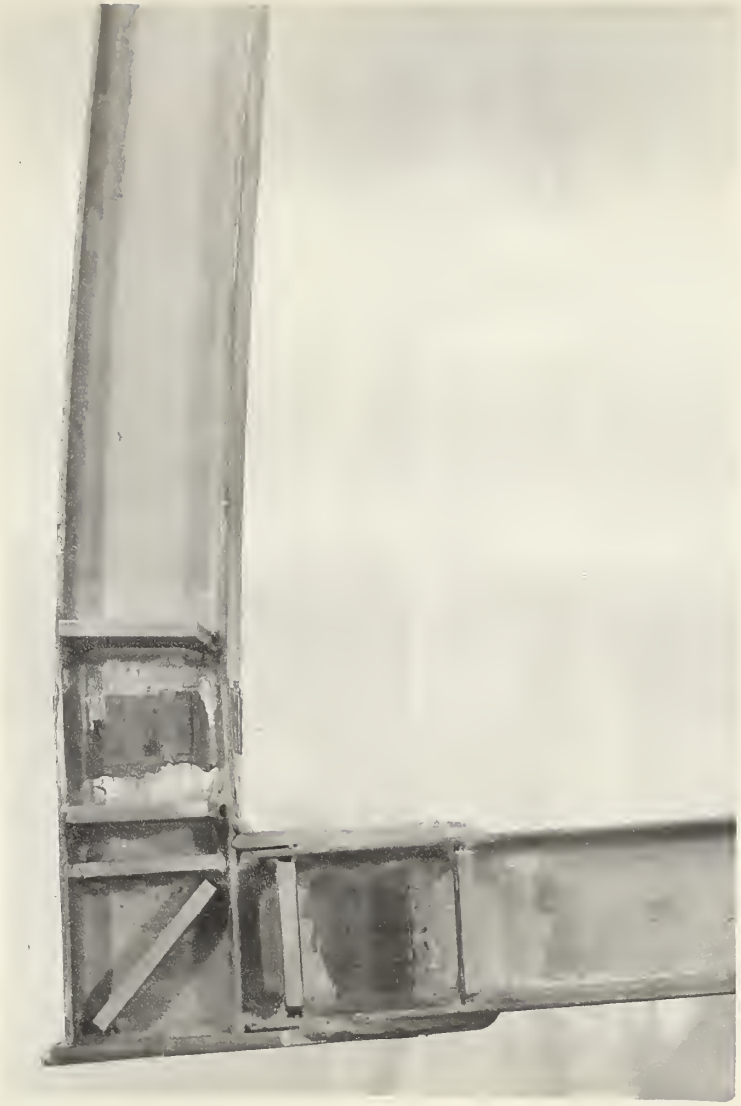

FIG. 47 – PLASTIC HINGE IN LEFT COLUMN – FRAME NO. 1

FIG. 48 – PLASTIC HINGE IN RIGHT COLUMN – FRAME NO. 1

FIG. 49 – BUCKLED PORTION OF LEFT COLUMN – FRAME NO. 1

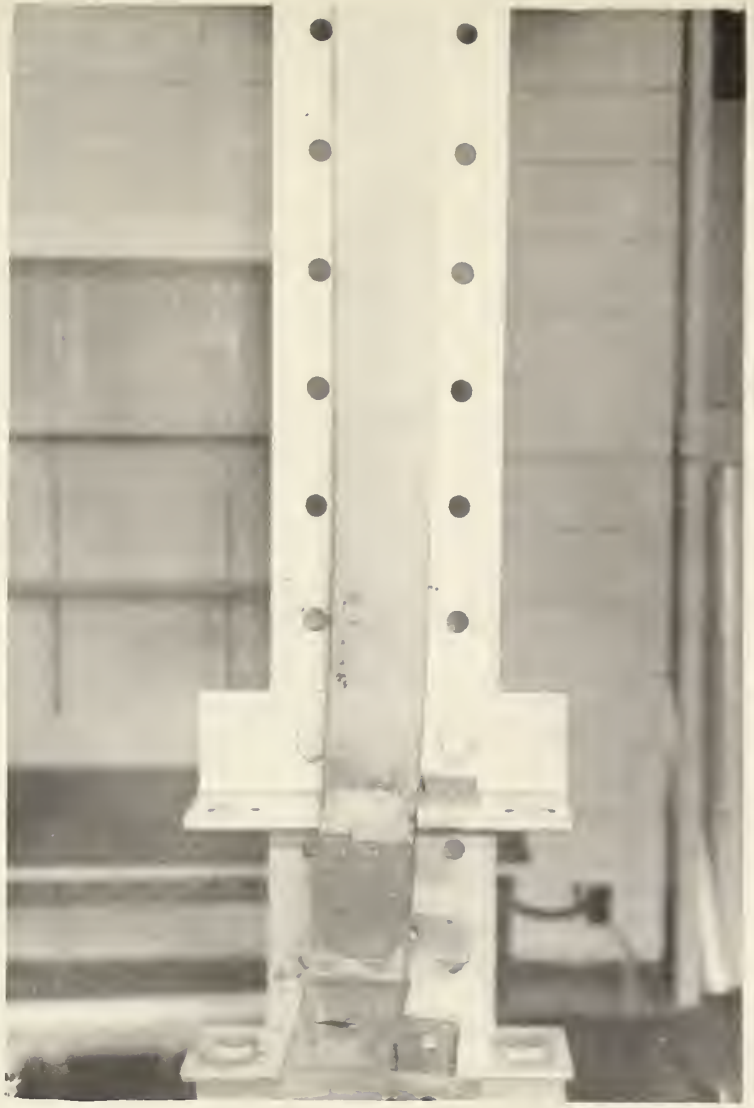

FIG. 50 – BUCKLED PORTION OF RIGHT COLUMN – FRAME NO. 1

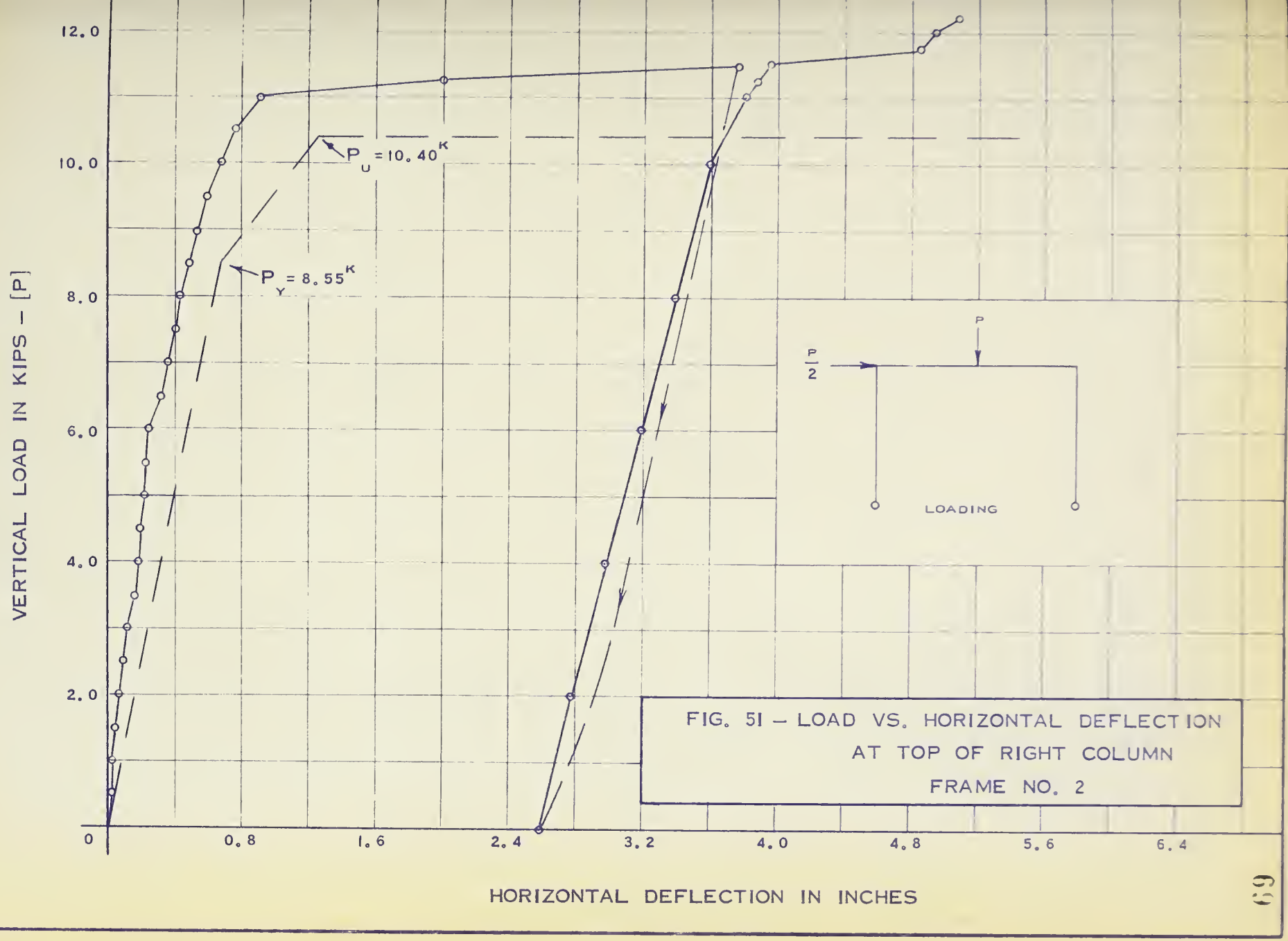

FIG. 51 – LOAD VS. HORIZONTAL DEFLECTION AT TOP OF RIGHT COLUMN FRAME NO. 2

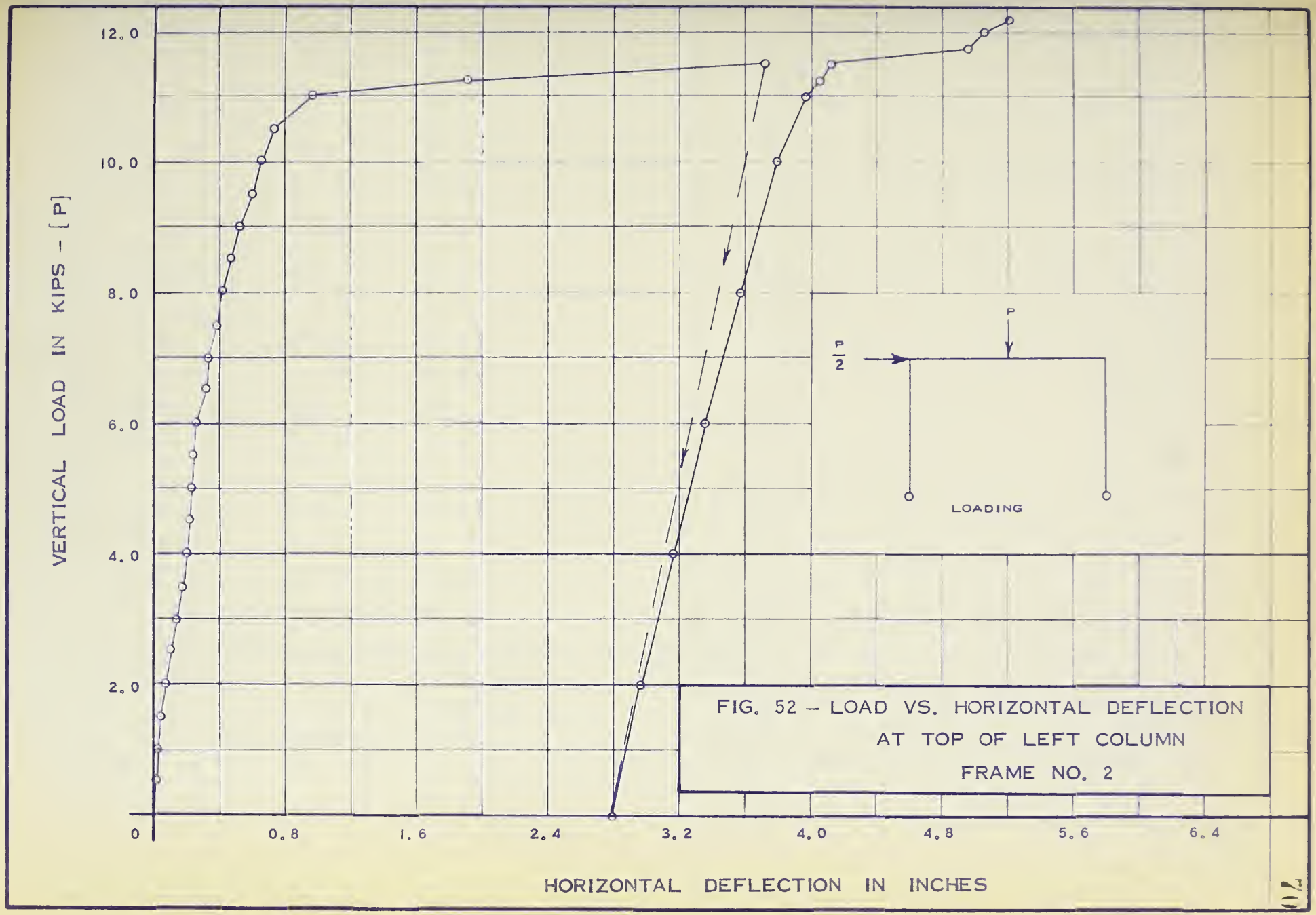

FIG. 52 – LOAD VS. HORIZONTAL DEFLECTION AT TOP OF LEFT COLUMN FRAME NO. 2

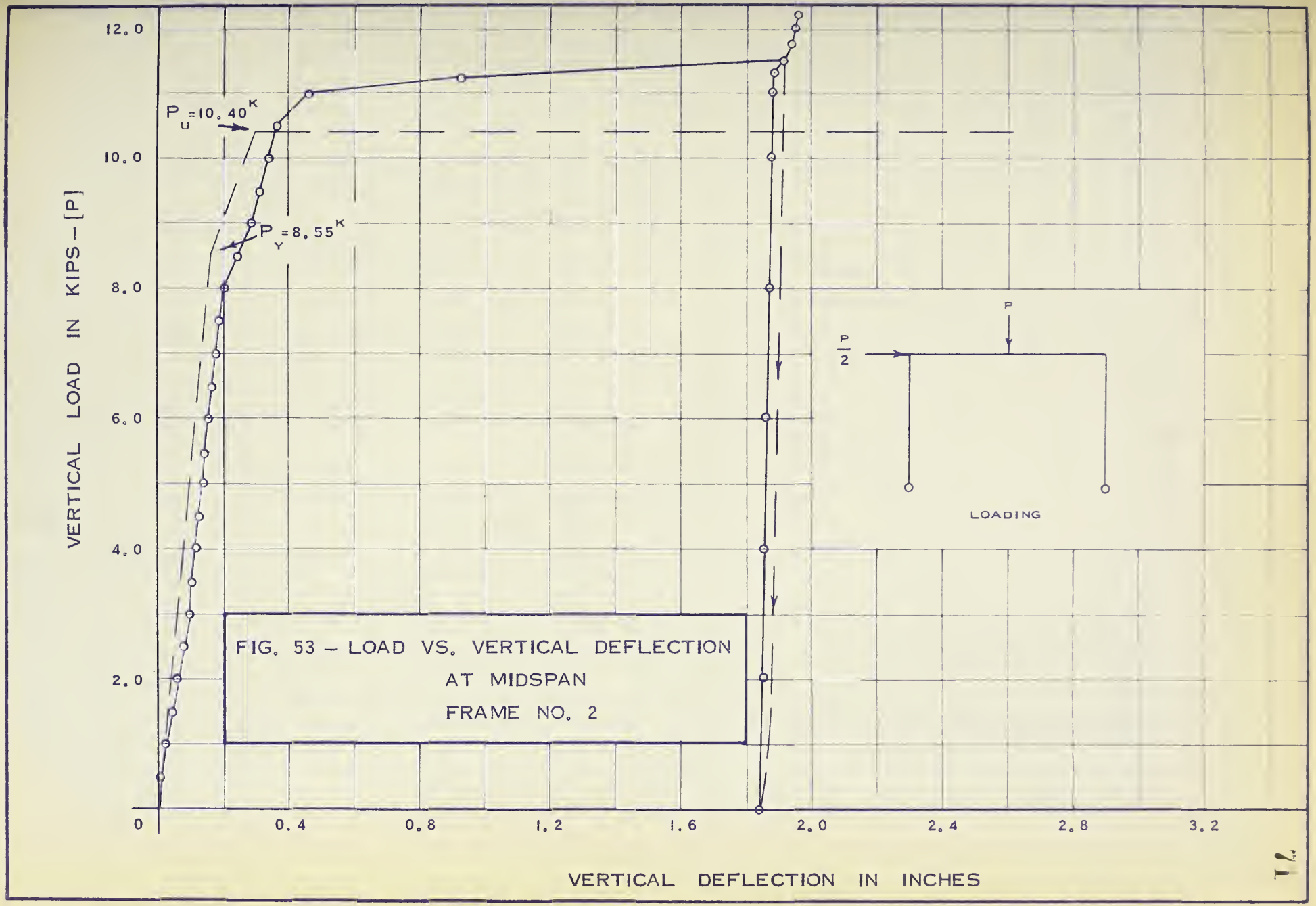
12.0
10.0
8.0
6.0
4.0
2.0
0
0.4
0.8
1.2
1.6
2.0
2.4
2.8
3.2
VERTICAL LOAD IN KIPS – [P]
VERTICAL DEFLECTION IN INCHES
$P_U = 10.40^K$
$P_Y = 8.55^K$
P
P/2
LOADING
FIG. 53 – LOAD VS. VERTICAL DEFLECTION
AT MIDSPAN
FRAME NO. 2

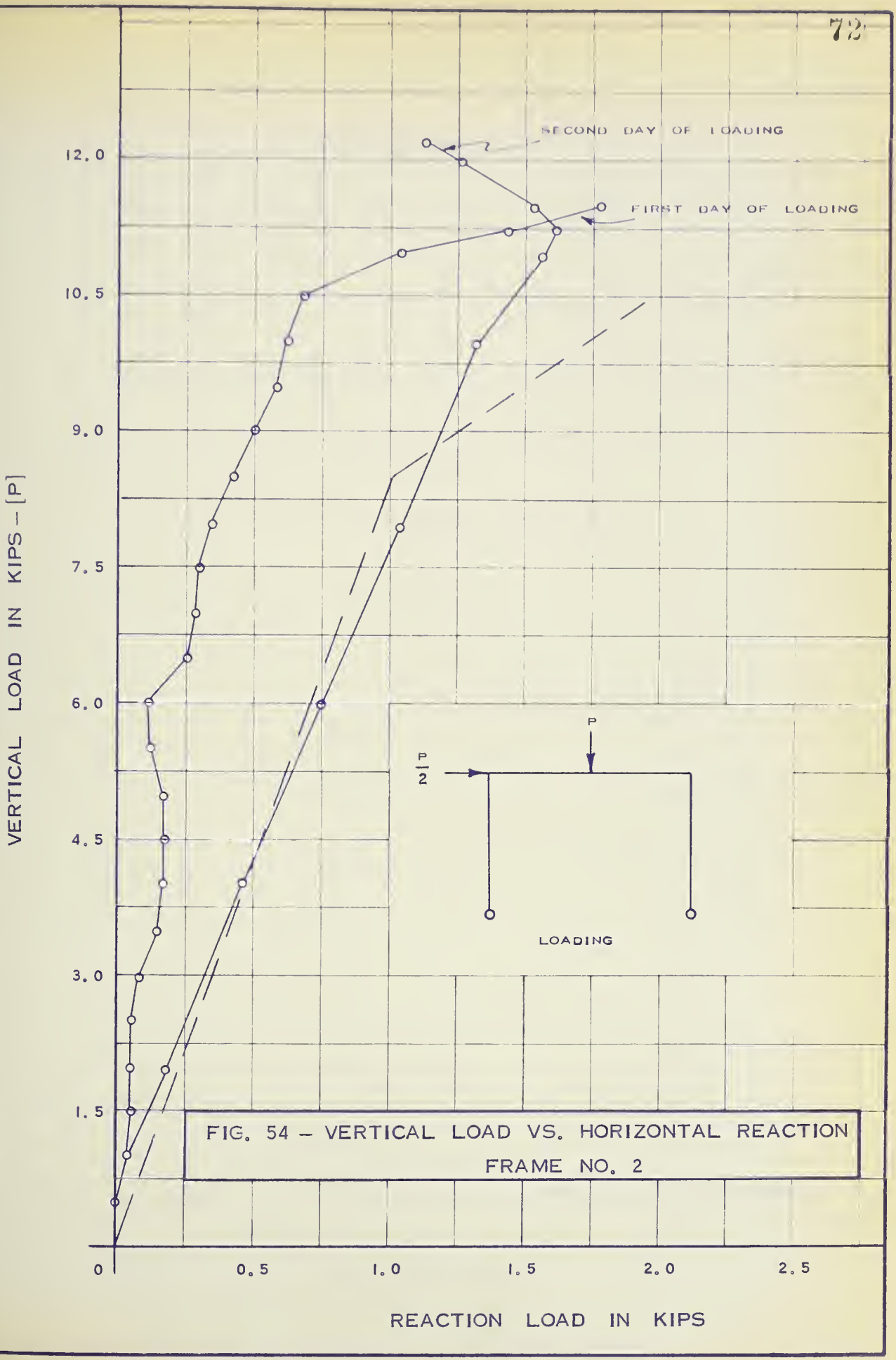

FIG. 54 – VERTICAL LOAD VS. HORIZONTAL REACTION
FRAME NO. 2

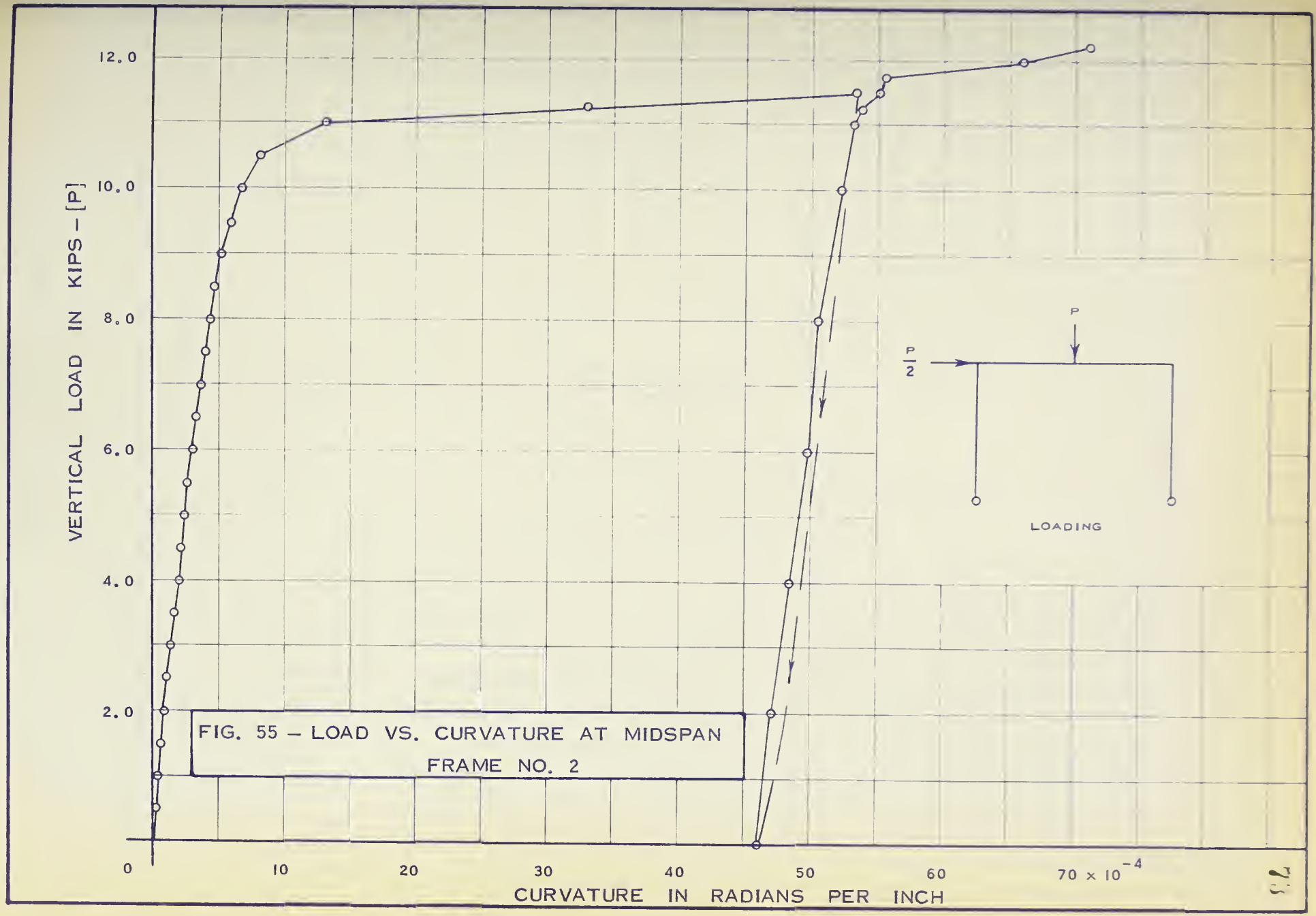

FIG. 55 – LOAD VS. CURVATURE AT MIDSPAN
FRAME NO. 2

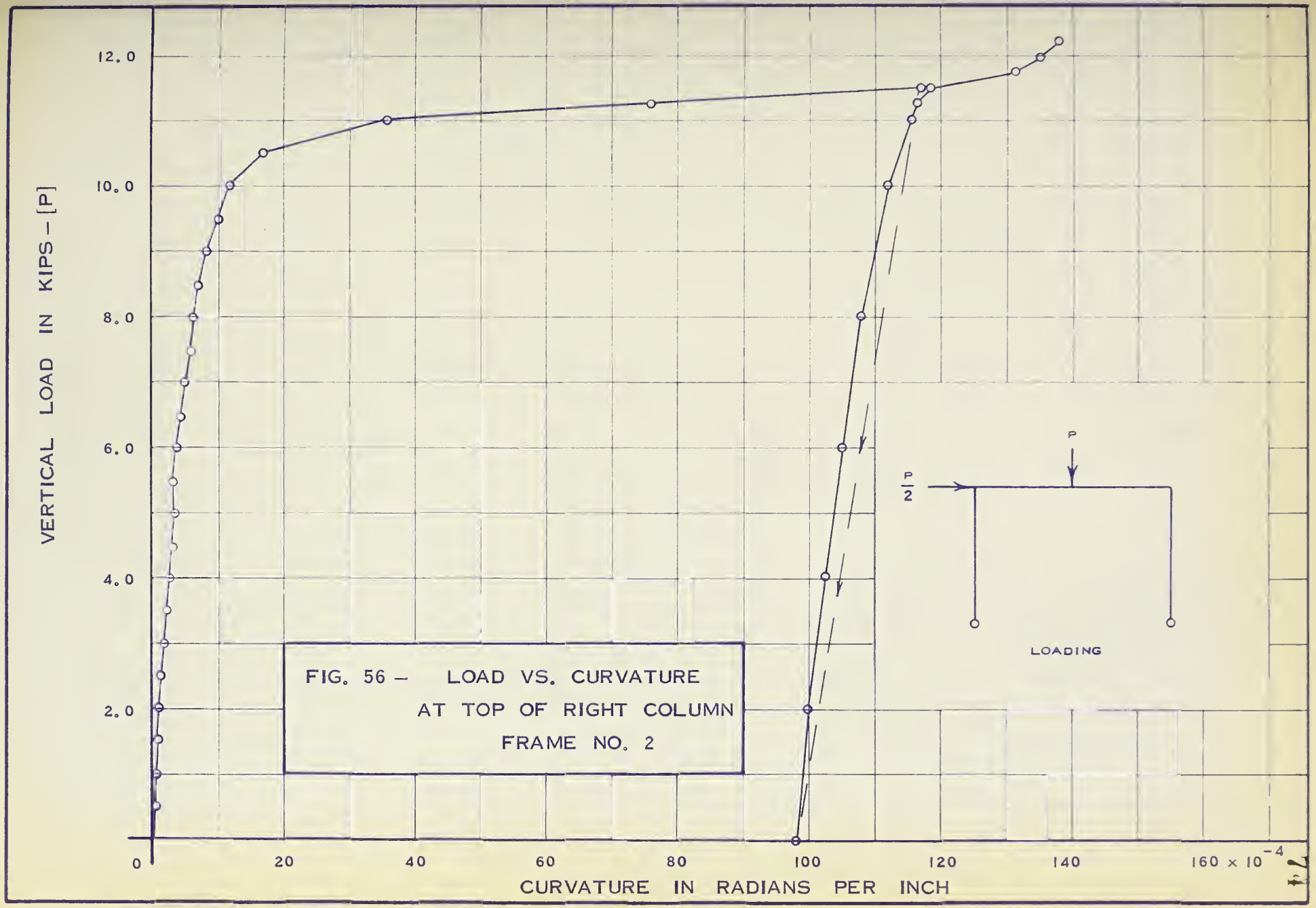

FIG. 56 – LOAD VS. CURVATURE AT TOP OF RIGHT COLUMN FRAME NO. 2

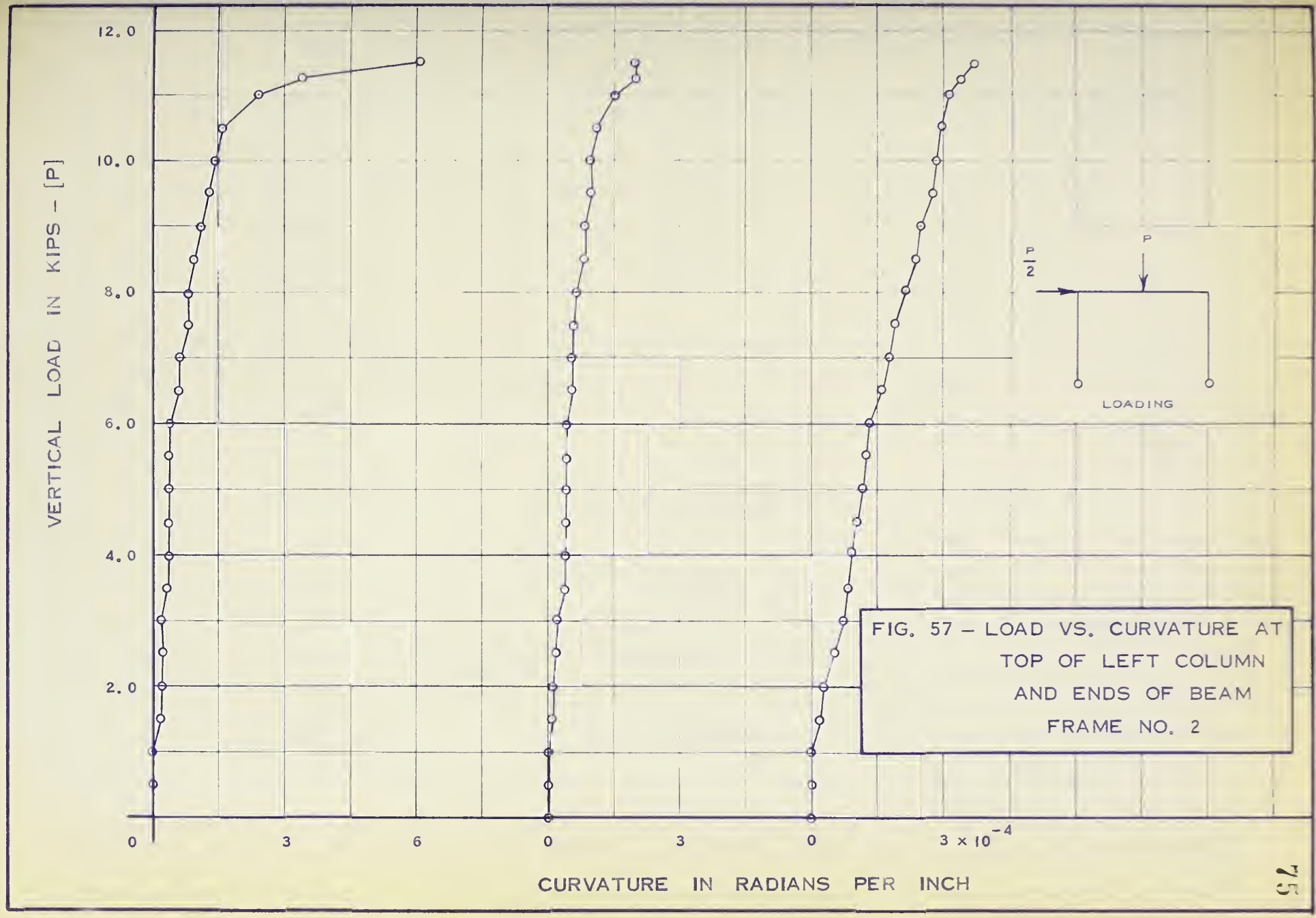

FIG. 57 – LOAD VS. CURVATURE AT TOP OF LEFT COLUMN AND ENDS OF BEAM FRAME NO. 2

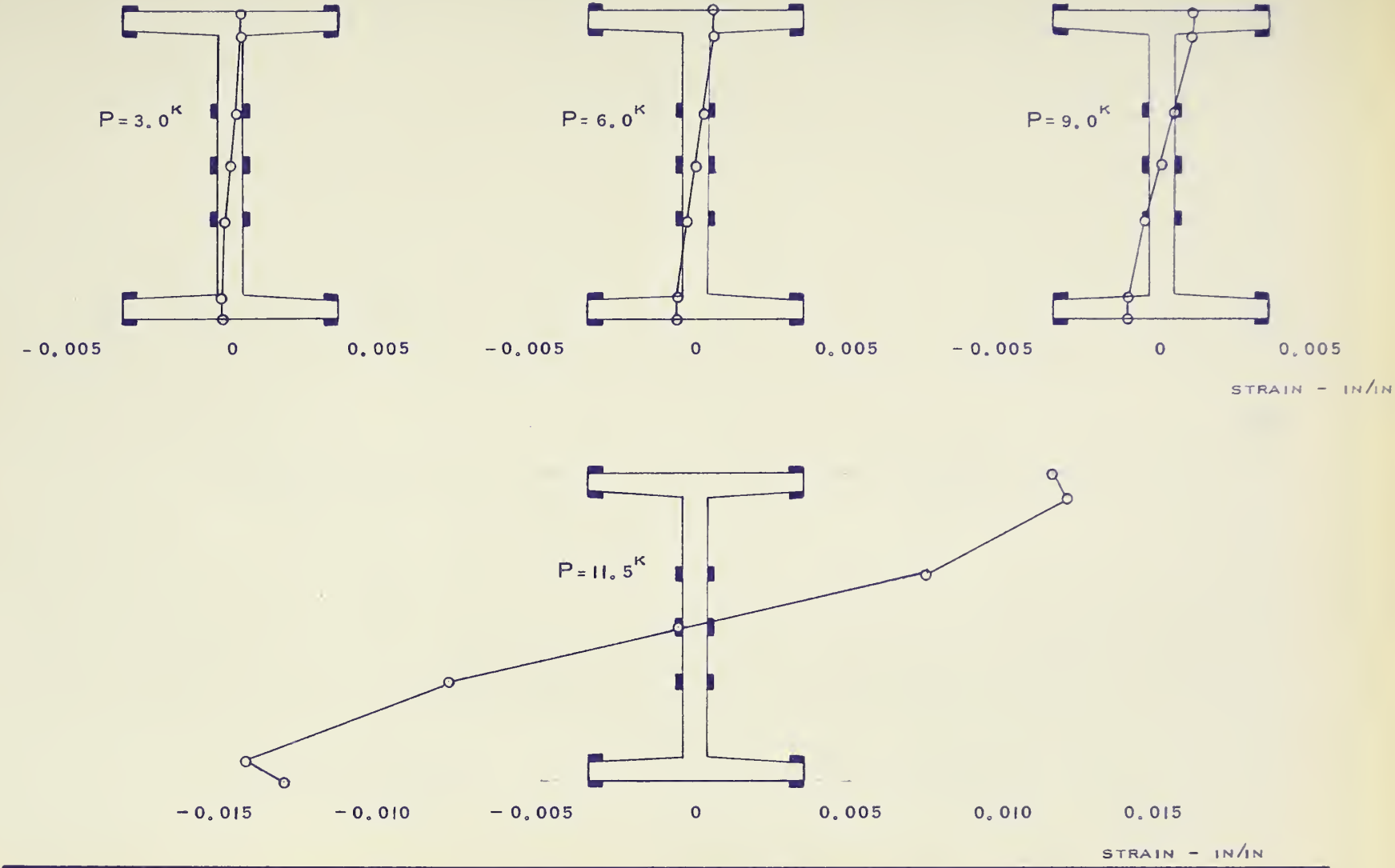

FIG. 58 – STRAIN DISTRIBUTION AT MIDSPAN – STRAINS MEASURED TO LEFT OF STIFFENER FRAME NO. 2

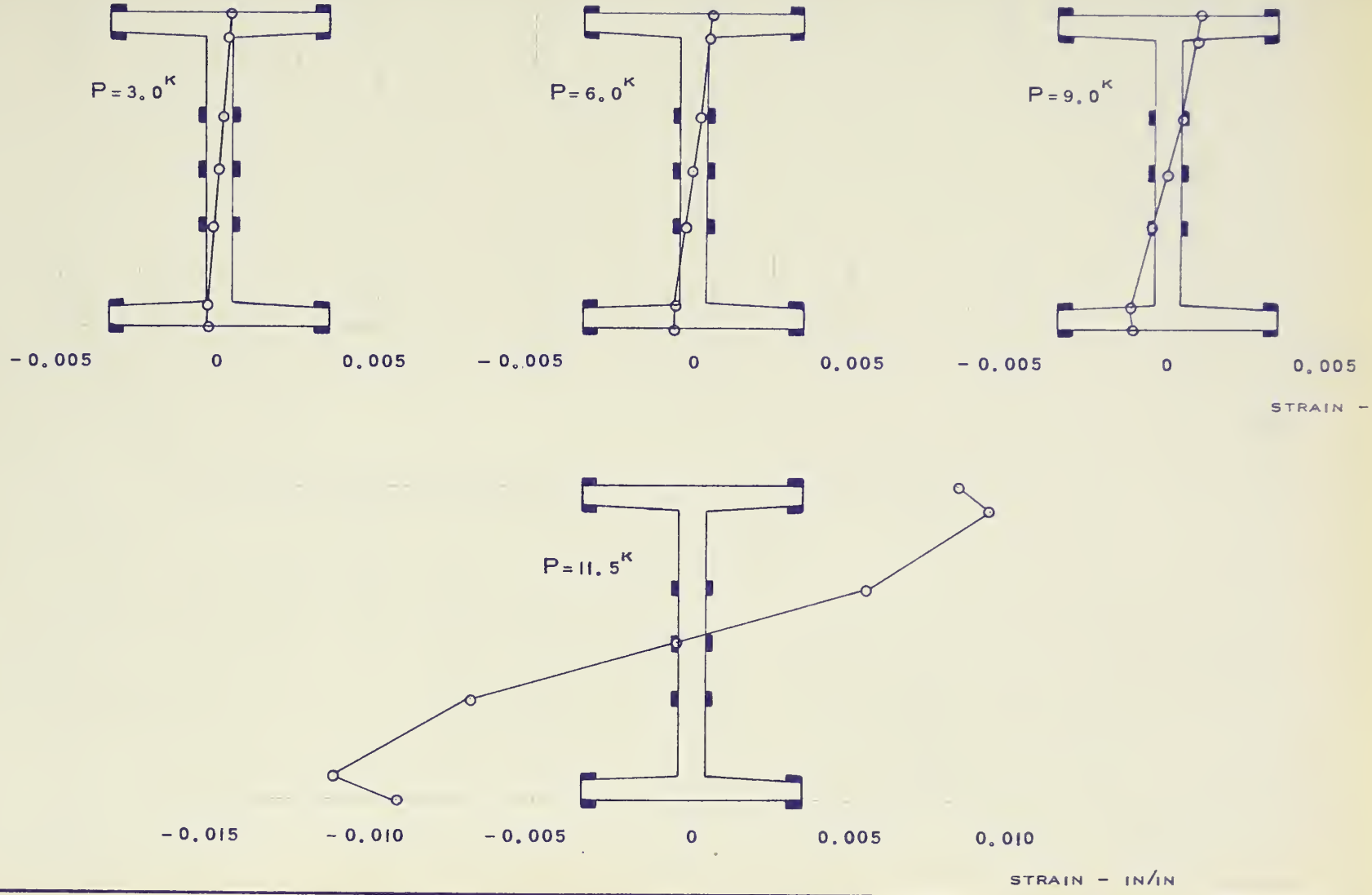

FIG. 59 – STRAIN DISTRIBUTION AT MIDSPAN – STRAINS MEASURED TO RIGHT OF STIFFENER FRAME NO. 2

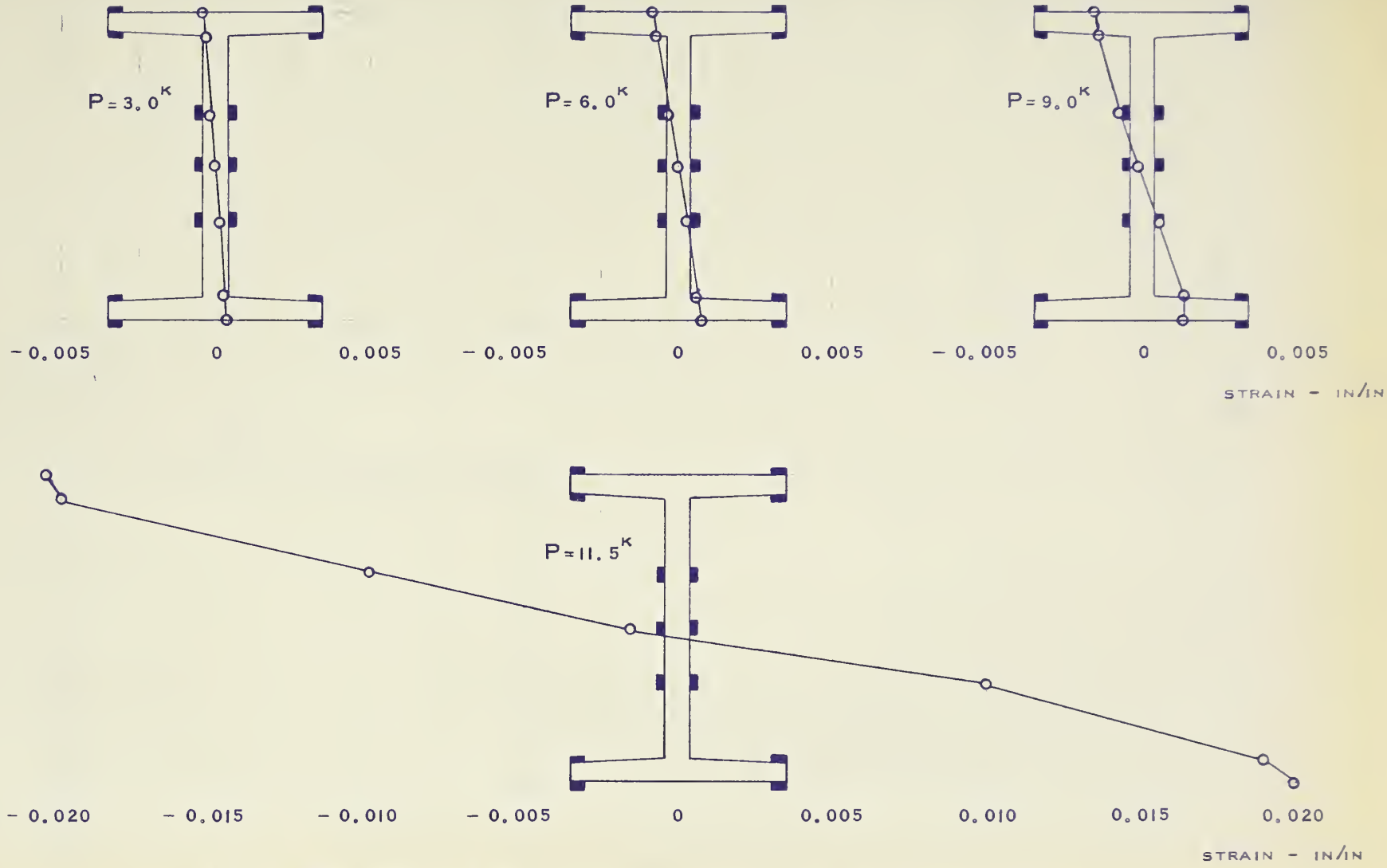

FIG. 60 – STRAIN DISTRIBUTION AT TOP OF RIGHT COLUMN
FRAME NO. 2

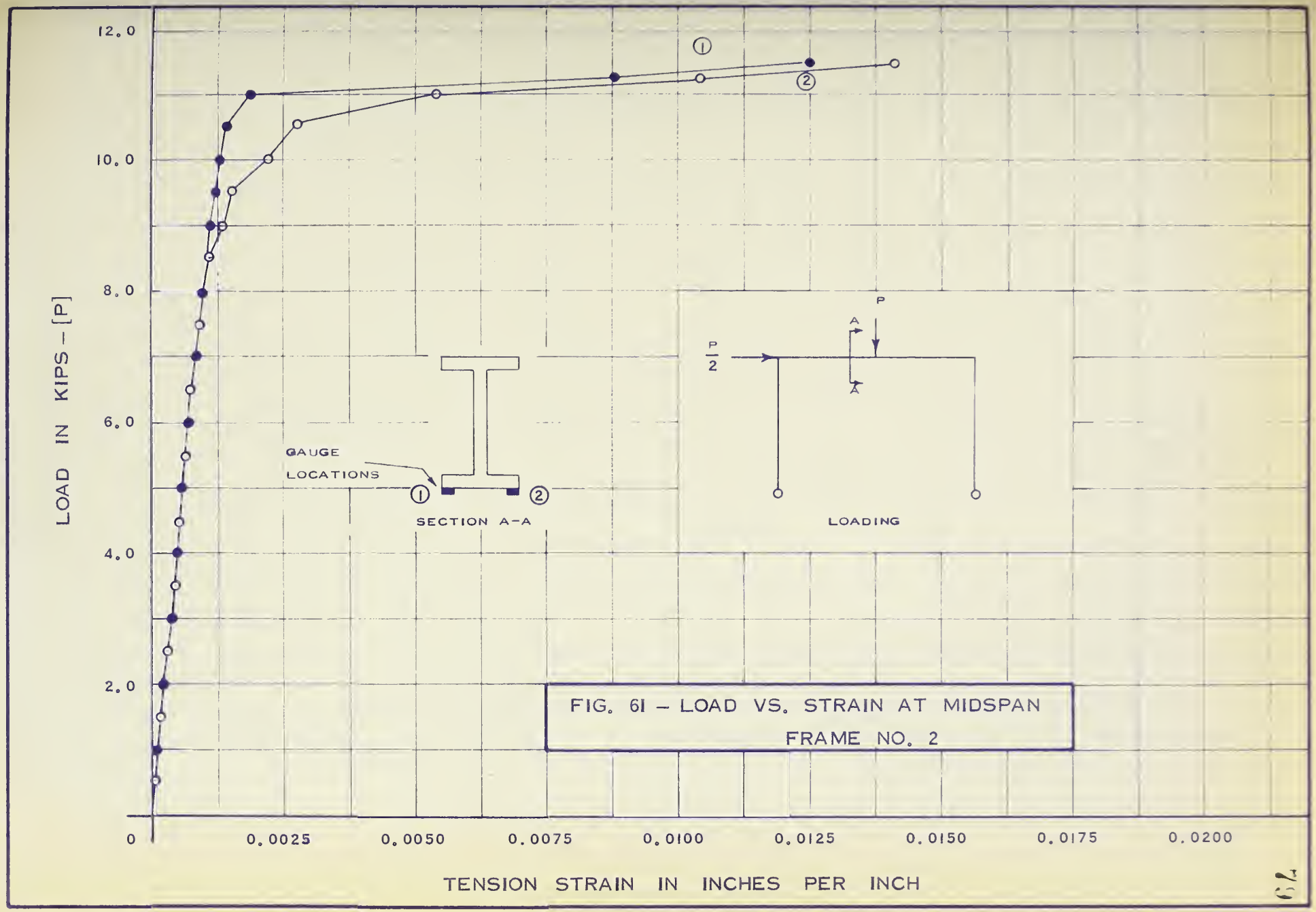

FIG. 61 – LOAD VS. STRAIN AT MIDSPAN
FRAME NO. 2

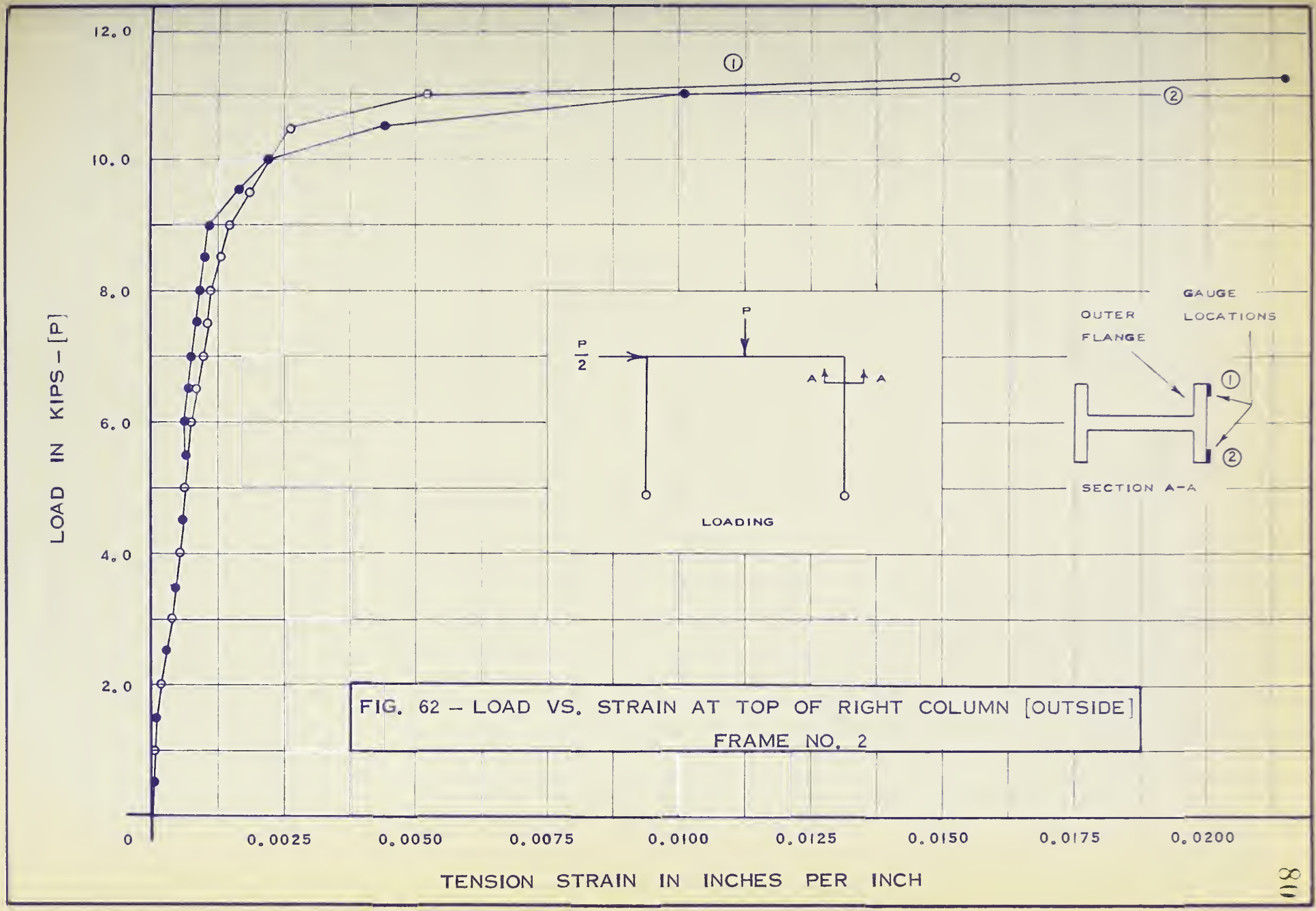

FIG. 62 – LOAD VS. STRAIN AT TOP OF RIGHT COLUMN [OUTSIDE]
FRAME NO. 2

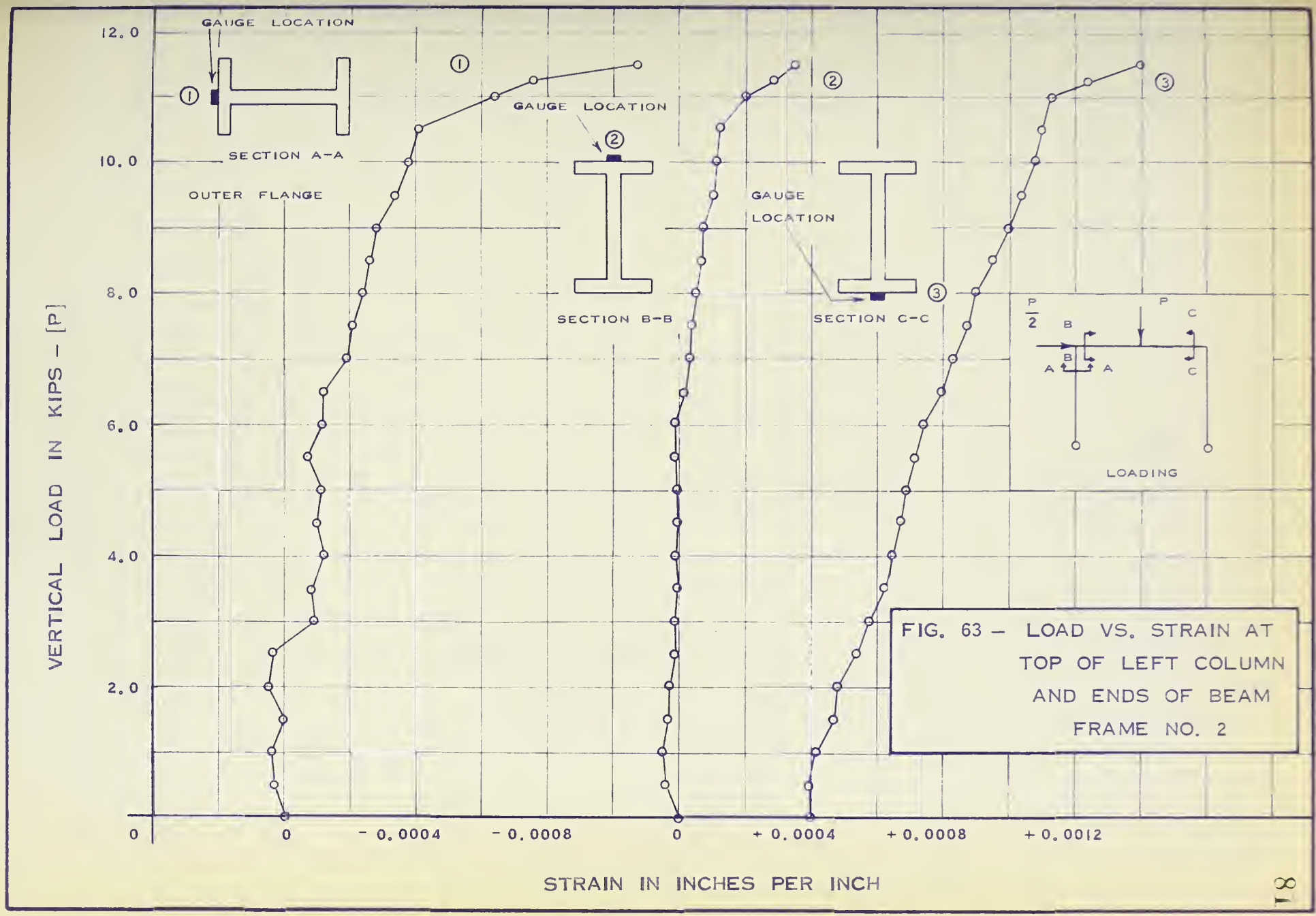

FIG. 63 – LOAD VS. STRAIN AT TOP OF LEFT COLUMN AND ENDS OF BEAM FRAME NO. 2

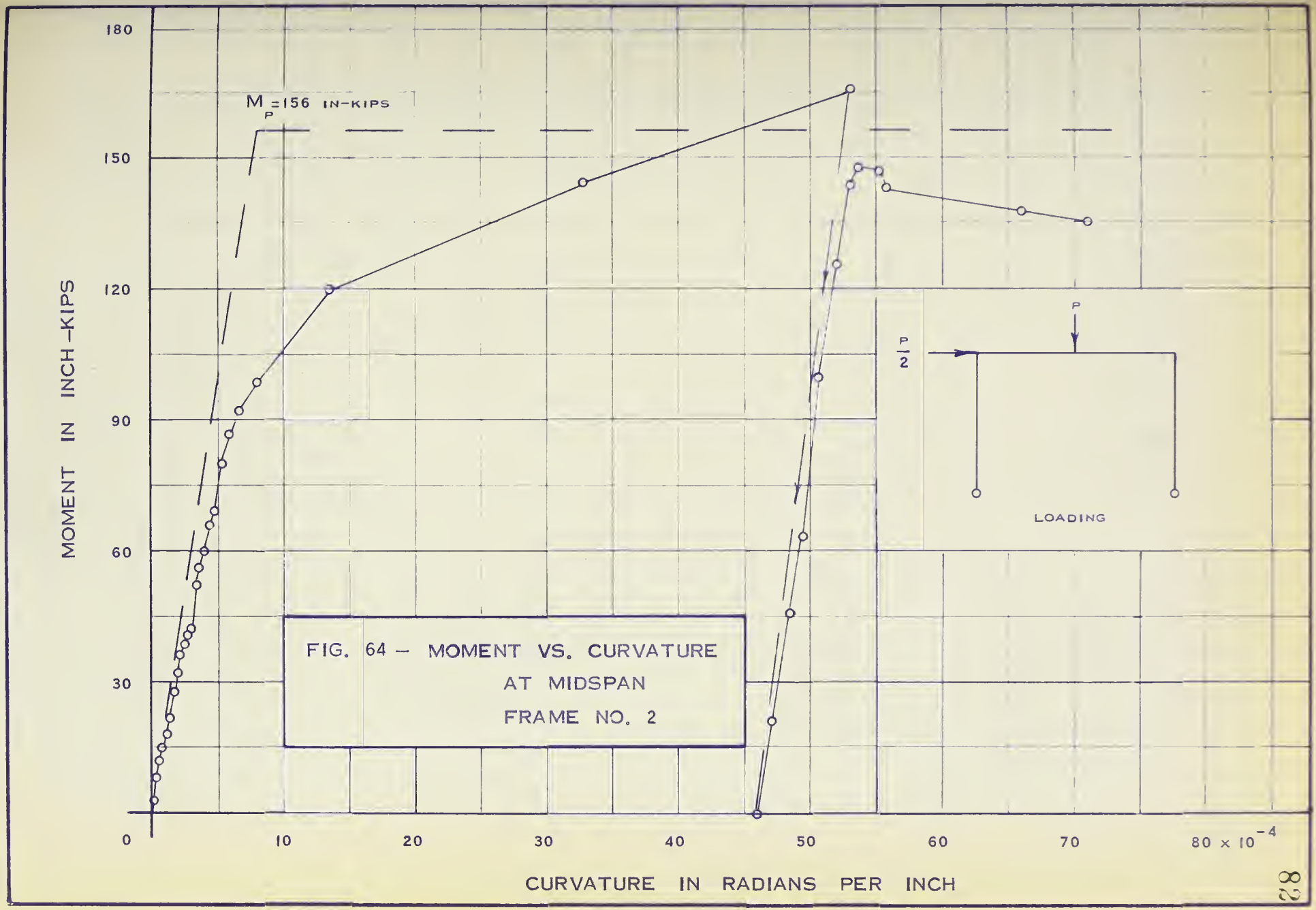

FIG. 64 – MOMENT VS. CURVATURE AT MIDSPAN FRAME NO. 2

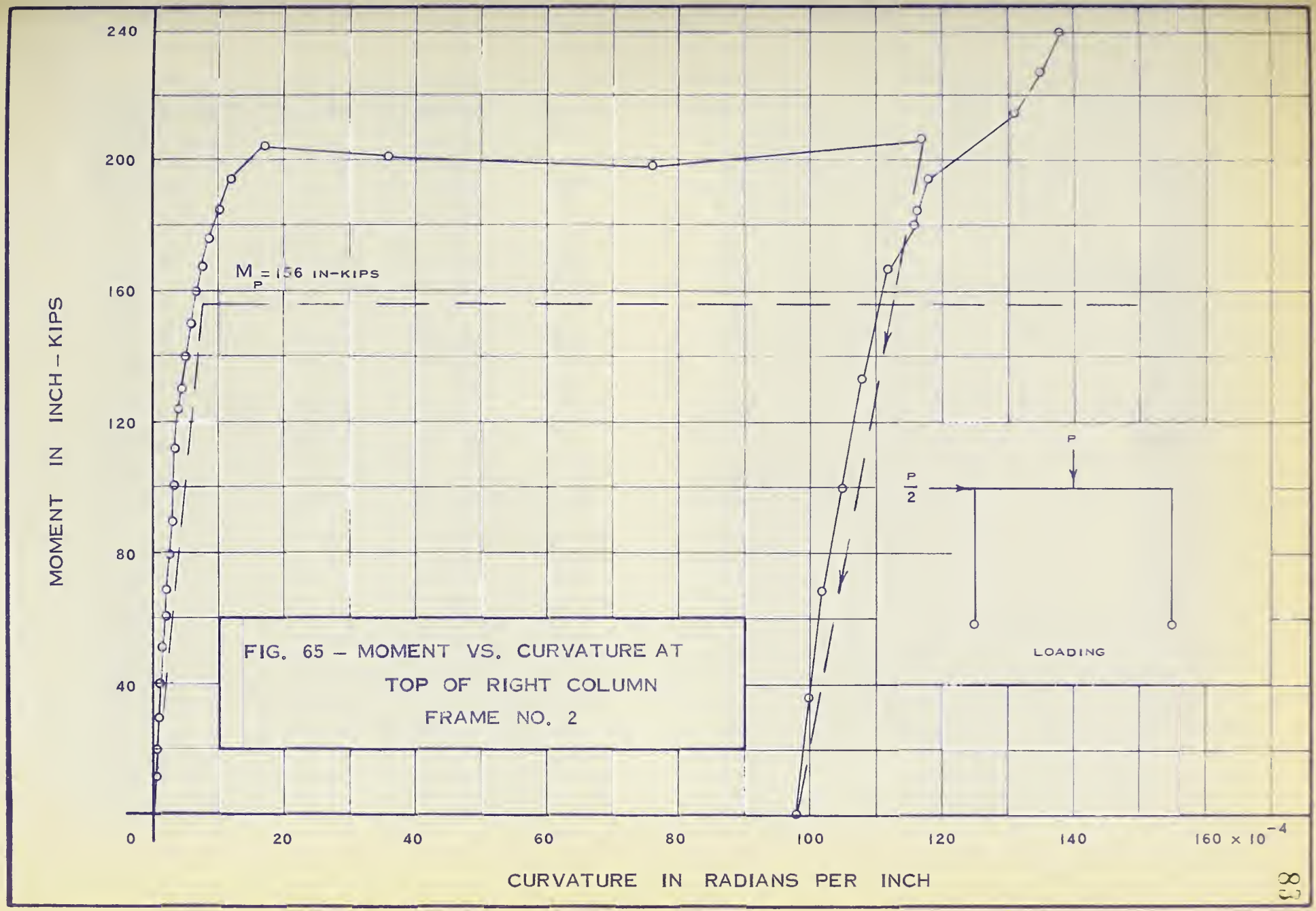

FIG. 65 – MOMENT VS. CURVATURE AT TOP OF RIGHT COLUMN FRAME NO. 2

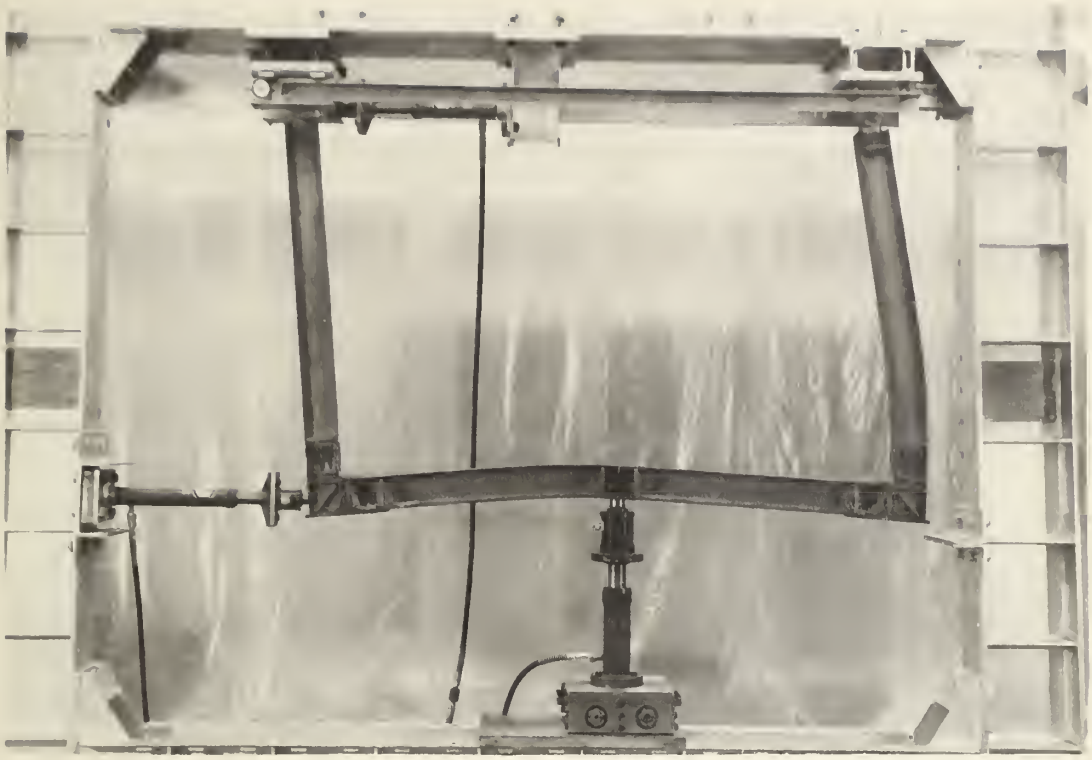

FIG. 66 – FRAME NO. 2 AFTER TEST

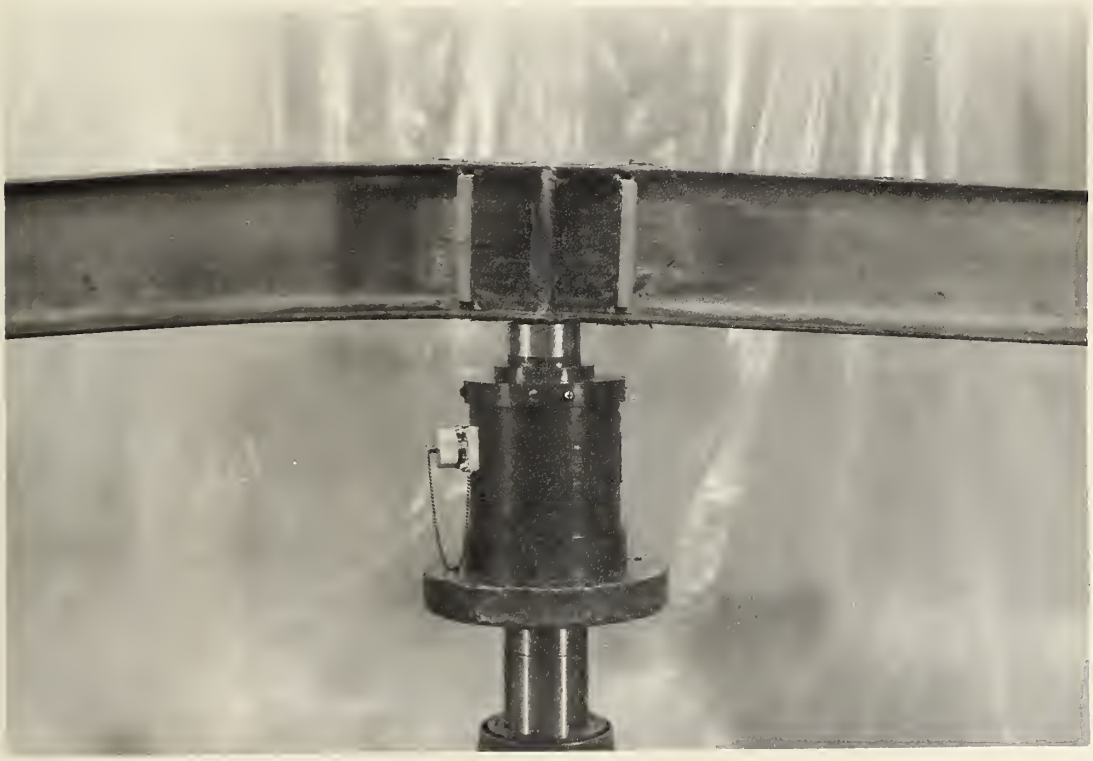

FIG. 67 – PLASTIC HINGE AT MIDSPAN OF BEAM – FRAME NO. 2

FIG. 68 – PLASTIC HINGE IN RIGHT COLUMN – FRAME NO. 2

FIG. 69 – BUCKLED PORTION OF RIGHT COLUMN – FRAME NO. 2

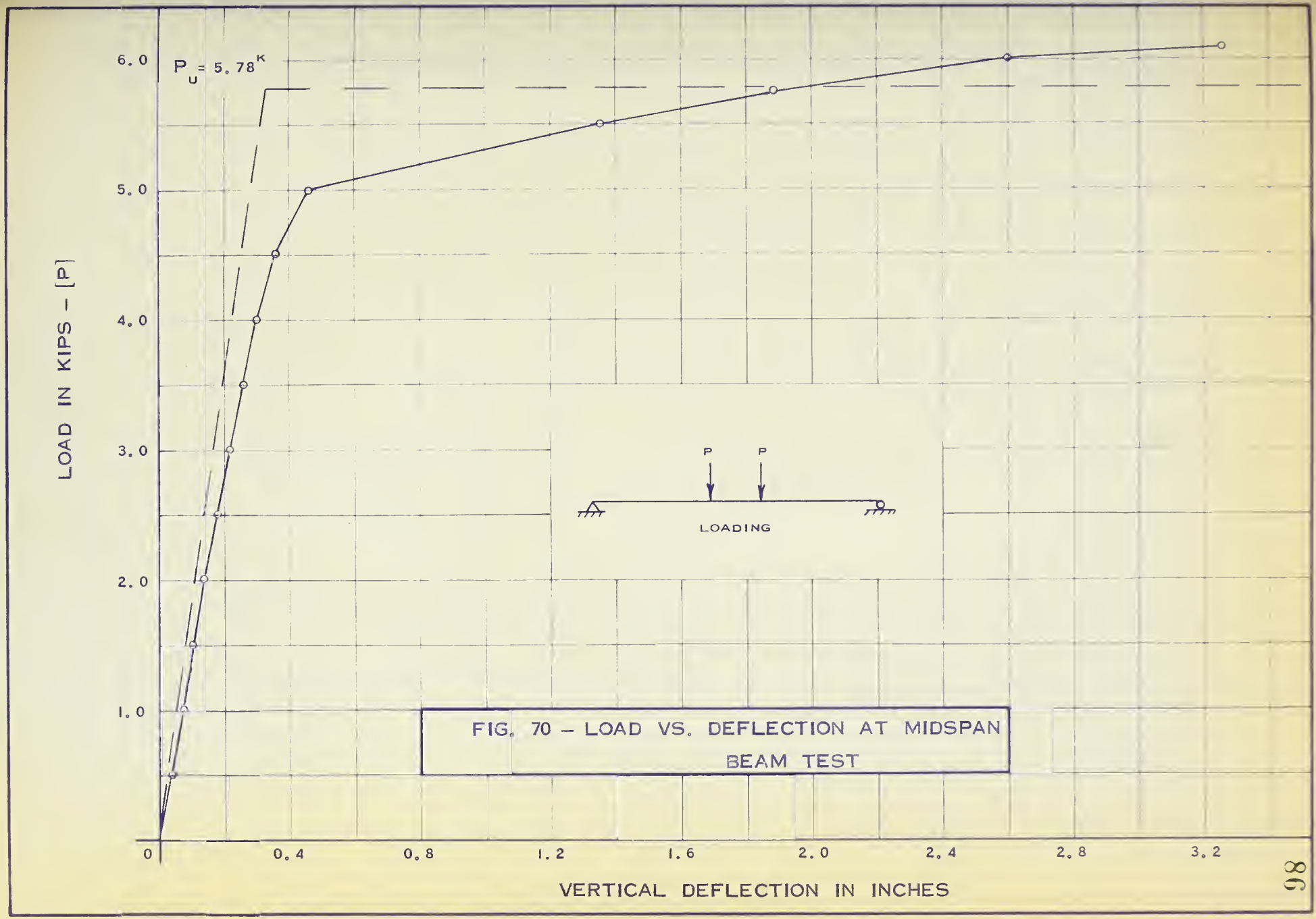

FIG. 70 – LOAD VS. DEFLECTION AT MIDSPAN BEAM TEST

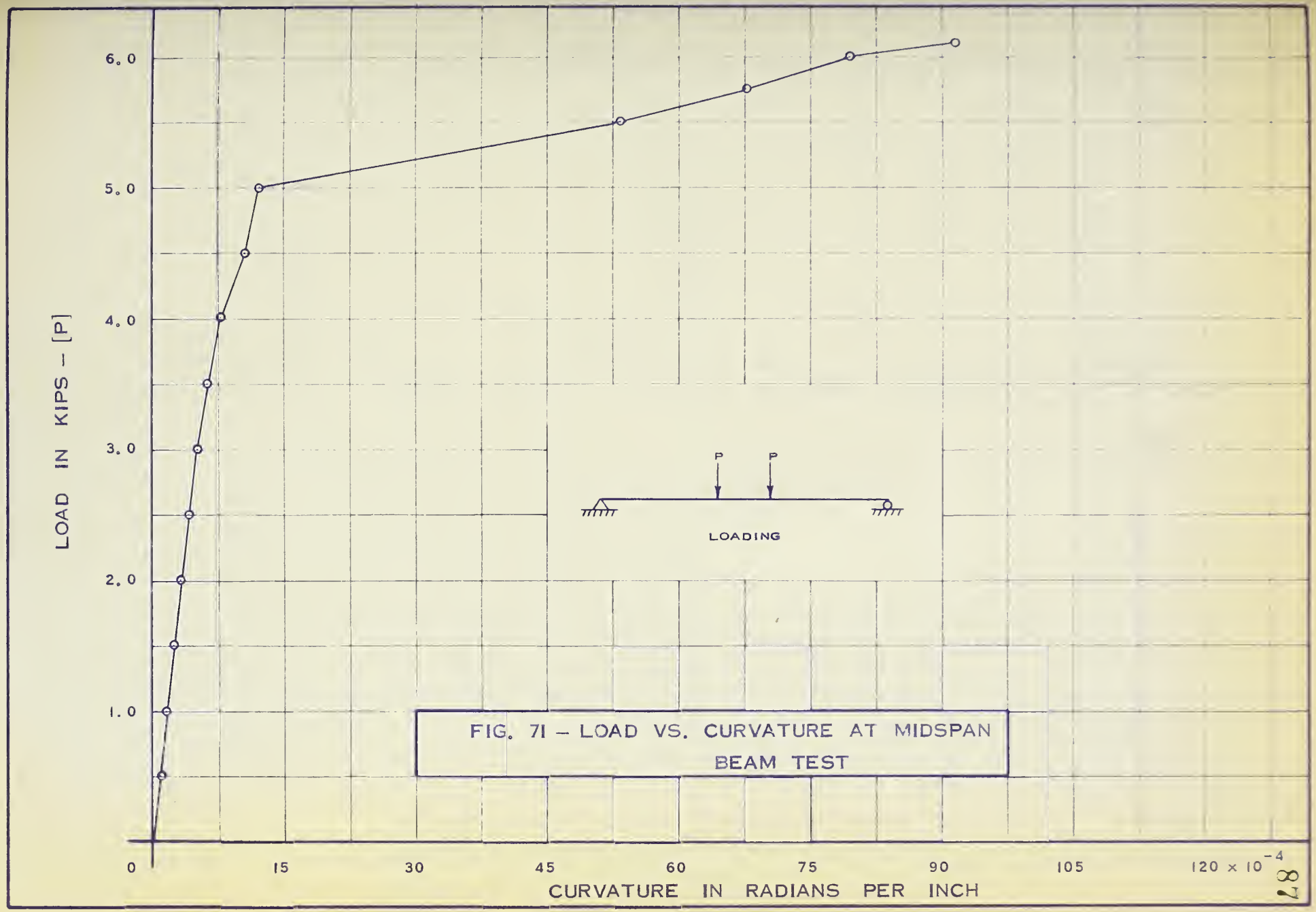

FIG. 71 – LOAD VS. CURVATURE AT MIDSPAN
BEAM TEST

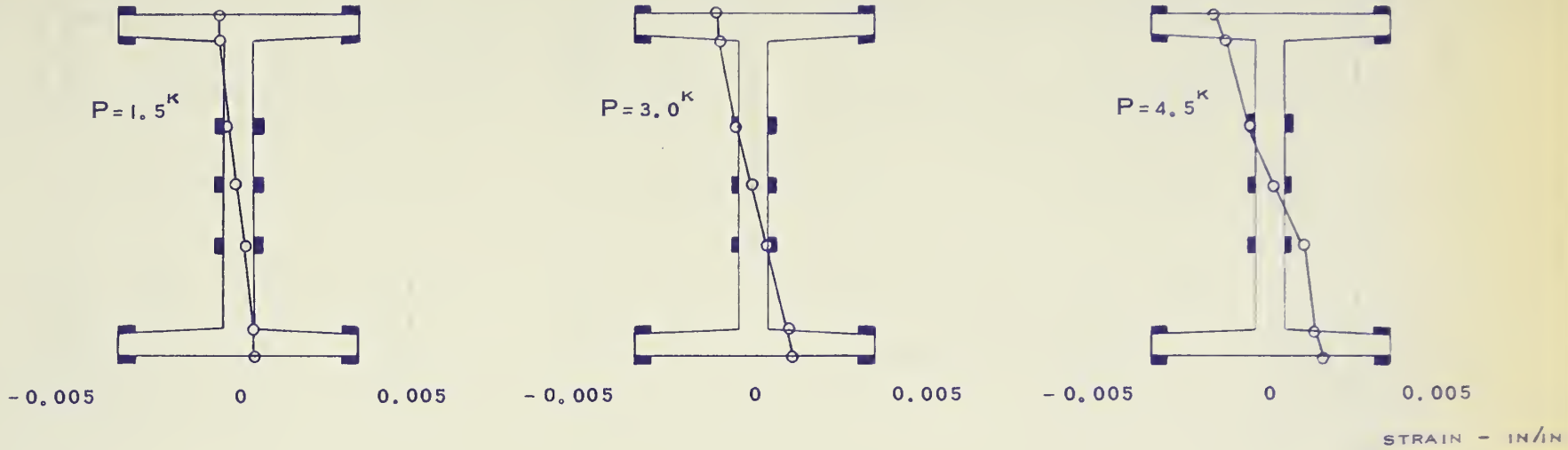

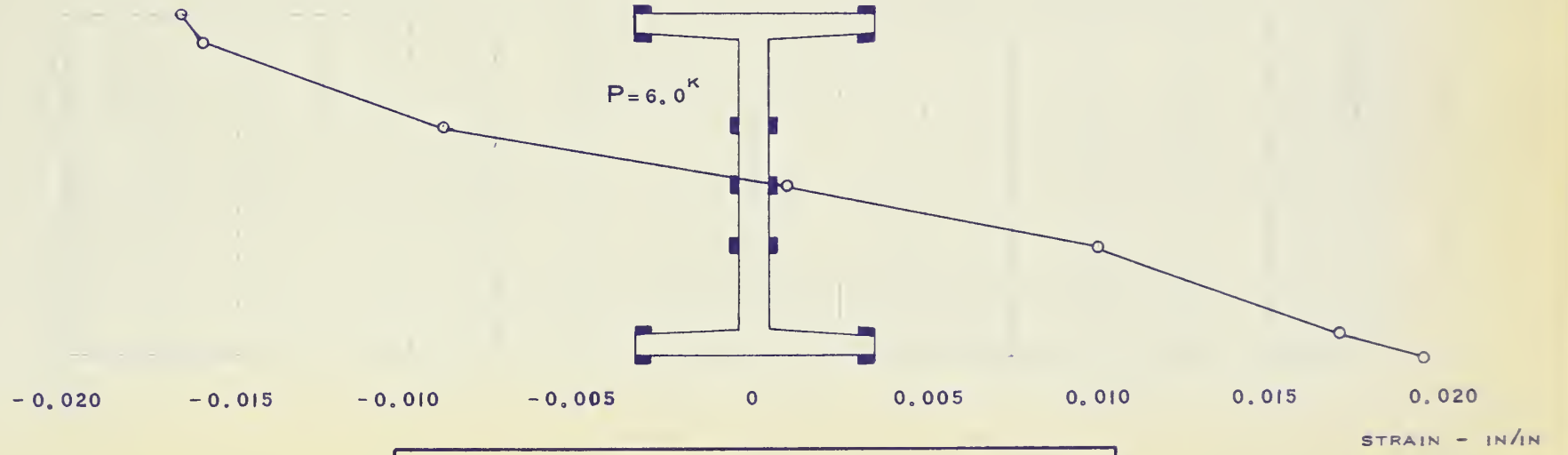

FIG. 72 – STRAIN DISTRIBUTION AT MIDSPAN BEAM TEST

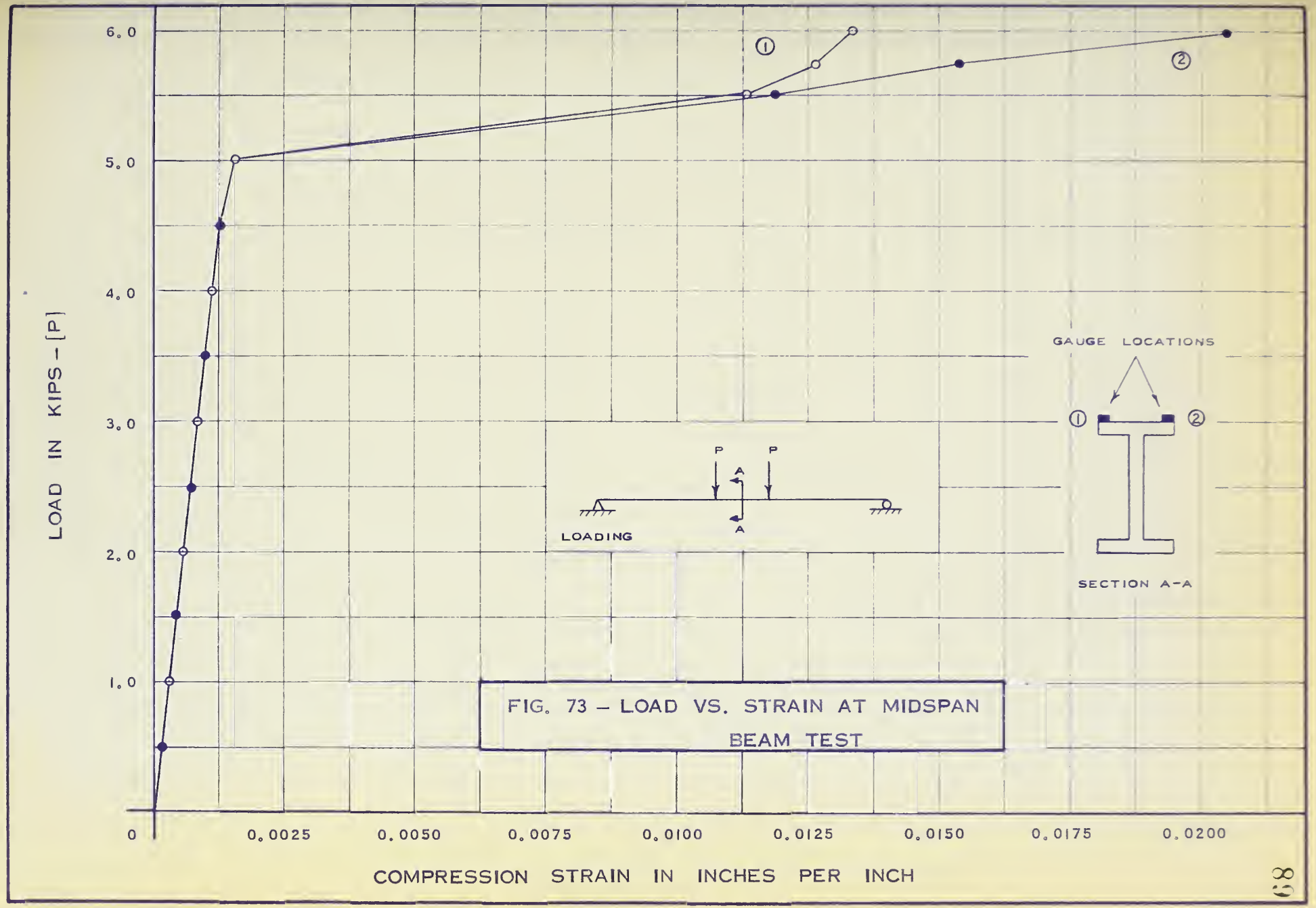

FIG. 73 – LOAD VS. STRAIN AT MIDSPAN BEAM TEST

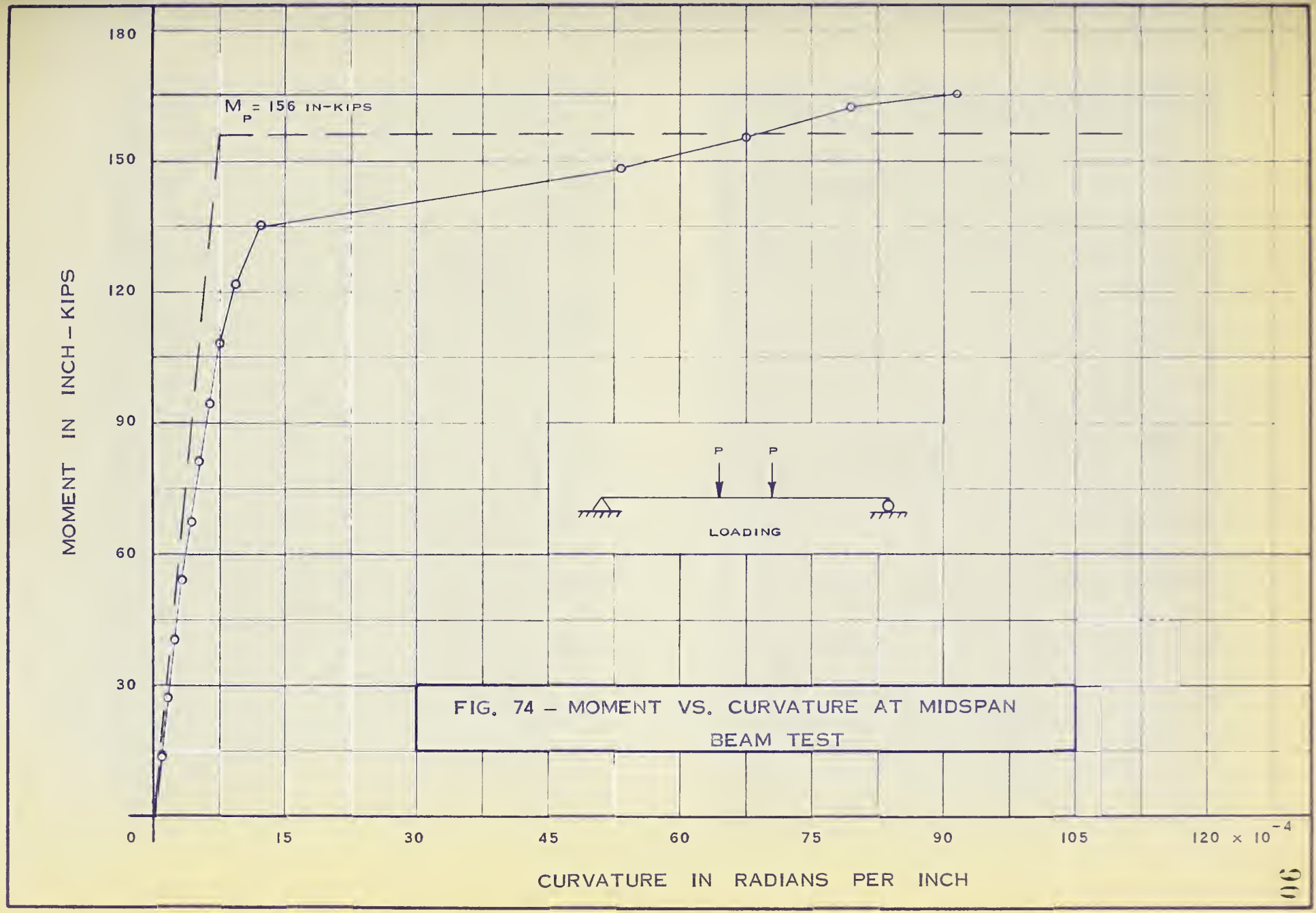

FIG. 74 – MOMENT VS. CURVATURE AT MIDSPAN BEAM TEST

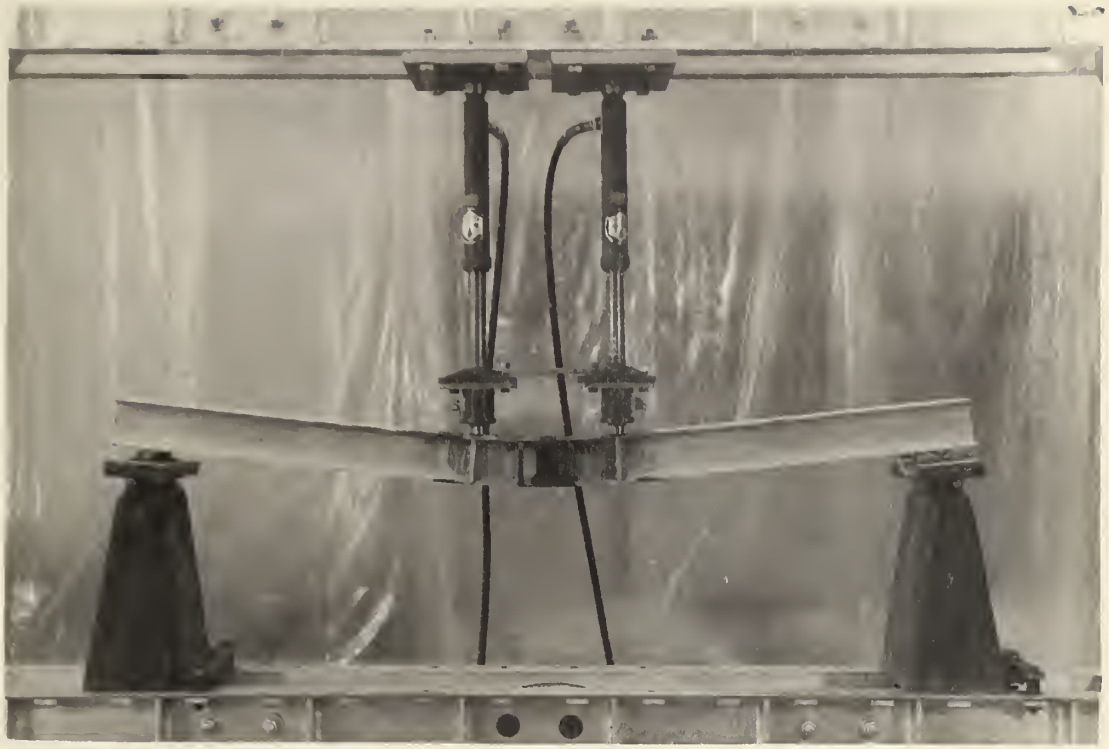

FIG. 75 – BEAM AFTER TEST

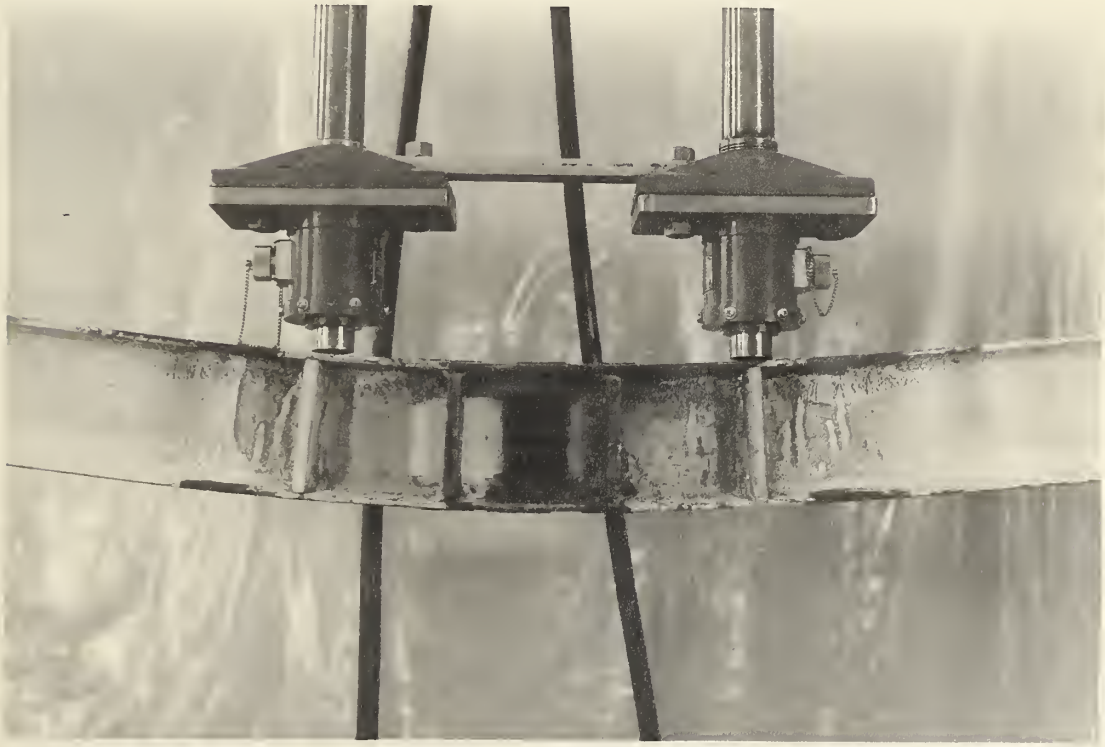

FIG. 76 – PLASTIC HINGE AT MIDSPAN OF BEAM

CHAPTER 10: DISCUSSION

10-1 Material Properties

The average value of 29.8×10^6 psi for the modulus of elasticity obtained from the coupon tests agrees favourably with the usual value for mild steel. The yield point stress values for the two web coupons were 39.3 ksi and 39.5 ksi, while the values for the two flange coupons were 38.5 ksi and 38.6 ksi. This difference was not expected due to the fact that the flanges were rolled thinner than the web. However, the differences were small, and a yield stress value of 39.0 ksi was used in all calculations.

In conducting the coupon tests, load was applied in 500 pound increments. This loading simulated the frame loading in that the frame loading was also applied in increments. The mill reports show a yield point stress of 46.5 ksi, approximately 19 percent in excess of that determined for the coupons above. The main factor contributing to this discrepancy is probably the rate of straining. The maximum specified A.S.T.M. strain rate of 1/16 inch per minute per inch of gauge length would probably be used for the mill tests, whereas the strain rate in the frame tests was much slower. It is a well established fact that an increase in the rate of straining results in an increase in the value of the yield stress.[10] Tall[11] reports that yield stresses found at normally accepted mill testing speeds can be as much as twenty percent greater than what he refers to as the "static yield stress", or the yield stress found at zero strain rate. The "static yield stress" is considered a logical yield stress to use for the theoretical calculations since most structural

loads are usually static. It would appear then that the yield stresses pertinent to this investigation are close to this "static yield stress". Assuming that stress is directly proportional to strain up to the yield stress, the corresponding yield strain is

$$\frac{39.0}{29.8 \times 10^{3}} = 0.131 \times 10^{-2} \text{ inches per inch.}$$

The two properties determined from the stress-strain relationship drawn by the recorder have values much lower than expected. The average strain-hardening moduls, E_{st}, (calculated from the slope of the initial portion of the strain-hardening region) was determined as 99.3 ksi. Beedle[1] suggests a value of 700 ksi for the strain-hardening modulus. The strain at the onset of strain-hardening, e_{st}, determinded directly from the stress-strain graph, was 0.75×10^{-2} inches per inch, which is only six times the yield strain. Beedle suggests a value for the e_{st}/e_{y} ratio of 12.0. Both the values for E_{st} and e_{st} are much lower than those commonly listed in literature. Although both these properties are extremely variable in nature, such a large discrepancy suggests that possibly the coupons were not representative samples of the frame material.

Measurements of the section dimensions compare closely with handbook values so tabulated values of the section properties were used in all calculations.

10-2 Residual Stresses

Residual stresses in a rolled section are due to differential cooling and cold-bending. In this investigation, residual stresses were calculated from the residual strain measurements, and found to

be a maximum of 13,000 psi in the flanges, or approximately one-third of the yield point stress of the steel. Therefore, a section under an applied load experiences initial yielding at a load approximately one-third lower than that predicted by theoretical calculations. At Lehigh University,[5,6] maximum residual stresses in large wide flange sections were found to be approximately 0.3 times the yield stress. The distribution of the residual strains, as shown in Figures 25 and 26, appear to be caused by local bending and therefore are not necessarily indicative of the residual cooling stresses in the frames.

10-3 Beam Test Results

Results of the beam test are presented in Figures 70 to 76 inclusive. In the load-deflection graph (Figure 70), the experimental curve is linear up to a load of 4.0 kips, at which load the curve begins to bend slightly. This value agrees favourably with the theoretical value if residual stresses are included. Since the magnitude of the residual stress is approximately one-third of the yield stress, initial yielding should begin at 5.78 x 0.67 = 3.9 kips. A sharply defined collapse load occurs at 5.0 kips; however, due to the strain-hardening effects, load increases past the theoretical ultimate load of 5.78 kips to a final value of 6.1 kips, at which point the test was stopped. The shape of the load vs. curvature diagram shown in Figure 71 is very similar to that of the load-deflection curve.

In Figure 72, strain distributions are shown for loads of 1.5, 3.0, 4.5, and 6.0 kips. At a load between 5.0 and 5.5 kips, strains equal to 0.0075 inches per inch (the strain value calculated

as the strain at the initiation of strain-hardening) are attained in the flanges. At 6.0 kips, practically the entire section has experienced strains beyond the strain-hardening strain.

Figure 73 shows a plot of load vs. strain. The inequality of strains at the edges of the flange shows the tendency for lateral buckling at the midspan, although the beam was well supported. Small eccentricities in the applied loads would presumably produce the tendency to bend about the weak axis.

The experimental moment-curvature relationship is shown in Figure 74. Residual stresses cause the moment-curvature relationship to become non-linear at a moment approximately equal to 108 inch-kips. This curve closely follows the theoretical curve (including strain-hardening effects) shown in Chapter 1.

10-4 Frame No. 1

Test results for Frame No. 1 are presented in Figures 27 to 50 inclusive. Frame No. 1 was subjected to a concentrated vertical force at the midspan of the beam. Calculations in accordance with the simple plastic theory indicated that the frame should form a beam mechanism and collapse when the magnitude of the applied vertical load reached 17.33 kips. These calculations are based on the assumption that the plastic hinges occur at the corners of the line diagram formed by the centerlines of the frame members.

In the theoretical calculations, the effect of axial force was neglected. The Commentary on Plastic Design in Steel[12] states that for strong-axis bending, the influence of axial force may be neglected if P is less than 15 percent of P_y where P is the axial force on the member and P_y is the concentric load that would cause yielding of the entire column cross-section. The resulting error

due to this approximation is less than 5 percent. In Frame No. 1, the computed axial loads on the columns were 8.67 kips at the theoretical ultimate load. P_y for the 4 I 9.5 section = σ_y x A = 39.0 x 2.76 = 107.5 kips. Thus the ratio of P/P_y was approximately 0.08, well below 0.15. Thus, the effects of axial load should therefore be less than 5 percent.

Similarily, shear force was neglected in theoretical ultimate load calculations. The Commentary[12] recommends a maximum allowable shear force of V_{max} = 18.0 wd, where "w" is the web thickness and "d" is the total section depth. For the 4 I 9.5 section this gives a maximum allowable shear value of approximately 23.5 kips. For Frame No. 1 the maximum theoretical shear in the columns at ultimate load was 3.25 kips and in the beam 8.67 kips, both well below the recommended maximum value of 23.5 kips. Therefore the value of ultimate load should not be affected by shearing force.

A plot of load vs. vertical deflection at the beam midspan of Frame No. 1 is shown in Figure 27. The experimental curve follows the theoretical curve quite closely up to the theoretical ultimate load, although the deflections are slightly in excess of those calculated by the simple plastic theory. At a load of approximately 9 kips, the experimental curve gradually departs from a straight line. This value agrees favourably with the theoretical value if residual stresses are included. Since the magnitude of the residual stress is approximately one-third of the yield stress, the formation of the first plastic hinge should begin at 13.3 x 0.67 = 8.9 kips. Beyond the theoretical ultimate load, increased deflection could only be attained by increasing the load. The test was discontinued at a load of 20.0 kips, and three weeks later was resumed and continued

to a final load of 23.0 kips which was approximately 33 percent in excess of the predicted ultimate load. The increase in load for a small additional deflection as shown in Figure 27 is probably due to the difference in load application and additional friction in the apparatus. For Frame No. 1 the increase in load capacity was 7.5 percent. Frame No. 2, loaded the following day after being previously tested to ultimate load, did not exhibit this increase in load capacity. The first portion of Test No. 1 was stopped to allow for additional lateral supports to be fastened to the columns. Nevertheless, lateral buckling produced final failure during the second portion of the test. Load was still increasing when the test was stopped.

Figure 28 is a plot of load vs. horizontal deflection at the top of both columns. These positions were not expected to deflect appreciably, but it is interesting to note their shape is similar to that of Figure 27. Both curves indicate that the ultimate load was equal to approximately 18 kips. Once again, the curves do not indicate a sharply defined collapse load but rather increase at a distinct slope.

Vertical load vs. horizontal reaction is plotted in Figure 29. The experimental results agree very closely with the theoretical curve. This theoretical curve was plotted on the basis of an elastic analysis, with load varying linearly with horizontal reaction up to the formation of the first plastic hinge. At this point the load-deflection curve varies linearly at a different slope up to the calculated ultimate load. For additional load beyond the theoretical collapse load, the experimental curve of load vs. reaction continues on a definite upward slope.

Figures 30 to 33 inclusive are plots of experimental load-curvature data. They show that rotations at the midspan of the beam were greatest, while the rotations at the tops of the columns were almost identical to one another. Values for curvature at the beam midspan exceed those at the columns by approximately 38 percent. As was the case for the load-deflection plots, an increase in load capacity was observed when the test frame was reloaded. This characteristic is not in evidence in the load-curvature plot for Frame No. 2 (Figure 56). Rotation indicator data at the ends of the beam are plotted in Figure 33. In theoretical calculations, the curvature at the ends of the beam was assumed to remain proportional to load throughout the entire test, since this section was stiffened to prevent the formation of a plastic hinge. The observed departure from a linear relationship is probably due to the extreme rotations of the hinges in the columns.

Strain distributions are shown in Figures 34 to 37 for loads of 5, 10, 15 and 20 kips. Strains are plotted for the beam midspan (both sides of the stiffener), and at the top of both columns. As can be seen from Figures 34 and 35, at a load of 15 kips, the strains have not reached the strain-hardening strain of 0.0075 inches per inch. At a load of between 16.0 and 17.0 kips, the compression flange reaches the strain-hardening strain. This fact can be seen in Figure 38. At a load of 17.0 kips, strains of at least 0.0075 inches per inch were recorded at the gauge locations on the web (not including the gauge mounted at the neutral axis, whose readings remained in the elastic range throughout the test). At a load of 20.0 kips, all but a small portion of the section is completely in the strain-hardening region. The strains at the tops of the columns

did not reach the strain-hardening strain until a load of 18.5 kips. As can be seen from Figures 36 and 37, portions of the web reached the strain-hardening strain at 20.0 kips.

Figures 38 to 41 are plots of load vs. strain. They record readings obtained from strain gauges located at the edges of the compression and tension flange. Differences in the two "SR-4" gauge readings for the same flange indicate a tendency for lateral buckling. Figure 38 indicates there was little tendency for Frame No. 1 to buckle at the midspan. However, Figures 39 and 40 indicate definite tendencies towards lateral buckling in the columns. Indeed lateral buckling actually occurred as shown in the photographs in Figures 49 and 50. Figure 41 indicates strains of very small magnitude at the ends of the frame beam. This was expected, since these particular sections were well stiffened with flange plates.

The National Building Code[13] specified that all plastic hinge locations except the last one to form shall be adequately braced to resist lateral and torsional displacement. The laterally unsupported distance to adjacent support points need not be less than

$$L_{cr} = (60 - 40 \frac{M}{M_p}) r_y \quad \text{nor less than } 35 r_y,$$

where: L_{cr} is the laterally unsupported distance;

r_y is the radius of gyration of the member about its weak axis;

M is the lesser of the moments at ends of the unbraced segment;

and

M_p is the plastic moment.

For the 4 I 9.5 section, r_y is 0.58 inches. $35 r_y$ gives a minimum required spacing between lateral supports of twenty inches. The small projecting angles on the lateral support channels were

spaced approximately twelve inches apart which was less than the required minimum spacing and was sufficient to prevent lateral buckling of the beam. According to the National Building Code Specifications, lateral support is not needed in the region where the last plastic hinge forms. This stipulation is sufficient for design since collapse is assumed at the formation of the last plastic hinge. However, where large deflections and rotations are produced after the theoretical collapse load, provision should be made to support the remaining hinge locations as well. The support system used in this investigation did not prove to be entirely satisfactory and should be improved for future investigations.

Moment-curvature relationships at the beam midspan and the tops of the two columns are shown in Figures 42 and 44 inclusive. The moment-curvature relationships at midspan closely follows the theoretical curve up to a moment value of approximately 100 inch-kips, at which time it begins to depart from the theoretical. This is a direct cause of residual stresses in the section. Calculations for the theoretical moment-curvature relationship appear in Appendix A. The experimental curve increases at an approximate constant slope once the theoretical ultimate moment has been reached. Strain-hardening causes the moments to increase at approximately a constant rate. When the frame was reloaded, a definite increase in moment occurred corresponding to the abrupt load increase for the load-deflection and load-curvature curves. Figures 43 and 44 are almost identical, indicating that the hinges in each column rotated approximately the same amount. The moment did not attain the theoretical plastic moment value, M_p, during the first portion of the test. However, during the second part, the moment reached and exceeded M_p. One

possible reason is suggested for the low moment-curvature relationships in Figure 43 and 44. In Figure 29, lower values are indicated for the reaction load than shown on the theoretical curve (dotted line). This discrepancy resulted in moment values lower than theoretical.

Figure 45 gives a general view of Frame No. 1 after testing. Figures 46 to 48 show closeup views of the hinges. As can be seen from these photographs, all hinges formed approximately where they were predicted. It is significant that the connections showed no signs of distress due to the imposed loading. This behaviour was also observed in Frame No. 2. It would appear, therefore, that relatively simple connections, when properly stiffened to withstand the high shear stresses,will not fail prematurely before the ultimate strength of the frame is developed.

There does not seem to be any apparent relationship between the moment-curvature relationship for the beam and that for the frame at the beam midspan. It is interesting to note that the strain-hardening strain is reached at midspan in Frame No. 1 before relatively large deflections are encountered, while in the beam, the strain-hardening strain is reached after the actual collapse load and after the beam has experienced considerable deflection. This was expected due to the difference in loading systems.

One factor that may have contributed to early strain hardening in the frames is the low value for the strain-hardening strain, e_{st}. The value obtained from the test coupons for e_{st} was only $6e_y$, whereas most tests on mild steel report values for e_{st} equal to 12-15 e_y.

In summarizing the results for Frame No. 1, the effect of strain-hardening on the ultimate load is two-fold: 1. Strain-hardening begins after the formation of the first plastic hinge but slightly

before the theoretical ultimate load. 2. Strain-hardening increases the load capacity beyond the calculated ultimate load. The slope of the load-deflection curve beyond the ultimate load is $\frac{P}{\delta}$ = 1.7 kips per inch. The reloading curve was disregarded. Dividing the slope by E_{st}, the strain-hardening modulus, the following expression is obtained:

$$\frac{P/\delta}{E_{st}} = \frac{1.7}{99.3} = 1.72 \times 10^{-2} \text{ kips /in/ ksi}$$

This value allows for future comparisons with similarily loaded frames having different material properties.

10-5 Frame No. 2

Test results for Frame No. 2 are shown in figures 51 to 69 inclusive. This frame was subjected to a concentrated vertical force at the midspan of the beam and a concentrated horizontal force equal to half of the vertical force and applied at the top of one column. Calculations in accordance with the simple plastic theory indicated that the frame would form a composite mechanism and collapse when the magnitude of the applied vertical and horizontal loads reached 10.40 kips and 5.20 kips respectively. Axial load and shear force were neglected in making theoretical ultimate load calculations, as they were for Frame No. 1.

In figure 51, vertical load is plotted against horizontal deflection at the top of the right column which was the location of the first plastic hinge. All test results for Frame No. 2 were plotted in relation to vertical load values, and thus whenever load is mentioned, it will refer to the vertical load unless stated otherwise. Load remained proportional to horizontal deflection up to a value of 6.0 kips. Beyond this load, deflections increased at a more rapid rate. It was predicted that the load vs. deflection

relationship would change slope at a value of 8.55 x 0.67 = 5.70 kips, since the residual stresses were approximately one-third of the yield stress. Between 6.0 and 9.5 kips, the experimental load-deflection curve remained linear. There is a sharply defined collapse load at 11.0 kips, approximately 6 percent in excess of the theoretical ultimate load. Strain-hardening effects caused the load to increase to a value of 11.5 kips, at which the test was discontinued to make apparatus adjustments. Reloading began the next day, and the curve does not show any abrupt load increase as did Frame No. 1. The test was terminated at a load of 12.25 kips, approximately 18 percent in excess of the theoretical ultimate load. A significant feature of the curve is the fact that deflections remained lower than the theoretical values throughout the entire test. This same characteristic was noted for a similar loading condition in the University of California tests.(8)

In Figure 52, load is plotted against horizontal deflection at the top of left column. Although no plastic hinge formed here, it is interesting to note that this curve is almost identical to Figure 51. In theory, deflections at the tops of both columns are assumed equal. Load vs. vertical deflection at the beam midspan is presented in Figure 53. Up to the calculated ultimate load, deflections are slightly larger than predicted. A sharply defined collapse load occurs at a value of 11.0 kips. The test was discontinued at a load of 11.50 kips, or approximately 11 percent greater than the theoretical collapse load. During the second portion of the test the following day, no significant deflections occurred before the test was terminated.

Figure 54, a plot of load vs horizontal reaction, shows

poor correlation of observed values with the theoretical curve (shown in dotted lines). All reaction values are lower than those calculated. The discrepancy may be explained, in part, by the frictional force acting at the roller mechanism under the vertical jack. The magnitude of the force would be the product of the coefficient of friction and vertical load, and would act in a direction opposite to the applied horizontal force. This would tend to decrease the magnitude of the horizontal reactions. The second experimental curve, (to the right of the initially plotted curve), is the actual relationship occurring when the frame was reloaded the second day. It would appear that once the mechanism has formed, the actual horizontal reactions agree much closer with the theoretical values. Also, load vs. reaction relationship would be affected by the degree of tightness at the left horizontal reaction assembly. From the appearance of the curve, this would appear to be a logical explanation for the large discrepancies from the theoretical curve.

Load vs. curvature relationships are presented in Figures 55 to 57. The relationships at midspan and at the top of the right column have similar shapes, although the curvatures for the latter are twice those recorded at the midspan. This fact clearly indicates that the first plastic hinges to form experience the largest rotations. Although the load-curvature relationship at the top of the left column, shown in Figure 57, becomes non-linear, the magnitudes of curvature remain small. Curvatures at the ends of the beam, as expected, have even lower values.

Strain distributions are shown in Figures 58 to 60 for loads of 3,6,9, and 11.5 kips. Strains are plotted for the beam midspan

(both sides of the stiffener), and at the top of the right column. The compression flange attained a strain of 0.0075 inches per inch at approximately 11.0 kips at the plastic hinge in the right column. At a load of 11.5 kips, practically all the section is in the strain-hardening range (Figure 60). Strains of 0.0075 inches per inch or greater first occurred in the flanges at midspan of the beam (to the left of the stiffener) at a load of 11.25 kips. Strains to the right of the stiffener at midspan reached the strain-hardening strain in the flanges at 11.50 kips. The fact that greater strains occurred to the left of the midspan is clearly shown in Figures 66 and 67. The plastic hinge actually formed about 4 inches to the windward side of the midspan. It is obvious that the hinge formed at a point which combined the highest moment with the section offering the least resistance to flexure. Vertical bearing stiffeners were welded at the center of the beam to prevent web crippling under the vertical concentrated load, and therefore strengthened this particular section. This, together with the fact that the moment gradient from the midspan to the windward column is relatively flat (see Figure A2 in Appendix) probably forced the hinge to form to the windward side of the midspan.

Figures 61 to 63 present load vs. strain relationships. In Figure 61, little lateral buckling tendency in the beam is evident, indicating the beam was satisfactorily supported against bending about its weak axis. However, at the right column, lateral buckling is evident, as shown graphically in Figure 62 and pictorially in Figure 69. Although lateral support was provided, it apparently was not sufficient. Nevertheless, loads beyond the theoretical ultimate were attained. As expected, the curves of

Figure 63 for positions at the top of the left column and at the ends of the beam showed strains of extremely small magnitude.

Moment-curvature relationships are shown for the beam midspan and the right column in Figures 64 and 65. In general, both curves show poor agreement with the theoretical curves. The discrepancy in the curves indicates the measurements of the horizontal reaction is in error, as shown in Figure 54. For the results obtained in Figure 64, the moment was computed using the left horizontal reaction force, which was much lower than the theoretical value. For the results obtained in Figure 65, the moment was computed using the right horizontal reaction force. It is obvious that this force was much higher than expected, since it was assumed to be simply the difference between the applied horizontal load and the left horizontal reaction.

Strain-hardening, therefore begins to affect the action of Frame No. 2 at a load approximately equal to the theoretical ultimate load. The increase in load beyond P_u may be expressed as follows:

$$\frac{P}{\delta_h} = 0.175 \text{ kips per inch}$$

Dividing by E_{st}, $\frac{P/\delta_h}{E_{st}} = \frac{0.175}{99.3} = 1.76 \times 10^{-3}$ kips/in/ksi

where δ_h is the horizontal deflection at the right column. Different relationships would be expected for different loading conditions.

The following two suggestions are presented for

consideration in future investigations.

1. A more elaborate device for laterally supporting the columns is necessary if deflections and rotations of large magnitude are desired.
2. The present electrical stress-strain recorder on the universal testing machine is unsatisfactory for obtaining accurate graphical results for the modulus of elasticity, the strain-hardening modulus, and the strain at the onset of strain-hardening. A device that would expand the strain scale to a large degree is necessary.

CHAPTER 11: CONCLUSIONS

11-1 Summary

Conclusions based on the results of this investigation are summarized as follows:

1. Values of modulus of elasticity and yield point stress as determined from coupon tests, compared favourably with standard values. Values of E_{st} (strain-hardening modulus) and e_{st} (strain at the onset of strain-hardening) were much lower than standard values.
2. Residual stresses were found to have a maximum value of approximately one-third the yield point stress at the flange tips.
3. Residual stresses resulted in initial yielding at values lower than predicted by the simple plastic theory.
4. Actual load-deflection curves for frames may be predicted with satisfactory accuracy up to the theoretical ultimate load.
5. Strain-hardening developed at approximately ultimate load and resulted in an increase in load carrying capacity that was proportional to deformation.
6. Strains, deflections, and rotations at the first plastic hinge were considerably greater than at hinges formed later; thus strain-hardening had the greatest effect at the first plastic hinge location.
7. Failure mechanisms formed as predicted by the simple plastic theory. In both frames, the cause of final failure was lateral buckling of the columns.
8. Instrumentation designed to measure horizontal reactions, rotations, and loads functioned favourably.

BIBLIOGRAPHY

1. Beedle, L.S., "Plastic Design of Steel Frames," Wiley, 1958.

2. Longworth, J., "Basic Concepts of Plastic Design," Proceedings, Conference on Recent Developments in Structural Engineering, U. of A., March, 1961.

3. Morrison, I.F., Ford, G., "The Physical Properties of Solid Materials", Hamly Press, 1955.

4. Knudsen, K.E., Yang, C.H., Johnston, B.G., Beedle, L.S., "Plastic Strength and Deflections of Continuous Beams," Welding Journal Supplement, Vol. 32, 1953.

5. Luxion, W.W., Johnston, B.G., "Plastic Behaviour of Wide Flange Beams," Welding Journal Supplement, Vol. 27, 1948.

6. Huber, A.W., Beedle, L.S., "Residual Stress and the Compressive Strength of Steel," Welding Journal Supplement, Vol. 33, 1954.

7. Ruzek, J.M., Knudsen, K.E., Johnston, E.R., Beedle, L.S., "Welded Portal Frames Tested To Collapse", Welding Journal Supplement, Vol. 33, 1954.

8. Popov, E.P., McCarthy, R.E., "Deflection Stability of Frames Under Repeated Loads," Journal of the Engineering Mechanics Division, Proceedings of the American Society of Civil Engineers, January, 1960.

9. Channon, J.R., "The Ultimate Load Capacity of Steel Frames," U. of A. Master Thesis, 1961.

10. Neal, B.G., "The Plastic Methods of Structural Analysis," Wiley, 1957.

11. Tall, L., "Material Properties of Structural Steel," Fritz Laboratory Report No. 220A. 28A, 1958.

12. ASCE Manual No. 41, "Commentary on Plastic Design in Steel," Welding Research Council and the American Society of Civil Engineers, 1961.

13. Part 4 (Design) Section 4.6, "Steel Construction," National Building Code of Canada, 1960.

14. Schilling, C.G., Schutz, F.W., Beedle, L.S., "Behaviour of Welded Single-Span Frames Under Combined Loading," Welding Journal Supplement, Vol. 35, 1956.

15. Beedle, L.S., Huber, A.W., "Residual Stress and the Compressive Properties of Steel," Fritz Laboratory Report No. 220A. 27,1957.

16. Longworth, J., "Some Secondary Factors in Plastic Design," Proceedings, Conference on Recent Developments in Structural Engineering, U. of A., March, 1961.

17. Murray, D.W., "Methods of Plastic Analysis," Proceedings, Conference on Recent Developments in Structural Engineering, U. of A., March, 1961.

18. Murray, D.W., "Instability Problems in Design," Proceedings, Conference on Recent Developments in Structural Engineering, U. of A., March, 1961.

19. Timoshenko, S.P., "Theory of Elastic Stability", McGraw-Hill, 1961.

APPENDIX A: CALCULATIONS BASED ON THE SIMPLE PLASTIC THEORY

A-1 Ultimate Load Calculations

Calculations based on the mechanism method of analysis are presented in this section for the ultimate load for the test frames and test beam. That mechanism forming at the lowest load is the actual failure mechanism and has a moment diagram that does not exceed the plastic moment at any section of the structure. The calculations included in this section refer to the failure mechanism which gives the true ultimate load in each case. Moment diagrams for the true ultimate loads are shown to indicate that the plastic moment has not been exceeded at any section of the frame.

(a) Frame No. 1

The loading for Frame No. 1 is shown in Figure A1(a). Possible plastic hinge locations are at sections 2, 3, and 4. A beam mechanism is formed as shown in Figure A1(b) with plastic hinges located at all three possible locations. In Figure A1(b), the frame, subjected to the ultimate load P, is given a virtual vertical displacement δ at the midspan of the beam. According to the theory of virtual work, the external work done by the applied loads in moving through their virtual displacements is equal to the internal work done by the plastic hinges as they rotate. The work done by each plastic hinge is equal to the plastic moment at the hinge times the angle through which it rotates. External work done by this vertical load is then:

$$W_e = P \times \delta = \frac{P L \theta}{2} \qquad \text{since} \quad \delta = \frac{L \theta}{2}$$

The plastic hinges at the corners have each rotated through an angle θ and the hinge at the beam midspan through an angle 2θ as

indicated by the diagram. The total internal work is:

$$W_i = M_p \times \theta + M_p \times 2\theta + M_p \times \theta = 4M_p\theta$$

Equating the external work to the internal work gives:

$$\frac{P\,L\,\theta}{2} = 4M_p\theta \qquad \text{or } P = \frac{8M_p}{L}$$

$$M_p = \sigma_y \times Z$$

σ_y = 39.0 ksi (from coupon test results)

Z for 4 I 9.5 = 4.0 in.^{3} L = 72 in.

Therefore M_p = 39.0 x 4.0 = 156 inch kips.

Substituting these values in the equation for P give:

$$P = \frac{8 \times 156}{72} = 17.33 \text{ kips}$$

Solving for the reactions:

$$H_1 = H_5 = \frac{3M_p}{2L} = \frac{3 \times 156}{2 \times 72} = 3.25 \text{ kips}$$

$$V_1 = V_5 = \frac{P}{2} = \frac{17.33}{2} = 8.67 \text{ kips}$$

The reactions are shown in Figure A1(b). The moment diagram for the ultimate load is shown in Figure A1(c).

$$M_3 = 36V_1 - 48H_1$$

$$= 36 \times 8.67 - 48 \times 3.25$$

$$= 312 - 156 = 156 \text{ inch-kips} = M_p$$

It is apparent that the plastic moment has not been exceeded at any section of the frame and that the full plastic moment acts at the predicted plastic hinge locations.

(b) Frame No. 2

The loading for Frame No. 2 is shown in Figure A2(a). Possible plastic hinge locations are at sections 2, 3, and 4 for the combined loading. Since the frame is indeterminate to the first degree,

it is possible to have two independent mechanisms and one composite mechanism. After analyzing these different possibilities, it was found that the composite mechanism shown in Figure A2(b) with plastic hinges at sections 3 and 4 formed at lowest load. Note that the plastic hinges have been assumed to form at the corners of the line diagram.

In Figure A2(b), the frame, loaded as shown, is given a virtual vertical and horizontal displacement, δ_1 and δ_2 respectively. The total external work done is:

$$W_e = P\delta_1 + \frac{P}{2}\delta_2 \qquad \delta_1 = \frac{L}{2}\cdot\theta \quad \delta_2 = \frac{2L\theta}{3}$$

$$W_e = \frac{PL\theta}{2} + \frac{PL\theta}{3} = \frac{5PL\theta}{6}$$

The plastic hinges at the midspan and the leeward column corner are each rotated through an angle 2θ. The total internal work is:

$$W_i = M_p \times 2\theta + M_p \times 2\theta = 4M_p\theta$$

Equating the external work to the internal work gives:

$$\frac{5PL\theta}{6} = 4M_p\theta \quad \text{or} \quad P = \frac{24M_p}{5L} = \frac{24 \times 156}{5 \times 72}$$

$$P = 10.40 \text{ kips} \qquad \frac{P}{2} = 5.20 \text{ kips}$$

Solving for the reactions:

$$H_5 = \frac{M_p}{2/3L} = \frac{3 \times 156}{2 \times 72} = 3.25 \text{ kips}$$

$$H_1 = \frac{P}{2} - H_5 = \left(\frac{24M_p}{5L}\right)\frac{1}{2} - \frac{3M_p}{2L} = \frac{9M_p}{10L} = \frac{9 \times 156}{10 \times 72} = 1.95 \text{ kips}$$

$$M_1 = \frac{P}{2} \times 48 + P \times 36 - V_5 \times 72 = 0$$

$$V_5 = \frac{60P}{72} = \frac{60 \times 10.40}{72} = 8.67 \text{ kips}$$

$$M_5 = \frac{P}{2} \times 48 - P \times 36 + V_1 \times 72 = 0$$

$$V_1 = \frac{12P}{72} = \frac{12 \times 10.40}{72} = 1.73 \text{ kips}$$

These reactions are shown in A2(b).

The moment diagram for the ultimate load is shown in Figure A2(c). Moments are plotted on the tension side of the members.

$$M_2 = H_1 \frac{2L}{3} = \frac{9M_p}{10L} \times \frac{2L}{3} = \frac{3M_p}{5}$$

Since the moment is not greater than M_p at any section, the correct solution has been obtained.

(c) Beam

The loading for the beam is shown in Figure A3(a). Plastic hinges will form at sections 2 and 3, directly under the two concentrated loads. A beam mechanism is formed as shown in Figure A3(b). In actual fact, one large plastic hinge will form over the entire 12 inch section between the loads. The maximum moment as shown in Figure A3(c) is $\frac{9}{22}$ PL. Equating this to the plastic moment,

$$M_p = \frac{9}{22} PL \qquad L = 66 \text{ inches}$$

$$P = \frac{22M_p}{9L} = \frac{22 \times 156}{9 \times 66}$$

$$P = 5.78 \text{ kips}$$

A-2 Elastic Analysis of Frames

Reactions and moments for the frames subjected to unit loads are shown in this section. These calculations are necessary in order to make subsequent theoretical deflection calculations.

(a) Frame No. 1

Calculated moments and reactions for the statically

indeterminate frame loaded with a unit vertical load at the midspan of the beam are shown in Figure A4(a). The frame has been solved using the Müller Breslau theory. The frame is made statically determinate by replacing the hinge with a roller at the right support (condition "O"). A horizontal unit load acting to the right at the roller (condition " $X_a = -1$") produces moments and reactions shown in Figure A4(c).

The horizontal deflection at the right support for condition "O", δ_{oa}, can now be solved using the Müller Breslau tables.

$$\delta_{oa} \times EI = \frac{4 \times 1.5 \times 6}{2} = 18$$

The horizontal deflection at the right support for condition " $X_a = -1$," δ_{aa}, can also be solved using the same tables.

$$\delta_{aa} \times EI = \frac{2 \times 4 \times 16}{3} + 6 \times 16 = 42.67 + 96 = 138.67$$

The horizontal reaction at the right support of the indeterminate frame is therefore:

$$H_5 = \frac{\delta_{oa}}{\delta_{aa}} = \frac{18}{138.67} = 0.13$$

From this value for H_5, the remaining reactions and moments in the indeterminate frame are shown in Figure A4(a).

(b) Frame No. 2

Reactions and moments for Frame No. 2 loaded with a vertical to horizontal load ratio of 2:1 are shown in Figure A5(a). Calculations are similar to those for Frame No. 1.

A-3 Frame Deflection Calculations

(a) Frame No. 1

The first plastic hinge forms in this frame at the midspan,

since the largest bending moment (0.98 foot-kips) for the unit loading acts at this section, as shown in Figure A4. The first plastic hinge forms at a predicted load of $\frac{156}{0.98 \times 12} \times 1$ or 13.30 kips. The vertical deflection at the midspan of the beam for the 13.30 kip load can be determined using the moment diagram shown in Figure A4(a). The moments for the 13.30 kips load are obtained by multiplying the coefficients shown in this figure by 13.30 kips to obtain the final moments as shown in Figure A6(a). By equating the external work done by the unit load in moving through the deflection caused by the 13.30 kip load to the internal work done by the unit load moments during the same deflection, the following value for the vertical deflection at the midspan of the beam is obtained using Muller Breslau tables:

$$\frac{\delta_v \times EI}{1728} = \frac{2 \times 4 \times 0.52 \times 6.93}{3} + \frac{2 \times 1.04 \times 0.52 \times 6.93}{3} + \frac{3.92 \times 13.05 \times 0.98}{3}$$

$$= 9.60 + 2.50 + 16.75 = 28.85$$

$$E = 29.8 \times 10^3 \text{ ksi} \quad \text{(from coupon tests)}$$

$$I = 6.7 \text{ in}^4$$

$$\delta_v = \frac{28.85 \times 1728}{6.7 \times 29.8 \times 10^3} = 0.250 \text{ inches.}$$

The theoretical deflection at the midspan of the beam is then 0.250 inches.

The theoretical vertical deflection at the midspan of the beam at the predicted ultimate load of 17.33 kips was calculated using the slope-deflection equations. The moment diagram for the ultimate load and a free-body diagram for the

frame at ultimate load are shown in Figures A6(b) and A6(c).

The slope-deflection equations necessary to solve for the vertical deflection at the ultimate load are as follows:

Note: Clockwise moment and angle changes are considered positive.

$$\theta_a = \theta'_a + \frac{\delta_v}{L} + \frac{L}{3EI}\left(M_{AB} - \frac{M_{BA}}{2}\right)$$

where θ'_a is the slope at A due to a similar loading of a simply supported beam.

$$\theta_{21} = 0 + 0 + \frac{2L}{3 \times 3EI}\left(+M_p - 0\right) = \frac{2M_p L}{9EI}$$

$$\theta_{23} = 0 + \frac{2\delta_v}{L} + \frac{L}{2 \times 3EI}\left(-M_p + \frac{M_p}{2}\right) = \frac{2\delta_v}{L} - \frac{M_p L}{12EI}$$

$$\theta_{43} = 0 - \frac{2\delta_v}{L} + \frac{L}{2 \times 3EI}\left(+M_p - \frac{M_p}{2}\right) = -\frac{2\delta_v}{L} + \frac{M_p L}{12EI}$$

$$\theta_{45} = 0 + 0 + \frac{2L}{3 \times 3EI}\left(-M_p - 0\right) = -\frac{2M_p L}{9EI}$$

Plastic hinges form simultaneously at sections 2 and 4 to complete the mechanism at ultimate load. Immediately before the formation of these two hinges, continuity exists at both sections. Therefore, $\theta_{21} = \theta_{23}$ and $\theta_{34} = \theta_{43}$ just before the collapse mechanism is formed. Equating $\theta_{21} = \theta_{23}$ gives:

$$\frac{2M_p L}{9EI} = \frac{2\delta_v}{L} - \frac{M_p L}{12EI} \qquad \frac{2\delta_v}{L} = \frac{8M_p L}{36EI} + \frac{3M_p L}{36EI}$$

$$\delta_v = \frac{11M_p L^2}{72EI}$$

$$\delta_v = \frac{11 \times 156 \times 72 \times 72}{72 \times 29.8 \times 10^3 \times 6.7} = 0.620 \text{ inches}$$

The theoretical vertical deflection at the midspan of the beam is therefore 0.620 inches at ultimate load. After the ultimate load has been reached, the deflections will theoretically increase with

no increase in load, neglecting strain-hardening effects.

(b) Frame No. 2

The first plastic hinge forms in this frame at section 4, as shown in Figure A5(a), since the largest bending moment (1.52 foot-kips) for the unit loading acts at this section. The first plastic hinge occurs at a predicted load of $\frac{156}{1.52 \times 12} \times 1$ or 8.55 kips.

Using the theory of virtual work, deflections are calculated prior to the formation of the first plastic hinge. The frame is shown in Figure A7(a) loaded with 8.55 kip and 4.27 kip loads. Moments and reactions were determined by multiplying all values shown in Figure A5(a) by 8.55. Figure A7(b) shows the moments for a horizontal unit load applied at the top of the windward column. The horizontal deflection at the top of the windward column is obtained by equating the external work done by the unit load during the deflection of the frame in Figure A7(a). to the internal work done by the unit load moments during the same deflection. The calculation is obtained by using the Müller Breslau tables as follows:

$$\frac{\delta_h \times EI}{1728} = \frac{4 \times 4.1 \times 2}{3} + \frac{3 \times 2 \times 16.6}{6} - \frac{1.18 \times 8.40 \times 0.79}{6} + \frac{1.82 \times 13.0 \times 4.79}{6} + \frac{4 \times 13.0 \times 2.0}{3}$$

$$\frac{\delta_h \times EI}{1728} = + 10.9 + 16.6 - 1.3 + 18.9 + 34.6 = 79.7$$

$E = 29.8 \times 10^3$ ksi (from coupon tests)

$I = 6.7$ in^4

$$\delta_h = \frac{79.7 \times 1728}{6.7 \times 29.8 \times 10^3} = 0.690 \text{ inches.}$$

The theoretical horizontal deflection at the top of the windward column when the first plastic hinge forms is therefore 0.690 inches.

The theoretical vertical deflection at the midspan of the beam immediately prior to the formation of the first plastic hinge is calculated in a similar manner to that above. For this case, Figures A7(a) and A7(c) are combined. By equating the external work done by the unit load to the internal work done by the unit load moments during the deflection of the frame loaded with a vertical load of 8.55 kips and horizontal load of 4.27 kips, the following value for the vertical deflection at the beam midspan is then:

$$\delta_v \times EI = -\frac{4 \times 0.52 \times 4.1}{3} - \frac{1.04 \times 0.52 \times 13.79}{6} + \frac{1.96 \times 0.98 \times 22.39}{6} + \frac{1.18 \times 8.40 \times 2.35}{6} - \frac{0.78 \times 0.39 \times 5.57}{6} + \frac{1.04 \times 0.52 \times 31.57}{6} + \frac{4 \times 0.52 \times 13.0}{3}$$

$$\delta_v \times EI = -2.84 - 1.24 + 7.17 + 3.89 - 0.28 + 2.85 + 9.00 = 18.55$$

$$\delta_v = \frac{18.55 \times 1728}{29.8 \times 10^3 \times 6.7} = 0.161 \text{ inches.}$$

The theoretical vertical deflection at the midspan of the beam when the first plastic hinge forms is therefore 0.161 inches.

The theoretical deflections at the predicted ultimate load are calculated using the slope-deflection equations. The moment diagram for the ultimate load and a free-body diagram for the frame at ultimate load are shown in Figure A8(a) and A8(b). The slope-deflection equations necessary to solve for the horizontal and

vertical deflections at the ultimate load are as follows:

$$\theta_a = \theta'_a + \frac{\delta_v}{L} + \frac{L}{3EI}\left(M_{AB} - \frac{M_{BA}}{2}\right)$$

where θ'_a is the slope at A due to a similar loading of a simply supported beam.

$$\theta_{21} = 0 + \frac{3\delta_h}{2L} + \frac{2L}{3 \times 3EI}\left(-\frac{3}{5}M_p - 0\right)$$

$$= \frac{3\delta_h}{2L} - \frac{2M_pL}{15EI}$$

$$\theta_{23} = 0 + \frac{2\delta_v}{L} + \frac{L}{2 \times 3EI}\left(\frac{3}{5}M_p + \frac{M_p}{2}\right)$$

$$= \frac{2\delta_v}{L} + \frac{11M_pL}{60EI}$$

$$\theta_{32} = 0 + \frac{2\delta_v}{L} + \frac{L}{2 \times 3EI}\left(-M_p - \frac{3M_p}{10}\right)$$

$$= \frac{2\delta_v}{L} - \frac{13M_pL}{60EI}$$

$$\theta_{34} = 0 - \frac{2\delta_v}{L} + \frac{L}{2 \times 3EI}\left(M_p - \frac{M_p}{2}\right)$$

$$= -\frac{2\delta_v}{L} + \frac{M_pL}{12EI}$$

It can be seen from Figure A5(a) that the last plastic hinge forms at section 3. Just prior to the formation of this hinge, continuity must exist here, and therefore $\theta_{32} = \theta_{34}$.

$$\frac{2\delta_v}{L} - \frac{13M_pL}{60EI} = -\frac{2\delta_v}{L} + \frac{M_pL}{12EI}$$

$$\delta_v = \frac{3M_pL^2}{40EI}$$

$$\delta_v = \frac{3 \times 156 \times 72 \times 72}{40 \times 29.8 \times 10^3 \times 6.7} = 0.304 \text{ inches.}$$

Therefore, the theoretical vertical deflection at the midspan of the beam when the collapse mechanism forms is 0.304 inches.

No plastic hinge forms at section 2, therefore $\theta_{21} = \theta_{23}$.

$$\frac{3\delta_h}{2L} - \frac{2M_p L}{15EI} = \frac{2\delta_v}{L} + \frac{11M_p L}{60EI}$$

Substituting $\delta_v = \frac{3M_p L^2}{40EI}$ in the right hand side gives:

$$\frac{3\delta_h}{2L} = \frac{2M_p L}{15EI} + \frac{3M_p L}{20EI} + \frac{11M_p L}{60EI}$$

$$\frac{3\delta_h}{2L} = \frac{28M_p L}{60EI} \qquad \delta_h = \frac{14M_p L^2}{45EI}$$

$$\delta_h = \frac{14 \times 156 \times 72 \times 72}{45 \times 29.8 \times 10^3 \times 6.7} = 1.26 \text{ inches.}$$

Therefore, the theoretical horizontal deflection when the collapse mechanism just forms is 1.26 inches.

(c) Beam

The deflection at the midspan of a simply supported beam with two equal concentrated loads symmetrically placed is given by the expression:

$$\delta = \frac{Pa}{24EI} (3L^2 - 4a^2)$$

where: L - is the length of the beam, in this case 66 inches

a - is the distance from one support to the position of the first load, in this case 27 inches.

$$\delta = \frac{5.78 \times 27}{24 \times 29.8 \times 10^3 \times 6.7} (3 \times 66^2 - 4 \times 27^2)$$

$$\delta = 0.331 \text{ inches.}$$

Therefore, the theoretical deflection at the midspan of the beam at ultimate load is 0.331 inches.

A-4 Theoretical Moment-Curvature Relationship

The idealized moment-curvature diagram for any structural steel consists of two straight lines, neglecting strain-hardening. For moments less than the plastic moment, curvature is assumed to be directly proportional to the applied moments. When the ultimate moment is reached, curvature increases indefinitely with no increase in moment. Therefore, in order to draw the theoretical moment-curvature diagram for any section, it is necessary to calculate only the plastic moment capacity of the section and the curvature for that moment capacity.

The plastic moment for the 4 I 9.5 section was calculated previously and found to be 156 inch-kips. The section modulus for this section is 3.3 in^3. The theoretical curvature when the plastic moment capacity has just been reached is then calculated as follows:

$$\sigma_{max} = \frac{M_p}{S} = \frac{156}{3.3} = 47.3 \text{ ksi}$$

$$e = \frac{\sigma}{E} = \frac{47.3}{29.8 \times 10^3} = 1.59 \times 10^{-3} \text{ in/in}$$

$$\phi = \frac{e}{d/2} = \frac{1.59 \times 10^{-3} \times 2}{4} = 7.95 \times 10^{-4} \text{ radians/in.}$$

A-5 Calculated Moment-Curvature Relationships

The calculated moment at the midspan of the beam for Frame No. 1 is given by the following expression:

$$M_c = V_1 \times \frac{L}{2} - H_1 \times \frac{2L}{3} + H_1 \delta$$

where: V_1 - is the assumed vertical reaction at the left support,

$$= \frac{P}{2} \text{ kips}$$

H_1 - is the measured horizontal reaction at the left support, in kips

δ - is the deflection at midspan, in inches

$\frac{L}{2}$ - is the half-length of the beam section of the frame, in inches.

$\frac{2L}{3}$ - is the length of the column section of the frame, in inches.

The horizontal reaction H_1 is carried by the beam as an axial compressive force. In the plastic range, the beam deflection δ becomes large and the additional beam moment due to this axial force can no longer be neglected. Friction on the roller at the left reaction was neglected. The inclusion of this term would result in a moment increase of approximately 2 to 3 percent.

The calculated moment at the knees of Frame No. 1 is given by the following expression:

$$M_k = H \left(\frac{2L}{3} - 5 \right)$$

where: H - is the measured reaction as before, in kips

$\frac{2L}{3}$ - is the length of the column section of the frame, in inches

5 - is the distance from the mid-depth of the beam to the point at which rotation was measured, in inches.

The moments for Frame No. 2 were calculated in a similar manner as shown above. The moment at the midspan of the simple beam was calculated by simply multiplying the load P times the moment arm of 27 inches. In all cases, curvature was calculated by using the formula given in Chapter 5.

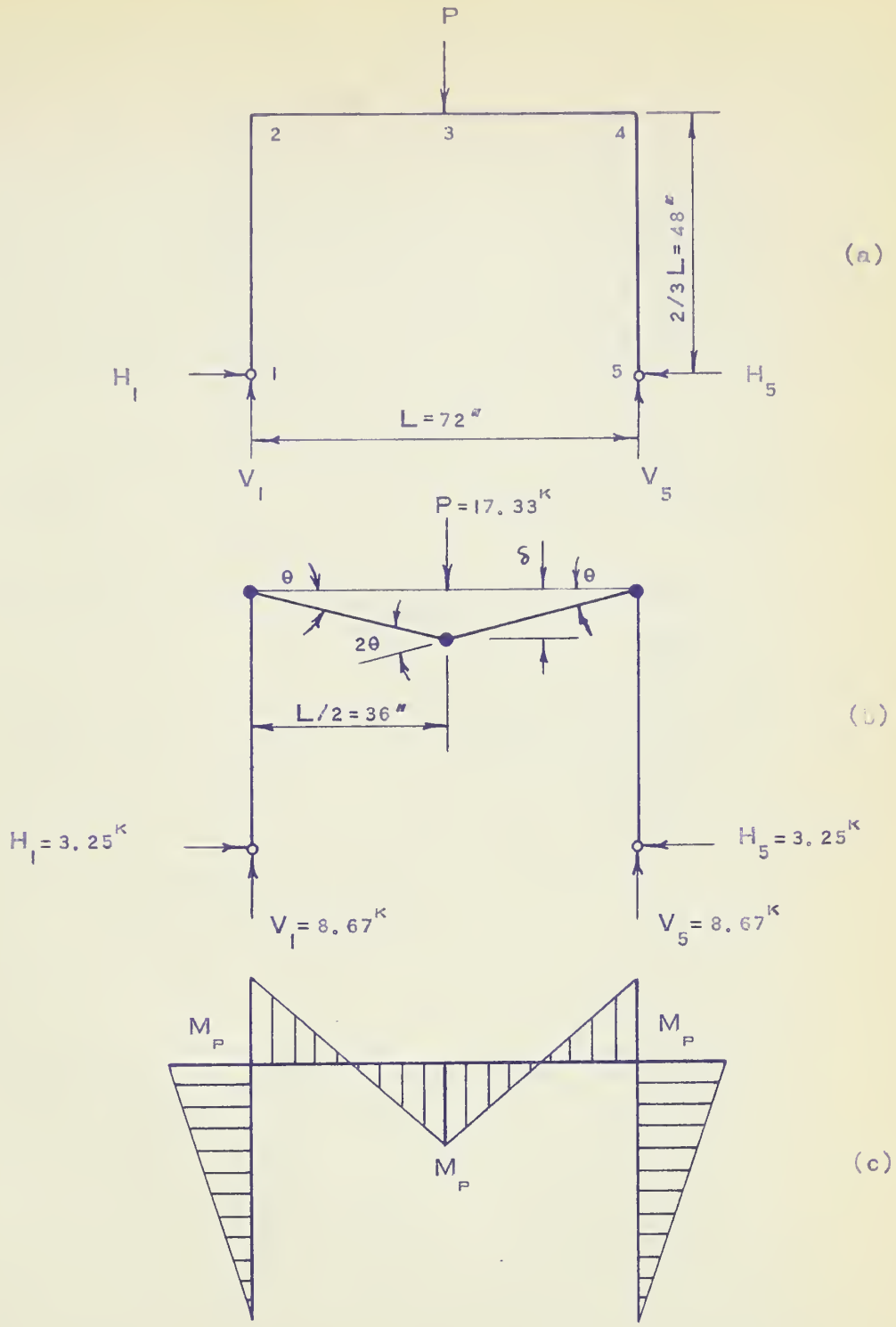

FIG. A1 — ULTIMATE LOAD ANALYSIS
FRAME NO. 1

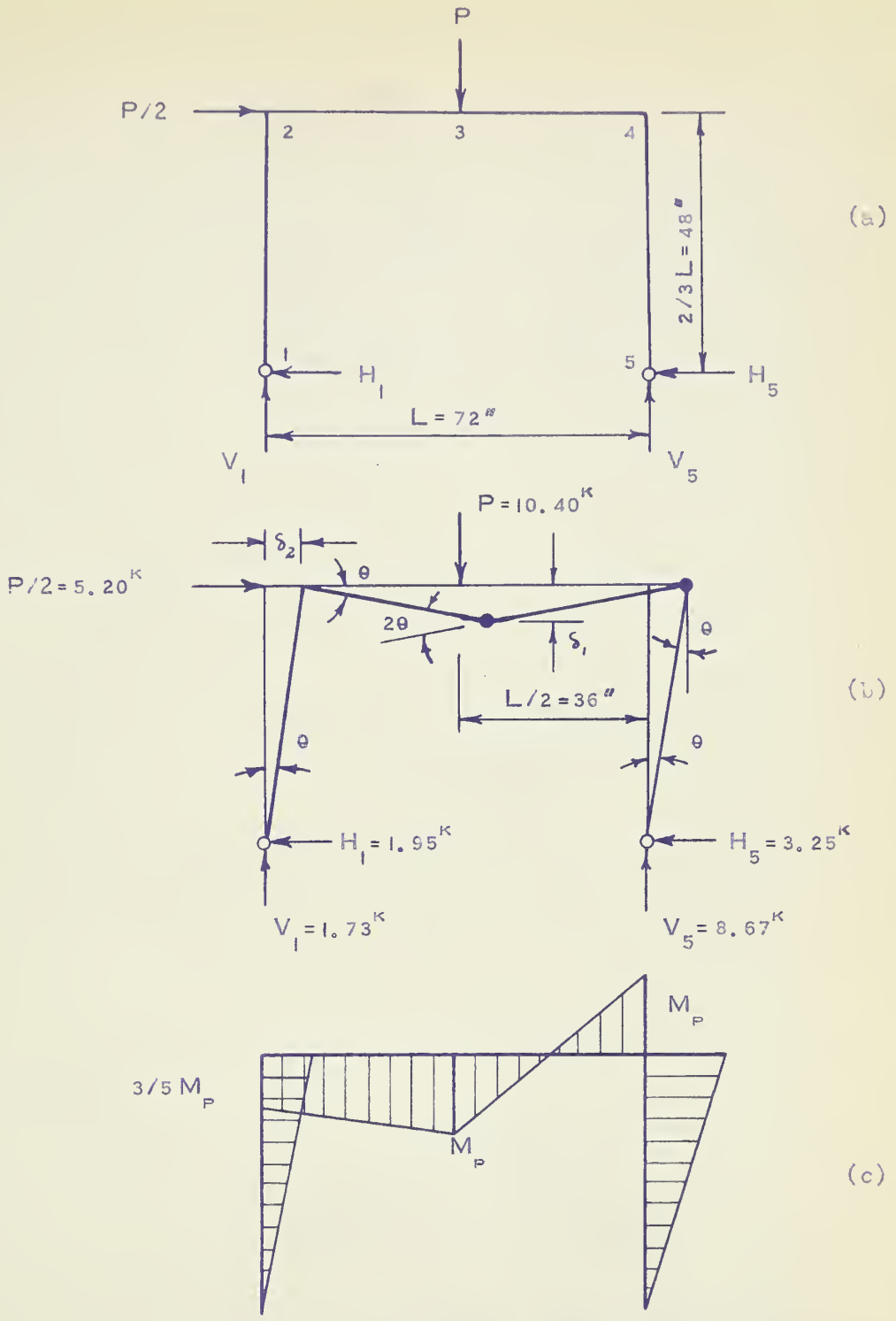

FIG. A2 – ULTIMATE LOAD ANALYSIS
FRAME NO. 2

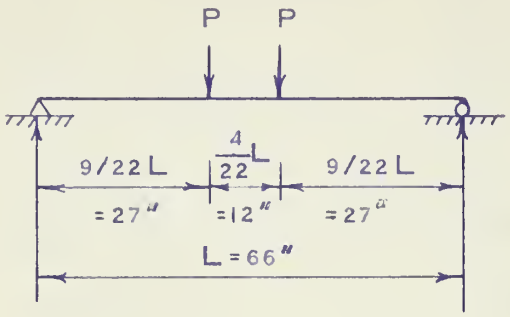

(a)

(b)

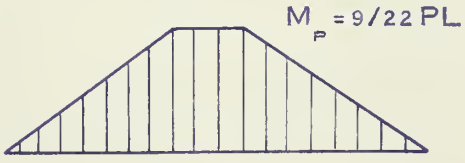

(c)

FIG. A3 – ULTIMATE LOAD ANALYSIS
BEAM

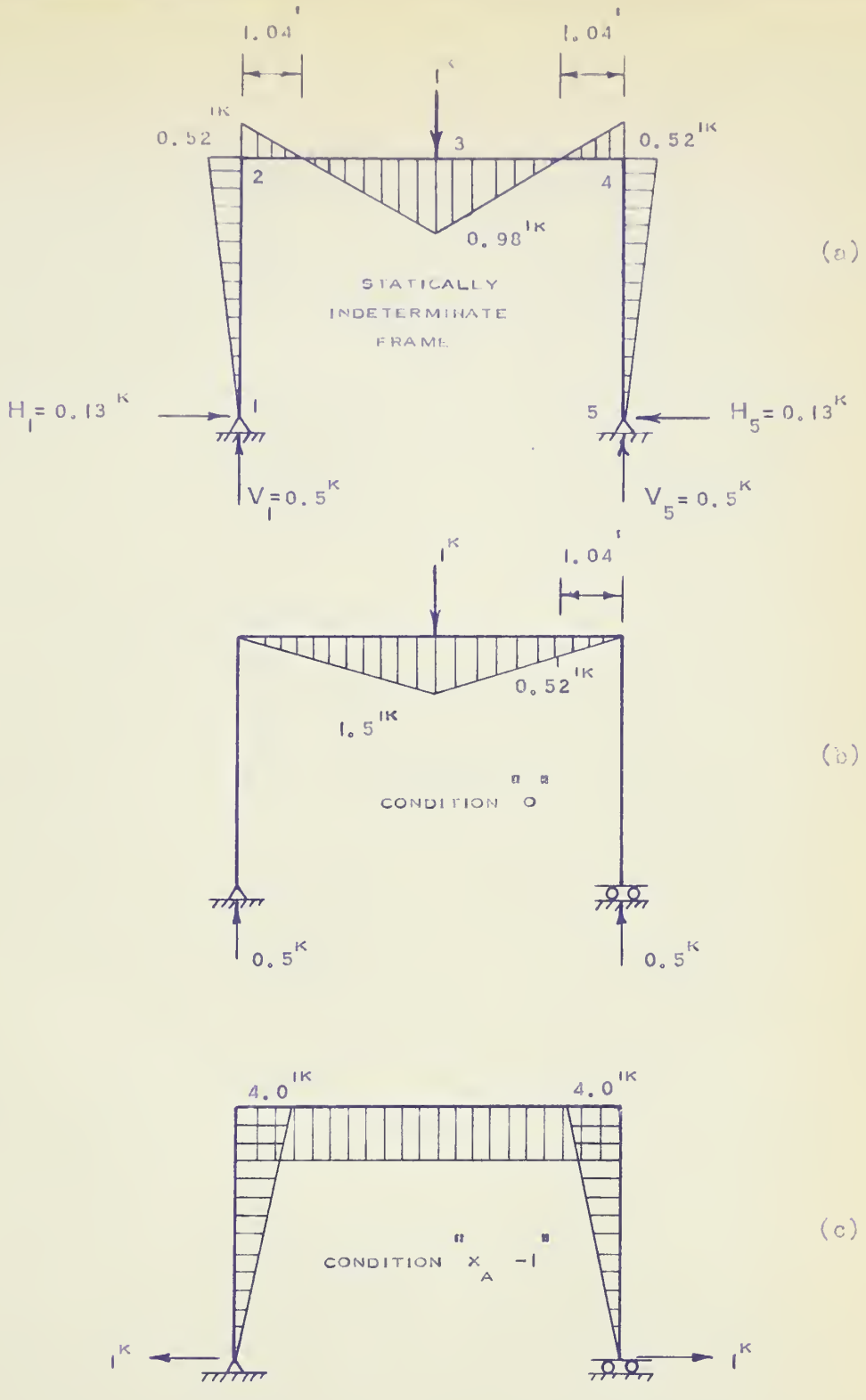

FIG. A4 – MOMENTS AND REACTIONS FOR UNIT LOAD FRAME NO. 1

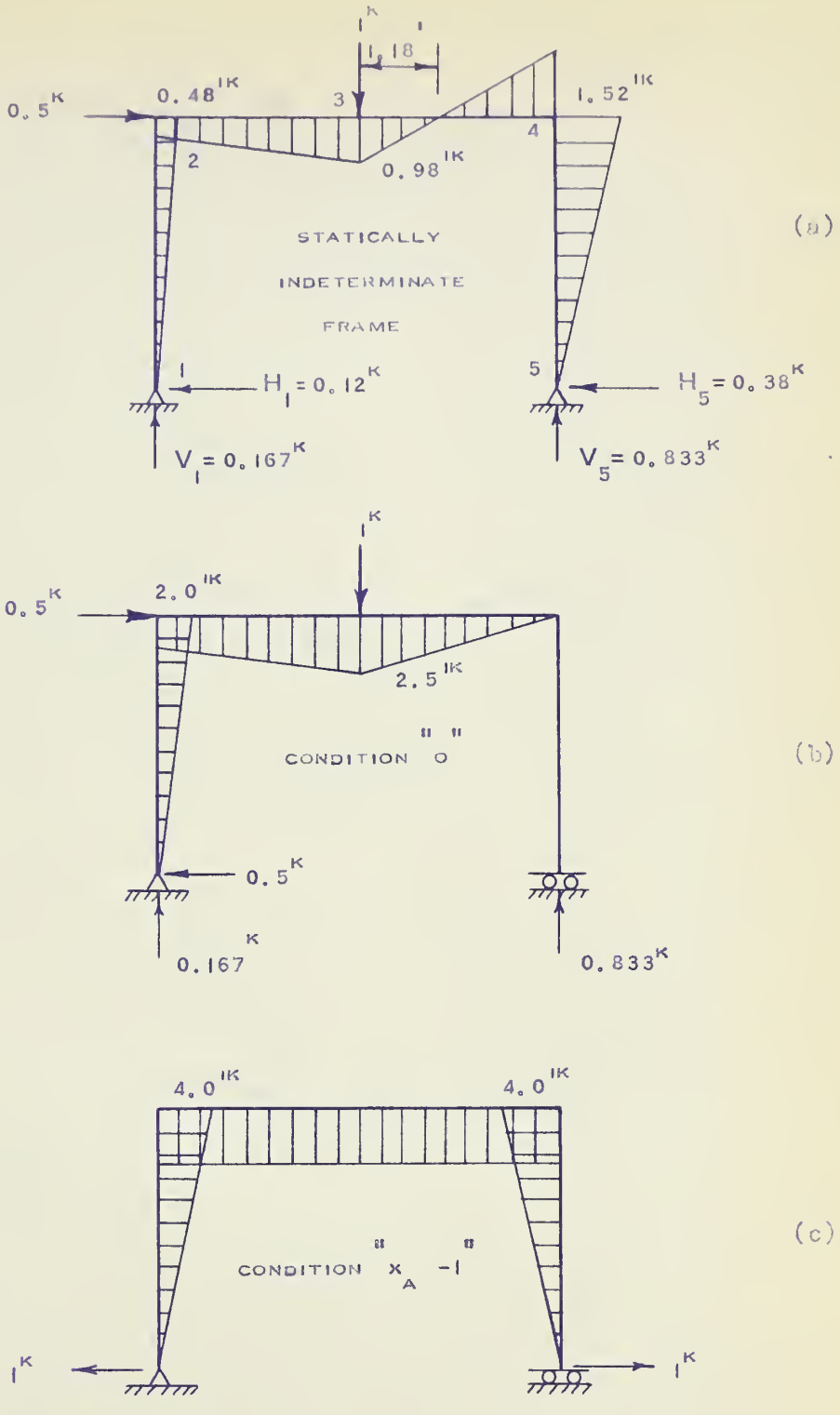

FIG. A5 – MOMENTS AND REACTIONS FOR UNIT LOADS

FRAME NO. 2

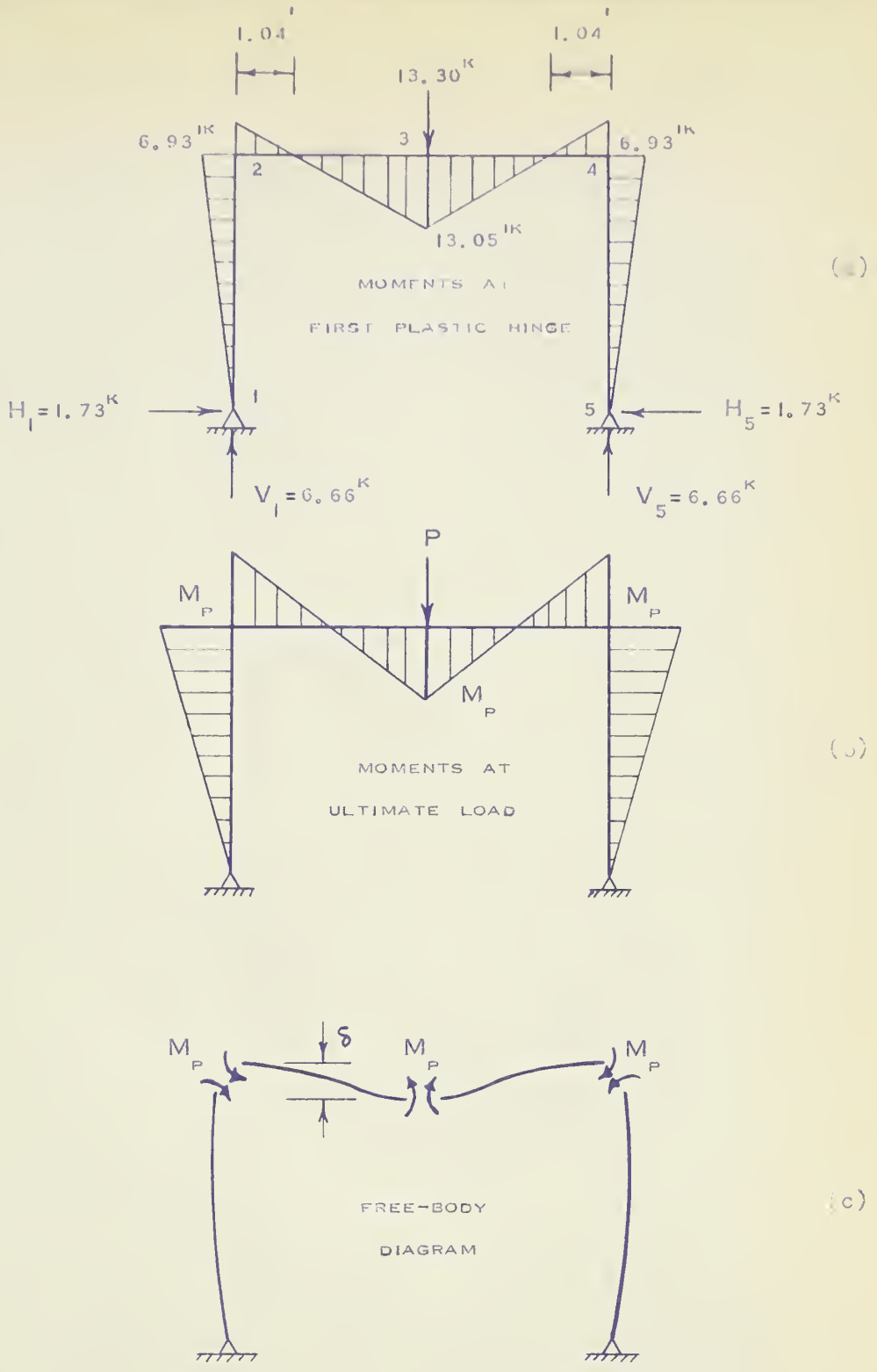

FIG. A6 – DEFLECTION ANALYSIS

FRAME NO. 1

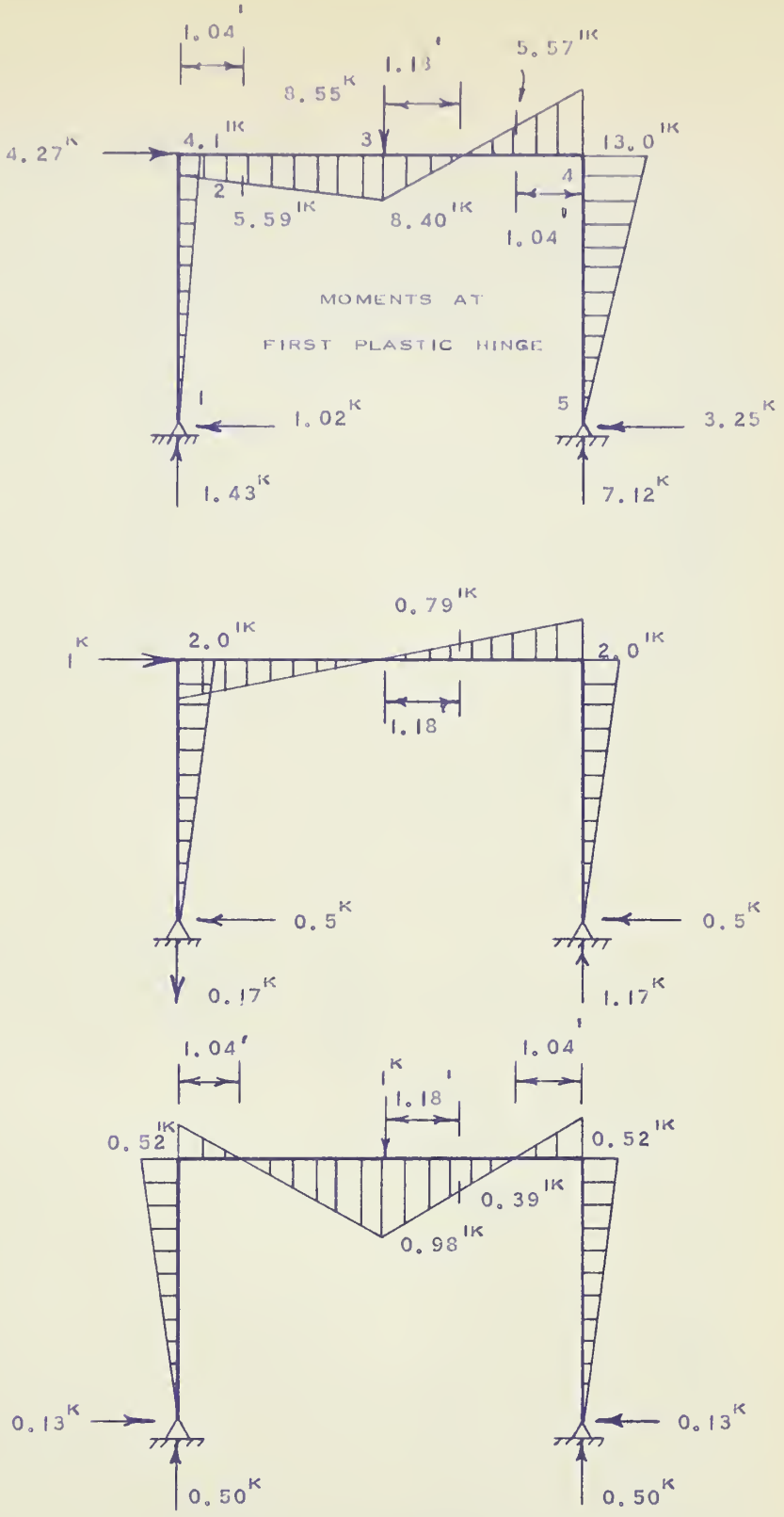

FIG. A7 – DEFLECTION ANALYSIS

FRAME NO. 2

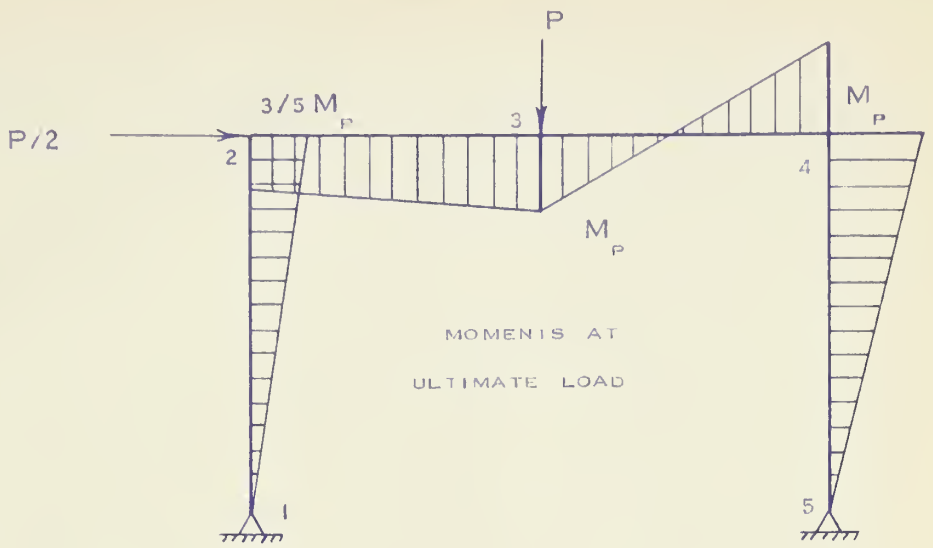

(a)

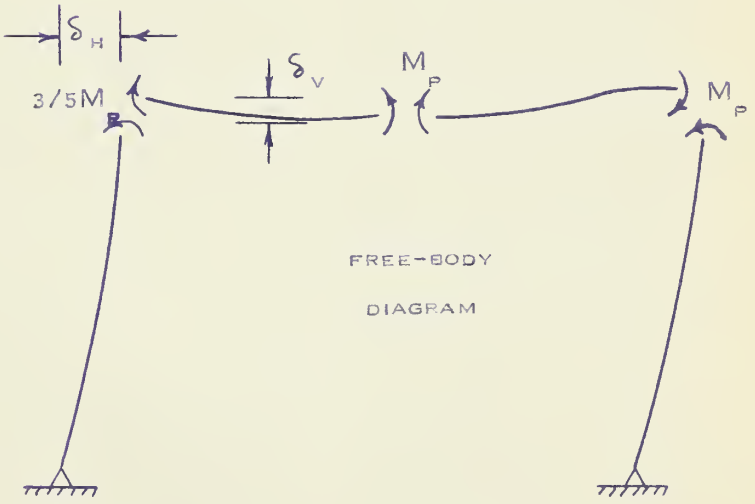

( )

FIG. A8 – DEFLECTION ANALYSIS

FRAME NO. 2